

UCLA

UCLA Electronic Theses and Dissertations

Title

Quantum Mechanics and Molecular Dynamic Investigations of Organic Reactions

Permalink

<https://escholarship.org/uc/item/9356s7tq>

Author

Mackey, Joel Loren

Publication Date

2015

Peer reviewed|Thesis/dissertation

UNIVERSITY OF CALIFORNIA

Los Angeles

Quantum Mechanics and Molecular Dynamic Investigations of Organic Reactions

A dissertation submitted

In partial satisfaction of the requirements for the degree

Doctor of Philosophy in Chemistry

By

Joel Loren Mackey

2015

© Copyright by
Joel Loren Mackey
2015

ABSTRACT OF THE DISSERTATION

Quantum Mechanics and Molecular Dynamic Investigations of Organic Reactions

By

Joel Loren Mackey

Doctor of Philosophy in Chemistry

University of California, Los Angeles, 2015

Professor Kendall N. Houk, Chair

This dissertation describes research in organic chemistry including quantum mechanical investigations of Diels-Alder reaction, 1,3-dipolar cycloadditions and bioorthogonal reactions, and dynamic investigations of several Cope rearrangements and the Bergman cyclization. Several of these projects are collaborations with experimentalist and some are original research projects.

Chapter 1 describes the regioselectivity and stereoselectivity aspects of the Diels-Alder reaction followed by a radical hydrodenitration reaction leading to a *trans*-fused ring system. Computations located a Diels-Alder and a hetero-Diels-Alder pathways with a sigmatropic rearrangement that takes the hetero-Diels-Alder intermediate to the Diels-Alder adduct.

Chapter 2 describes the study of strained cyclooctynes and their uses in bioorthogonal chemistry. Computational investigations of substituted BARAC analogs revealed that rates were

marginally affected by substituents, however, substituents located near the transition state of azide attack to the strained octyne dramatically slowed the reaction. Further investigation revealed a large steric dependence on rates of reaction.

Chapter 3 describes the study of nucleophilic attacks to silyl substituted arynes and the competing effects of sterics and aryne distortion. The nucleophilic attacks prefer addition at the *meta* site due to sterics but *ortho* attack due to the predistortion of the aryne. This predistortion favors the *ortho* attack due to the bond angles of the aryne being very close to what they are in the transition state. This was studied both experimentally and computationally and using the distortion/interaction model, it was determined that the flatter angle of an aryne will be favored for nucleophilic attack as the larger angle is close to what it needs to be in the resulting transition state.

Chapter 4 continues the exploration of substituted arynes with focus shifted to electron withdrawing groups. Based on previous models of aryne predistortion, the predicated site of attack is the *meta* position. Computations along with experiments confirm that nucleophilic attack is selective at the *meta* position. A mainstream approach to understand this reactivity is to invoke charge polarization of the bonds. A computational study of this charge polarization found that it was insignificant to be responsible for the observed regioselectivities and thus, predistortion is the main factor in determining selectivity. A predictive model can be used to predict the site of attack based simply on a reactant optimization and its predistortion of the alkyne.

Chapter 5 focuses on the mechanism and timing of bond formation for several Cope rearrangements and a Bergman cyclization. Certain substituted Cope systems have a shallow intermediate between reactant and product and depending on how a molecule enters the transition zone, it may skip this intermediate altogether. To study the crossing of the systems through the transition zone, molecular dynamics were employed. Initial structures are generated

using normal mode sampling techniques and then propagated toward the reactant and product. Depending on substitution patterns, the Cope rearrangement may have dissociative, associative or aromatic character in the transition state. Molecular dynamics were performed on cases that exhibit each of these characteristics. The associative system has the shallow intermediate that is skipped in some dynamic trajectories. The Bergman cyclization has a very deep well and dynamics have indicated that the intermediate is not skipped over.

The dissertation of Joel Loren Mackey is approved.

Neil Kamal Garg

Selim M Senkan

Kendall N. Houk, Committee Chair

University of California, Los Angeles

2015

TABLE OF CONTENTS

List of Figures.....	vi-viii
List of Schemes	ix
List of Tables	x
Acknowledgments.....	xi
Vita.....	xiii
1. Origins of stereoselectivity in the <i>trans</i> Diels-Alder paradigm.....	1
2. Reactivity of biarylazacyclooctynones in copper-free click chemistry.....	15
3. Steric effects compete with aryne distortion to control regioselectivities of nucleophilic additions to 3-silylarynes	39
4. The Role of Steric Effects, Charges, and Aryne Distortions on Regioselectivities of Aryne Reactions	51
5. Molecular Dynamic Investigations of Cope Rearrangements and a Bergman Cyclization: Probing the Nature of a Chameleonic Transition State	73

LIST OF FIGURES

1. Transition structures and adducts for the cycloaddition of 2,3-dimethyl-1,3-butadiene and 1-nitrocyclohexene.....	6
2. Summary of the low energy transition structures leading to the formation of the DA adduct	7
3. Transition structures for the cycloadditions of isoprene and 1-nitrocyclohexene	7
4. [3,3]-Sigmatropic rearrangement transition structures in the cycloaddition of isoprene and 1-nitrocyclohexene.....	8
5. Solvent effects on the energetics of the cycloadditions of 1,3-butadiene and 1-nitrocyclohexene.....	9
6. Bicyclic radicals and connecting transition structure, and hydrogen transfer TSs and dehydrodecalin products in the cycloaddition of 2,3-dimethyl-1,3-butadiene and 1-nitrocyclohexene.....	11
7. 6,5-Bicyclic radicals and connecting transition structure, and hydrogen transfer TSs and bicyclic products in the cycloaddition of 2,3-dimethyl-1,3-butadiene and 1-nitrocyclopentene ...	12
8. Reagent development for copper-free click chemistry	16
9. The distortion/interaction model	19
10. Bond angles and reactivities of BARAC analogs.....	22
11. Structural analysis of BARAC.....	23
12. Flagpole methyl substituents sterically hinder the transition state.....	26
13. Strain modulation through rehybridization	31
14. Under Curtin-Hammett conditions, BARAC's amide conformation influences reactivity and regioselectivity	34
15. Influence of 3-methoxy and 3-silyl substituents on aryne regioselectivity	40
16. Transition states for nucleophilic additions of benzylamine and aniline to 3-trimethylsilylbenzynes	45
17. Cycloaddition of methylazide with 3-trimethylsilylbenzynes	46
18. Geometry optimized structure of 3- <i>t</i> -butylbenzynes 6 and predicted regioselectivity	46
19. Charge-controlled, steric, and aryne distortion models	52
20. Geometry-optimized structures of 1a–1e (B3LYP) and regioselectivity predictions for nucleophilic attack based on the aryne distortion model	54
21. Geometry-optimized structures and NBO charges for benzyne (7) (B3LYP)	57
22. Geometry-optimized structure and NBO charges for 3-fluorobenzyne (1b) (B3LYP) and point charge analysis.....	58
23. NBO charges for 1b separated based on distortion or inductive effects	60
24. Geometry-optimized structure and NBO charges for 3-trimethylsilylbenzynes (8), in addition to charge distribution due to distortion or inductive effects	61
25. Benzyne internal angles and transition state for methyl azide / benzyne cycloaddition	62
26. Competing transition states for the addition of <i>N</i> -methylaniline and methyl azide to 3-fluorobenzyne (1b) and 3-chlorobenzyne (1c)	64
27. Tandem Aryne Trapping / Cross-Coupling Sequence.....	65
28. Nickel-catalyzed C–C and C–N bond forming reactions for the synthesis of functionalized benzotriazoles 11 and 12	66
29. A More O'Ferrall-Jencks plot showing the effects of substitution on the timing of bond formations during a Cope rearrangement.....	74
30. Three possible mechanisms for the Cope rearrangement	75

31. Computed reactants, transition states, intermediates and products.....	80
32. Contour maps of reactions 1, 2, 4, and 6.....	82
33. Overlay of starting points and trajectory paths on the PES contour map of reaction 1	85
34. Overlay of starting points and trajectory paths on the PES contour map of reaction 2	86
35. Overlay of starting points and trajectory paths on the PES contour map of reaction 4	87
36. Representative samples or a trajectory that bypasses the intermediate and a normal short trajectory.....	88
37. Overlay of starting points and trajectory paths on the PES contour map of reaction 6	90
38. Trajectories that lead to product and a trajectory that rebounds	91
39. Trajectory that recross in the Bergman reaction.....	92

LIST OF SCHEMES

1. <i>trans</i> Diels-Alder Paradigm Involving a <i>cis</i> -Dienophile.....	1
2. Cycloadditions of 1-Nitrocyclohexene and Hydrocarbon Dienes.....	2
3. Diels-Alder (DA) and Hetero-Diels-Alder (HDA) Cycloadditions of Nitroalkenes.....	2
4. Radical Hydrodenitration of the DA Adduct to Yield <i>trans</i> -Fused Decalins.....	3
5. Synthetic route to triethylsilylbenzyne	41
6. Reactions which illustrate the unique nature of the Cope and Bergman rearrangements.....	73

LIST OF TABLES

1. Reactivity and alkyne bond angles	29
2. Nucleophilic additions to triethylsilylbenzyne.....	42
3. Cycloaddition reactions with triethylsilylbenzyne.....	43
4. Nucleophilic additions to <i>t</i> -butylbenzyne	47
5. Addition of <i>N</i> -methylaniline to various benzynes.....	55
6. Cycloaddition of benzylazide with various benzynes	56
7. QM and electronic energetics for the Cope and Bergman reactions.....	78
8. Summation of trajectories performed on reactants	84

ACKNOWLEDGEMENTS

My wife, Katy, has been a most generous supporter of my graduate career. I could not have done this without her love and support during my time at UCLA. Our marriage has been an important support structure and help me through many tough situations. I would also like to acknowledge my mother Stephanie and step-father Bill for their continued support during my lifetime. They have always encouraged me to work towards my goals and achieve them.

I have to thank Professor Houk for his continued support and mentorship. Not only is he a brilliant and successful scientist, he is an excellent mentor that truly cares about his students' growth. I have always felt that he had my best interests at heart and truly wanted me to succeed. He was very understanding during some difficult times in my life, and I am forever grateful for that.

Several current and former Houk group members have been incredible helpful during my graduate studies: Robert Paton, Peng Liu, Hung Pham, Colin Lam, Blanton Martin, Nick Knutson, and Ashay Patel. These individuals have been excellent teachers and supporters during my graduate studies.

I thank my many collaborators – Professor Samuel J. Danishefsky, Professor Carolyn R. Bertozzi, Professor Neil K. Garg, and Professor Daniel A. Singleton – for the many important chemistry questions that I have studied.

Finally I would like to thank my mentor from my undergraduate university, Dr. Carl Kemnetz. His training and guidance lead to a passion for computations and opened the door for my studies at UCLA.

Chapter 1 is reprinted (adapted) with permission from “Origins of Stereoselectivity in the *trans* Diels–Alder Paradigm,” Paton, R. S.; Mackey, J. L.; Kim, W. H.; Lee, J. H.; Danishefsky, S. J.; Houk, K. N. *J. Am. Chem. Soc.*, **2010**, *132*, 9335–9340. Copyright 2010 American Chemical Society.

Chapter 2 is reprinted (adapted) with permission from “Reactivity of Biarylazacyclooctynones in Copper-Free Click Chemistry,” Gordon C. G.; Mackey, J. L.; Jewett, J. C.; Sletten, E. M.; Houk, K. N.; Bertozzi, C. R. *J. Am. Chem. Soc.*, **2012**, *134*, 9199–9208. Copyright 2012 American Chemical Society.

Chapter 3 is reprinted (adapted) with permission from “Steric Effects Compete with Aryne Distortion To Control Regioselectivities of Nucleophilic Additions to 3-Silylarynes,” Bronner, S. M.; Mackey, J. L.; Houk, K. N.; Garg, N. K. *J. Am. Chem. Soc.*, **2012**, *134*, 13966–13969. Copyright 2012 American Chemical Society.

Chapter 4 is reprinted (adapted) with permission from “The Role of Aryne Distortions, Steric Effects, and Charges in Regioselectivities of Aryne Reactions,” Medina, J. M.; Mackey, J. L.; Garg, N. K.; Houk, K. N. *J. Am. Chem. Soc.*, **2014**, *136*, 15798–15805. Copyright 2014 American Chemical Society.

In all these cases, the experiments were performed by collaborators and I did the calculations.

The American Chemical Society is acknowledged for blanket permission to reproduce my published manuscripts in this dissertation (chapters 1, 2, 3, and 4). Funding for my graduate studies was provided by the National Science Foundation (CHE-0548209) and computational resources were provided by the UCLA Institute for Digital Research and Education (IDRE) and the Hoffman2 cluster along with the Extreme Science and Engineering Discovery Environment (XSEDE) (CHE040014).

VITA

2005-2009

Quality Assurance Chemist

NuSil Silicone Technologies

Bakersfield, CA

2009

B. S., Chemistry

California State University, Bakersfield

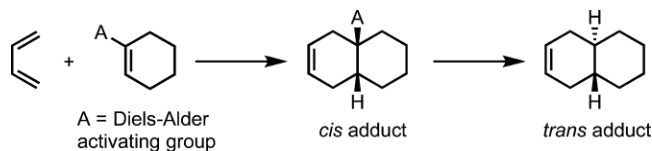
Bakersfield, CA

1. Origins of stereoselectivity in the *trans* Diels-Alder Paradigm

Introduction

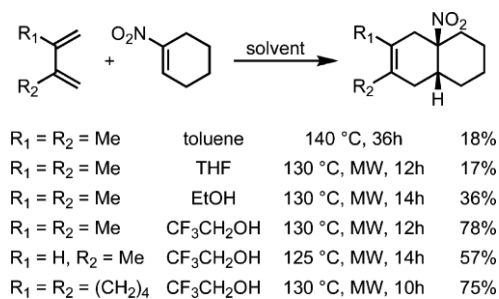
The critical role of the Diels-Alder reaction in organic synthesis is well appreciated. Diels-Alder cycloadditions produce *cis*-fused bicyclic systems from cyclic *cis*-dienophiles, providing a routine approach to the synthesis of complex molecules. Danishefsky and co-workers recently reported a departure from the *cis*-directed logic of the traditional Diels-Alder approach to encompass the formation of *trans*-fused products (i.e., the *trans* Diels-Alder paradigm).¹ This process formally involves reactions leading formally to the *trans*-fused adduct of a cycloalkene. This was achieved not via antarafacial cycloaddition, but instead by equipping an otherwise unreactive dienophile (such as cyclohexene) with a temporary, readily removable activating group. Following cycloaddition, the resultant *cis*-fused substructure is converted to the *trans*-series by removing the activating group and replacing it in a stereocontrolled fashion (Scheme 1).

Scheme 1. *trans* Diels-Alder Paradigm Involving a *cis*-Dienophile



The nitro group was chosen based on its dienophile activating properties, its known success in controlling Diels-Alder (DA) regioselectivity, and its ability to generate free radical intermediates. DA cycloadducts were obtained for the reaction between 1-nitrocyclohexene and a series of hydrocarbon dienes, although yields were adversely affected by the decomposition of 1-nitrocyclohexene. Alcoholic solvents, especially 2,2,2-trifluoro-ethanol, were found to improve yields of cycloaddition, and microwave irradiation was also helpful (Scheme 2).

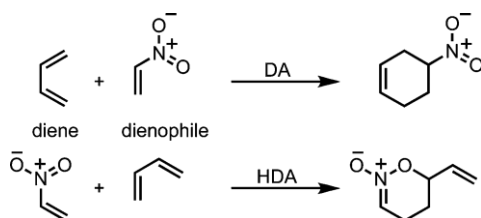
Scheme 2. Cycloadditions of 1-Nitrocyclohexene and Hydrocarbon Dienes^a



^a MW = microwave irradiation.

Nitroalkenes can function as either dienophiles or as hetero- dienes in Diels-Alder reactions (Scheme 3).² Denmark has shown that the reactions of nitroalkenes with cyclopentadiene can lead to mixtures of DA and hetero-Diels-Alder (HDA) cycloadducts.³⁻⁸ The DA adduct is favored under thermal conditions, but a Lewis acid can reverse the periselectivity to favor the HDA adduct. Calculations reveal that under thermal conditions this reaction proceeds initially via an *endo* DA transition state, which is then followed by a sigmatropic rearrangement of the *endo* adduct accounting for the formation of the hetero-Diels-Alder cycloadduct.⁹ Diels-Alder reactions of nitroethylene derivatives with cyclohexadiene yield a mixture of DA and HDA adducts. Subsequently the HDA adduct rearranges to the DA adduct upon heating at 80°C via a [3,3] sigmatropic rearrangement.¹⁰ Computational studies on microwave-assisted reactions of nitroheterocycles with dienes suggest that the DA adduct is formed via a tandem HDA/[3,3]-sigmatropic shift.¹¹

Scheme 3. Diels-Alder (DA) and Hetero-Diels-Alder (HDA) Cycloadditions of Nitroalkenes



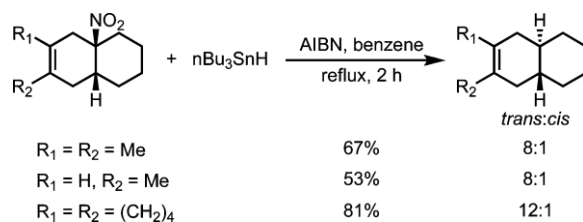
When reactants pass through an initial transition state into a flat area of an energy surface with multiple exit routes to products, reaction dynamics affect the selectivity. The products that

tend to form, arise from a direct continuation of the trajectories that passed through the initial transition state.¹²⁻¹⁴ In such cases, dynamics determine the selectivity in cases involving a bifurcating energy surface. Theoretical studies by Caramella showed that the dimerization of cyclopentadiene involves a bifurcating energy surface, and a transition state that is “bispericyclic”.¹⁵ Singleton has discussed the role of bifurcating energy surfaces in cycloadditions where there are competing [4 + 2] and [2 + 4] pathways.¹⁶ Bifurcating energy surfaces have now been implicated in determining the selectivity of a variety of Diels-Alder reactions.¹⁷⁻²¹

The removal of the activating nitro group was achieved by radical hydrodenitration, using tri-*n*-butyltin hydride and AIBN. The mechanism of this transformation presumably proceeds via trialkyltin radicals forming a Sn-O bond with the nitro group. Fragmentation gives rise to Bu₃SnONO and an (secondary or tertiary) alkyl radical.²² This transformation has been used successfully to reduce the nitro group of Diels-Alder cycloadducts.^{23, 24}

In Danishefsky’s recent work, the *cis*-fused ring junction characteristic of the Diels-Alder cycloaddition was converted to the desired *trans* stereochemistry for the decalins shown in Scheme 4. Radical hydrodenitration of 6,6-bicyclics formed from cycloaddition of nitrocyclohexene yielded the *trans* stereochemistry selectively, although 5,6-bicyclics from the cycloadditions of 1-nitrocyclopentene showed very little selectivity.

Scheme 4. Radical Hydrodenitration of the DA Adduct to Yield *trans*-Fused Decalins



To understand the factors that control the regioselectivity of the cycloaddition and how the *trans*-fused decalin geometry is ultimately furnished from the *cis*-fused cycloadduct, a computational study using density functional theory (DFT) calculations was undertaken.

Computational Methods

All geometry optimizations were performed with Gaussian 09 using the B3LYP density functional with the 6-31G(d) basis set.²⁵ A fine grid density was used for numerical integration. Radical species were optimized with unrestricted (UB3LYP) density functional calculations. We have shown previously that this level of electronic structure theory is capable of providing ground-state and transition-state geometries for organic radicals that agree well with more elaborate calculations, and that the results obtained agree quantitatively with experiment.²⁶ We have also performed single point energy calculations with M06-2X/UM06-2X density functional theory (DFT)²⁷ that are expected to deliver a more accurate treatment of medium-range correlation effects, such as van der Waals interactions. Such calculations give improved thermodynamics for C-C bond forming reactions.²⁸ Energetics were also evaluated with the B2-PLYP double-hybrid density functional,²⁹ again to ensure that our conclusions are robust across different theoretical methods. Single point calculations with a larger 6-311+G(d,p) basis set have been also performed to confirm that the basis-set size does not affect the conclusions drawn. Harmonic vibrational frequencies were computed for all optimized structures to verify that they were either minima (zero imaginary frequencies) or transition states (a single imaginary frequency). Zero-point energies (unscaled) are included in all thermodynamic quantities. The effects of solvation on the reaction energetics were evaluated using a conductor-like polarizable continuum solvation model (CPCM).³⁰ The solute surface was defined by UAKS radii in each case.³¹

Results and Discussion

The cycloaddition between 2,3-dimethyl-1,3-butadiene and 1-nitrocyclohexene was investigated, and transition structures (TSs) for both the Diels-Alder (1-nitrocyclohexene behaving as dienophile) and the hetero-Diels-Alder (1-nitrocyclohexene behaving as heterodiene) reactions were successfully located, as shown in Figure 1. The activation barriers for the competing DA and HDA mechanistic pathways are very similar at all of the levels of theory examined, so both

mechanisms are predicted to be competitive (see Supporting Information for a full comparison of energetics computed with different methods). The HDA TS with an isopropenyl group *endo* to the heterodiene is most favored by 1.1 kcal/mol. With the inclusion of solvation effects, the preference for the HDA TS rises to 1.5 kcal/mol. TSs for the regioisomeric HDA pathway were located (see Supporting Information) but lie around 10 kcal/mol higher in energy than those shown in Figure 1, and so can be discounted as a viable pathway. While the kinetics of DA and HDA pathways are predicted to be very similar, there is a large difference in the thermodynamics of the two processes; the DA adduct is over 18 kcal/mol more stable than the HDA adduct. B3LYP is expected to underestimate the exothermicity of the Diels-Alder reaction, due to a systematic error in computing π - σ energy changes. M06-2X calculated energetics, which are expected to be more accurate, predict that reactions are more exothermic than predicted by B3LYP as is found in other Diels-Alder processes.²⁸ However, the DA adduct is still much preferred over the HDA adduct, now by almost 21 kcal/mol. In experiment, only the DA adduct is observed. This may be explained by the HDA adduct undergoing a cycloreversion back to starting materials, which can undergo an essentially irreversible DA cycloaddition. However, we also located a transition structure corresponding to the [3,3]-sigmatropic rearrangement that provides an alternative pathway for the interconversion. The sigmatropic rearrangement of the HDA adduct is relatively facile in relation to the cycloaddition step, since this [3,3]-TS lies lower in energy than any of the cycloaddition TSs.

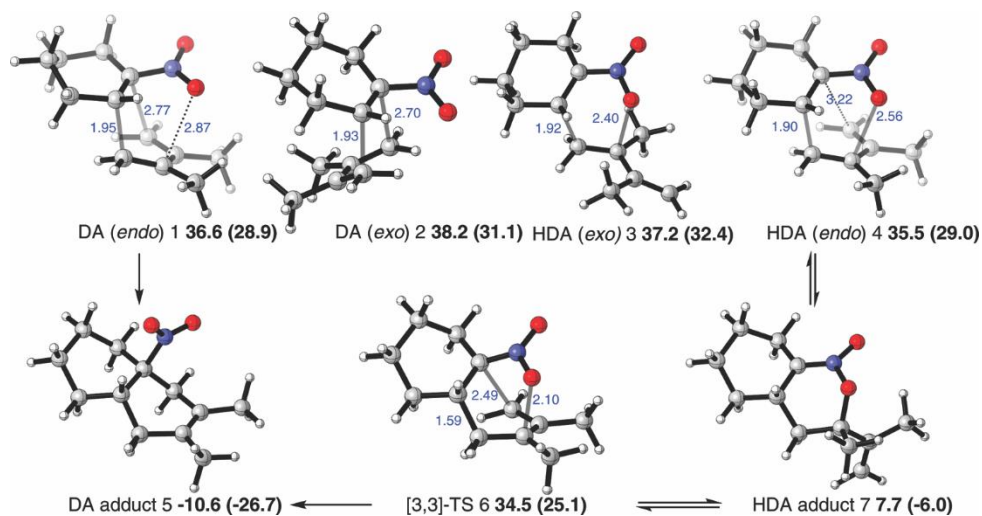


Figure 1. Transition structures and adducts for the cycloaddition of 2,3-dimethyl-1,3-butadiene and 1-nitrocyclohexene. Selected distances shown in Å, B3LYP/6-31G(d) relative free energies, with M06-2X/6-31G(d) in parentheses, shown in kcal/mol.

The geometries of the *endo* DA (1), *endo* HDA (4) and [3,3]-sigmatropic rearrangement (6) transition structures are rather similar, and lie within 2 kcal/mol in energy. The potential energy surface is very flat in the region of these structures. In the *endo* DA transition structure there is a C-O distance of 2.87 Å, which suggests that to some extent this structure can be considered as “bis-pericyclic”,^{9,12} with intermolecular distances reflective of both DA and HDA bond-forming reactions. Intrinsic Reaction Coordinate (IRC) calculations were able to locate the energy minima that connect these transition structures, and no bifurcations were found on the energy surface. However, the relative positions of the cycloaddition and sigmatropic rearrangement transition states may well influence the periselectivity due to the shape of the potential energy surface and corresponding dynamical influences. The key transition structures are summarized in Figure 2.

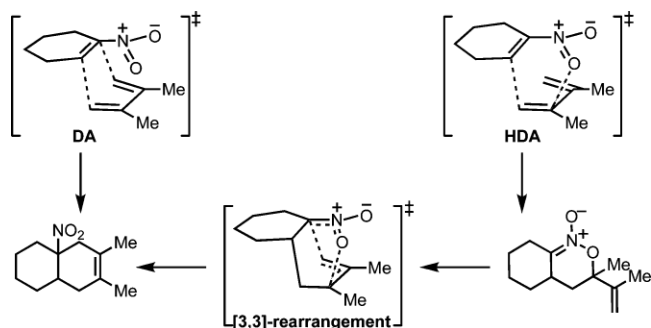


Figure 2. Summary of the low energy transition structures leading to the formation of the DA adduct.

The regioselectivity of an unsymmetrical diene (isoprene) was then investigated. Transition structures were located for the DA and HDA cycloaddition with 1-nitrocyclohexene. The *endo* transition structures are shown in Figure 3. The *exo* structures were located and all lie higher in energy than the corresponding *endo* structures (see Supporting Information). The HDA transition structures are found to be slightly favored kinetically, although thermodynamics favor the DA cycloadducts by over 19 kcal/mol.

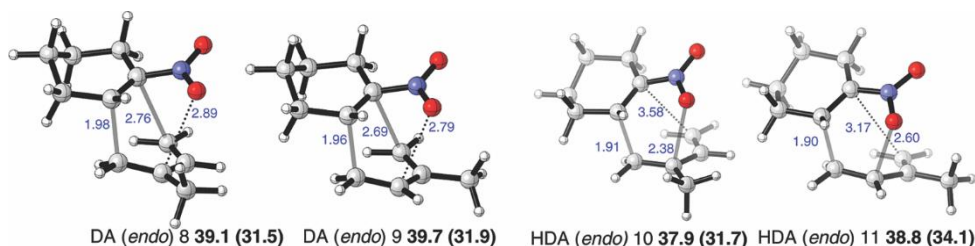


Figure 3. Transition structures for the cycloadditions of isoprene and 1-nitrocyclohexene. Selected distances shown in Å, B3LYP/6-31G(d) relative free energies, with M06-2X/6-31G(d) in parentheses, in kcal/mol.

[3,3]-Sigmatropic rearrangement transition structures were again located. These lie close in energy to the cycloaddition transition structures, as shown in Figure 4. Thus the sigmatropic rearrangement TS again presents an energetically accessible pathway for the HDA to interconvert to the DA adduct. Whereas the DA cycloadducts themselves are essentially isoenergetic, the transition structures leading to the *para*-substituted product are somewhat favored over their *meta*-substituted counterparts (DA: $\Delta\Delta G^\ddagger$ 0.6 kcal/mol, HDA: $\Delta\Delta G^\ddagger$ 0.9 kcal/mol, sigmatropic:

$\Delta\Delta G^\ddagger$ 1.6 kcal/mol). Experimentally, the reaction of isoprene and 1-nitrocyclohexene is unselective when performed in toluene, but in 2,2,2-trifluoroethanol the *para*-substituted product dominates in a 15:1 ratio. Computed relative free energies of the regioisomeric pathways performed with implicit solvation reproduce this trend, as the $\Delta\Delta G^\ddagger$ of DA and HAD pathways increase to 1.4 and 1.6 kcal/mol in favor of the *para*-substituted product. The M06-2X calculations predict that both direct DA and hetero-DA/sigmatropic rearrangement pathways are competitive, both forming the *para*-product.

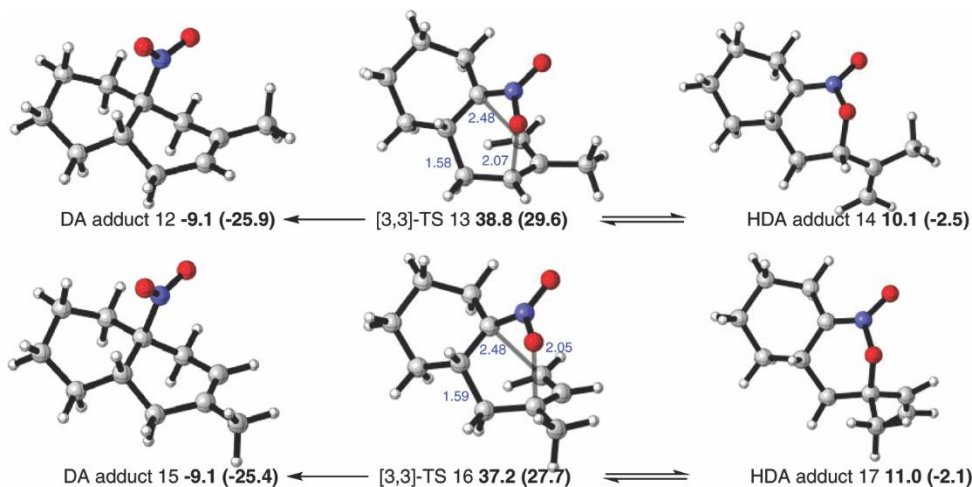


Figure 4. [3,3]-Sigmatropic rearrangement transition structures in the cycloaddition of isoprene and 1-nitrocyclohexene. Selected distances shown in Å, B3LYP/6-31G(d) relative free energies, with M06-2X/6-31G(d) in parentheses, in kcal/mol.

Experimentally, the use of a hydroxylic solvent resulted in improved cycloaddition yields. A substantial increase in yield was observed with 2,2,2-trifluoroethanol as solvent, particularly under microwave conditions. The effects of solvation were evaluated computationally with an implicit continuum model and also using explicit molecules of 2,2,2-trifluoroethanol, as shown in Figure 5. The inclusion of a hydrogen-bonded 2,2,2-trifluoroethanol molecule led to smaller activation barriers for HDA and sigmatropic rearrangement transition structures (we were unable to locate the DA transition structure), by around 4 kcal/mol. The thermodynamics of the Diels-Alder adduct and hetero-Diels-Alder adduct formation are changed only marginally by the

inclusion of solvent. Therefore the effects of an alcoholic solvent are to enhance reaction rates for all pathways. Energetics computed with an implicit solvent model led to the same conclusions, with the barrier heights in close quantitative agreement with those with an explicit molecule of alcohol. The origins of this rate enhancement are due to the partial charge separation in the DA and HDA transition structures: the charges on the 1-nitrocyclohexene moiety are -0.18 and -0.40 in the DA and HDA structures, respectively. Specific hydrogen bonding interactions with the nitro group are strengthened, as the computed Mulliken charge on each of the two oxygen atoms increases from -0.40 in the reactant to -0.45 and -0.47 in the DA and HDA transition structures, respectively.

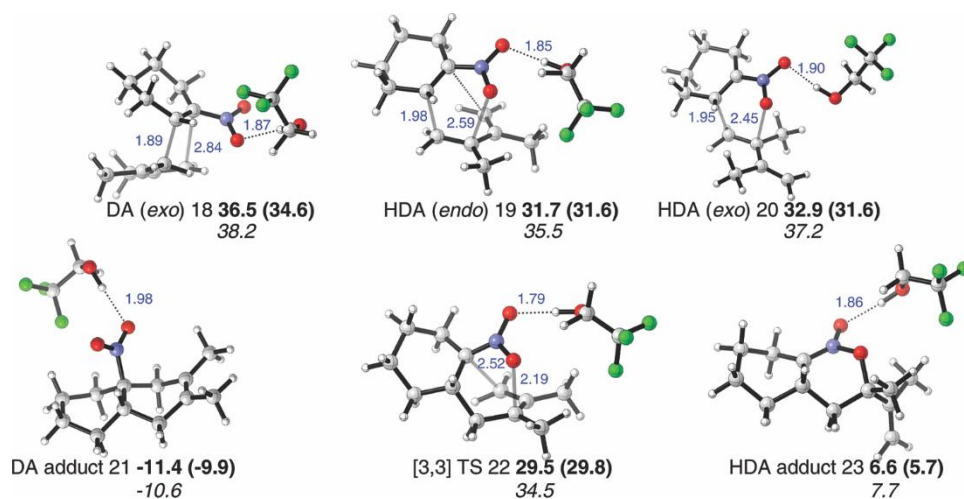


Figure 5. Solvent effects on the energetics of the cycloadditions of 1,3-butadiene and 1-nitrocyclohexene. Selected distances shown in Å, B3LYP/6-31G(d) relative free energies in kcal/mol, compared with implicit CPCM values in parentheses and gas-phase values in italics.

Conversion of Diels-Alder Adducts of 1-Nitrocyclohexene to the Formal *trans*

Diels-Alder Adducts of Cyclohexene.

Reductive hydrodenitration using tri-*n*-butyltin hydride in the presence of AIBN resulted in the formation of the denitrated *trans*-fused dehydrodecalin.¹ In the cycloaddition of 1-nitrocyclohexene to a range of dienes (2,3-dimethyl-1,3-butadiene, isoprene, 1,2-dimethylenecyclohexane and 2,3-diphenyl-1,3-butadiene) the initial *cis*-fused Diels-Alder

stereochemistry can be converted to a *trans*-fused dehydrodecalin with 7-12:1 diastereoselectivity.¹

We studied the stability and the interconversion of the tertiary carbon radicals formed in the radical denitration mechanism, and the irreversible hydrogen radical transfer from a trialkyltin hydride. The results are shown in Figure 6. Computations performed on the radical intermediates for the 2,3-dimethyl-1,3-butadiene/1-nitrocyclohexene Diels-Alder cycloadduct show that the observed *trans* selectivity in the hydrodenitration is a consequence of the greater thermodynamic stability of the *trans*-fused bridgehead radical over the *cis* form. The tertiary radicals are appreciably pyramidal, but the interconversion via a planar transition state is calculated to be energetically feasible, and is able to occur much faster than the radical trapping with a trialkyltin hydride. Transition structures were located for hydrogen transfer from trimethyltin hydride to form *trans*- and *cis*-dehydrodecalins. Both transition structures have large distances between carbon and tin, and so the TS relative energies simply reflect the stability of each of the radical geometries. Whereas the *cis*-radical lies 2.6 kcal/mol above the *trans*-radical, the transition states differ in energy by 2.5 kcal/mol. The greater stability of the *trans*-radical and transition state is due to the absence of any axial substituents in the latter. The products of hydrogen abstraction differ by 3.2 kcal/mol, due to the same repulsive interactions in the *cis*-product. The same energetic trends are manifested in the UM06-2X energetics, with the *trans*-radical, TS and product favored over the corresponding *cis*-pathway by 1.4, 2.8, and 2.3 kcal/mol. By way of comparison, *trans*-decalin (decahydronaphthalene) is favored over its *cis*-stereoisomer by 2.5-3.1 kcal/mol. The dehydrodecalin cycloadducts lack a 1,3-steric interaction in the *cis*-isomer that is present for decalin, so the expected energy difference between *cis* and *trans* forms of dehydrodecalin is expected to be smaller than 2.5 kcal/mol. Calculated free energy differences between *cis* and *trans* pathways for the hydrodenitration of 1,2-diphenyl dehydrodecalin and 1-methyl

dehydrodecalin are also in accord with the *trans*-selectivity of these systems (see Supporting Information).

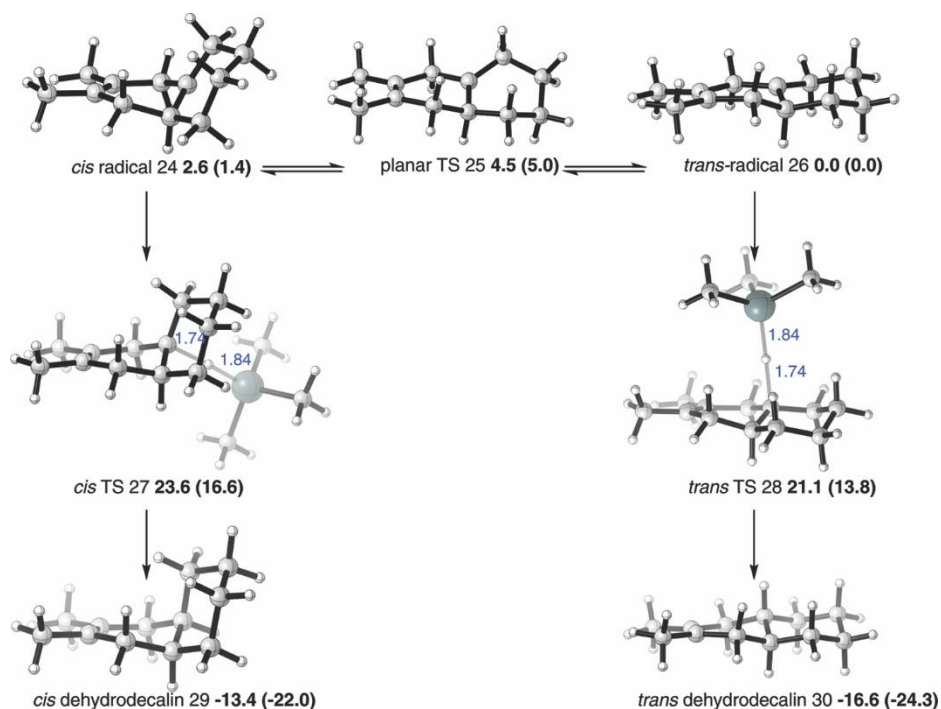


Figure 6. Bicyclic radicals and connecting transition structure, and hydrogen transfer TSs and dehydrodecalin products in the cycloaddition of 2,3-dimethyl-1,3-butadiene and 1-nitrocyclohexene. Selected distances shown in Å, UB3LYP/LANL2DZ relative free energies, UM06-2X/LANL2DZ in parentheses, in kcal/mol.

The origins of the poor *trans*-selectivity in the hydrogenation step when 1-nitrocyclopentene was used experimentally were also investigated, as shown in Figure 7. Unlike the 6,6-bicyclic radical in Figure 6, the 5,6-bicyclic adduct formed from the cycloaddition of 1-nitrocyclopentene is unable to adopt distinct *cis* and *trans* radical conformers after denitration. Therefore just a single radical conformer, planar about the radical carbon atom, results and this may react with trialkyltin hydride from either face. The UB3LYP relative free energies of the resulting two transition structures suggest these two pathways are isoenergetic, which is in accord with the low stereoselectivity of this process.

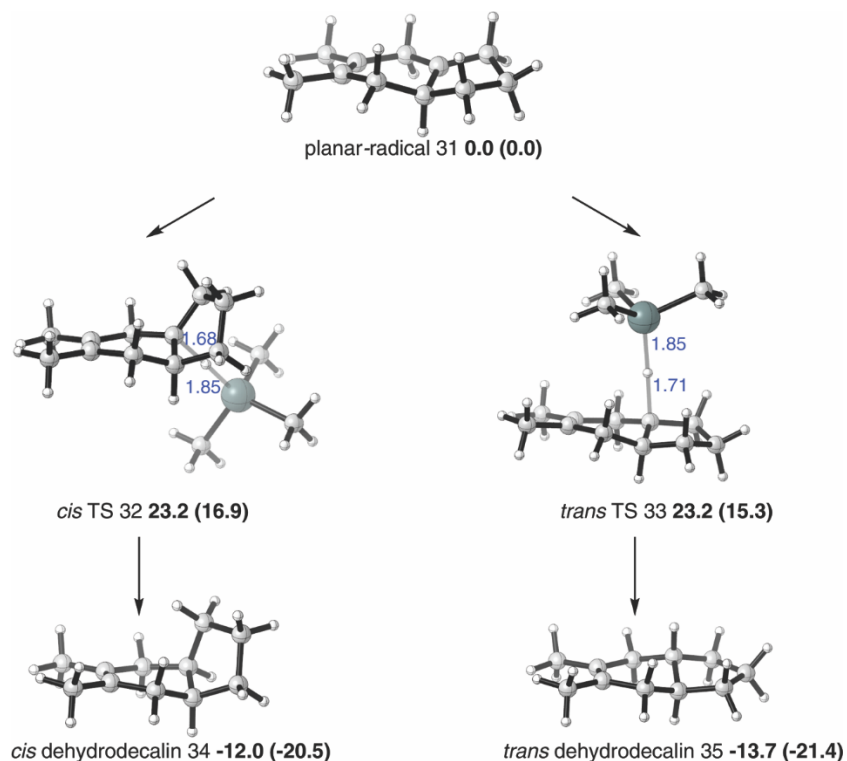


Figure 7. 6,5-Bicyclic radicals and connecting transition structure, and hydrogen transfer TSs and bicyclic products in the cycloaddition of 2,3-dimethyl-1,3-butadiene and 1-nitrocyclopentene. Selected distances shown in Å, UB3LYP/LANL2DZ relative free energies, UM06-2X/LANL2DZ in parentheses, in kcal/mol.

Conclusions

The origins of regioselectivity and stereoselectivity in the *trans*-selective Diels-Alder/hydrodenitration sequence developed by Danishefsky have been determined with density functional calculations. In the cycloaddition between 1-nitro-cyclohexene and a series of butadienes, the Diels-Alder adduct results from the Diels-Alder pathway but also by a hetero-Diels-Alder cycloaddition and subsequent [3,3]-sigmatropic rearrangement. The selectivity of the radical hydrodenitration step of 6,6-bicyclic adducts arises from the greater stability of the *trans*-decalyl radical intermediate and subsequent transition state involving hydrogen atom transfer.

Acknowledgment. This work was supported by NIH-GM36700 (K.N.H.), the Fulbright Commission, AstraZeneca and the Royal Commission for the Exhibition of 1851 (R.S.P).

Computer time was provided in part by the UCLA Institute for Digital Research and Education (IDRE).

Supporting Information Available: Absolute energies, Cartesian coordinates, imaginary frequencies, and full authorship of ref 25. This material is available free of charge via the Internet at <http://pubs.acs.org>.

References

- (1) Kim, W. H.; Lee, J. H.; Danishefsky, S. J. *J. Am. Chem. Soc.* **2009**, *131*, 12576–12578.
- (2) Denmark, S. E.; Thorarensen, A. *Chem. Rev.* **1996**, *96*, 137–165.
- (3) Denmark, S. E.; Kesler, B. S.; Moon, Y.-C. *J. Org. Chem.* **1992**, *57*, 4912–4924.
- (4) (a) Denmark, S. E.; Cramer, C. J.; Sternberg, J. A. *Helv. Chim. Acta* **1986**, *69*, 1971–1989. (b) Denmark, S. E.; Cramer, C. J.; Sternberg, J. A. *Tetrahedron Lett.* **1986**, *27*, 3693–3696.
- (5) Denmark, S. E.; Moon, Y.-C.; Senanayake, C. B. W. *J. Am. Chem. Soc.* **1990**, *112*, 311–315.
- (6) Denmark, S. E.; Moon, Y.-C.; Cramer, C. J.; Dappen, M. S.; Senanayake, C. B. W. *Tetrahedron* **1990**, *46*, 7373–7392.
- (7) Denmark, S. E.; Dappen, M. S.; Cramer, C. J. *J. Am. Chem. Soc.* **1986**, *108*, 1306–1307.
- (8) Denmark, S. E.; Stolle, A.; Dixon, J. A.; Guagnano, V. *J. Am. Chem. Soc.* **1995**, *117*, 2100–2101.
- (9) Celebi-Olcum, N.; Ess, D. H.; Aviyente, V.; Houk, K. N. *J. Org. Chem.* **2008**, *73*, 7472–7480.
- (10) Wade, P. A.; Murray, Jr., J. K.; Shah-Patel, S.; Le, H. T. *Chem Commun.* **2002**, 1090–1091.
- (11) Gomez, M. V.; Aranda, A. I.; Moreno, A.; Cossio, F. P.; de Cozar, A.; Diaz-Ortiz, A.; de la Hoz, A.; Prieto, P. *Tetrahedron* **2009**, *65*, 5328–5336.
- (12) Doubleday, C.; Nendel, M.; Houk, K. N.; Thweatt, D.; Page, M. *J. Am. Chem. Soc.* **1999**, *121*, 4720–4721.
- (13) Doubleday, C.; Suhrada, C. P.; Houk, K. N. *J. Am. Chem. Soc.* **2006**, *128*, 90–94.
- (14) Kless, A.; Nendel, M.; Wilsey, S.; Houk, K. N. *J. Am. Chem. Soc.* **1999**, *121*, 4524–4525.
- (15) (a) Toma, L.; Romano, S.; Quadrelli, P.; Caramella, P. *Tetrahedron Lett.* **2001**, *42*, 5077–5080. (b) Caramella, P.; Quadrelli, P.; Toma, L. *J. Am. Chem. Soc.* **2002**, *124*, 1130–1131. (c) Quadrelli, P.; Romano, S.; Toma, L.; Caramella, P. *Tetrahedron Lett.* **2002**, *43*, 8785–8789. (d) Quadrelli, P.; Romano, S.; Toma, L.; Caramella, P. *J. Org. Chem.* **2003**, *68*, 6035–6038.

- (16) Singleton, D. A.; Hang, C.; Szymanski, M. J.; Meyer, M. P.; Leach, A. G.; Kuwata, K. T.; Chen, J. S.; Greer, A.; Foote, C. S.; Houk, K. N. *J. Am. Chem. Soc.* **2003**, *125*, 1319–1328.
- (17) Ess, D. H.; Wheeler, S. E.; Iafe, R. G.; Xu, L.; Celebi-Olcum, N.; Houk, K. N. *Angew. Chem., Int. Ed.* **2008**, *47*, 7592–7601.
- (18) Celebi-Olcum, N.; Ess, D. H.; Aviyente, V.; Houk, K. N. *J. Am. Chem. Soc.* **2007**, *129*, 4528–4529.
- (19) Beno, B. R.; Houk, K. N.; Singleton, D. A. *J. Am. Chem. Soc.* **1996**, *118*, 9984–9985.
- (20) Khuong, K. S.; Jones, W. H.; Pryor, W. A.; Houk, K. N. *J. Am. Chem. Soc.* **2005**, *127*, 1265–1277.
- (21) Hayden, A. E.; DeChancie, J.; George, A. H.; Dai, M.; Yu, M.; Danishefsky, S. J.; Houk, K. N. *J. Org. Chem.* **2009**, *74*, 6770–6776.
- (22) Yoshikawa, M.; Okaichi, Y.; Cha, B. C.; Kitagawa, I. *Tetrahedron* **1990**, *46*, 7459–7470.
- (23) (a) Ono, N.; Miyake, H.; Kaji, A. *J. Chem. Soc., Chem. Commun.* **1982**, 33–34. (b) Ono, N.; Miyake, H.; Kaji, A. *J. Chem. Soc., Perkin Trans. 1* **1987**, 1929–1935.
- (24) Guy, A.; Serva, L. *Synlett* **1994**, 647–648.
- (25) Frisch, M. J.; et al. Gaussian 09, revision A.02; Gaussian, Inc.: Wallingford, CT, **2009**.
- (26) (a) Hayden, A. E.; Paton, R. S.; Becker, J.; Lim, Y. H.; Nicolaou, K. C.; Houk, K. N. *J. Org. Chem.* **2010**, *75*, 922–928. (b) Spellmeyer, D. C.; Houk, K. N. *J. Org. Chem.* **1987**, *52*, 959–974. (c) Montgomery, J. A., Jr.; Frisch, M. J.; Ochterski, J. W.; Peterson, G. A. *J. Chem. Phys.* **1999**, *110*, 2822–2827. (d) Luft, J. A. R.; Winkler, T.; Kessabi, F. M.; Houk, K. N. *J. Org. Chem.* **2008**, *73*, 8175–8181. (e) Leach, A. G.; Wang, R.; Wohlhieter, G. E.; Khan, S. I.; Jung, M. E.; Houk, K. N. *J. Am. Chem. Soc.* **2003**, *125*, 4271–4278.
- (27) Zhao, Y.; Truhlar, D. G. *Theor. Chem. Acc.* **2008**, *120*, 215–241.
- (28) Pieniazek, S. N.; Clemente, F. R.; Houk, K. N. *Angew. Chem., Int. Ed.* **2008**, *47*, 7746–7749.
- (29) Grimme, S. *J. Chem. Phys.* **2006**, *124*, 034108.
- (30) (a) Barone, V.; Cossi, M. *J. Phys. Chem. A* **1998**, *102*, 1995–2001. (b) Cossi, M.; Rega, N.; Scalmani, G.; Barone, V. *J. Comput. Chem.* **2003**, *24*, 669–681.
- (31) Takano, Y.; Houk, K. N. *J. Chem. Theory Comput.* **2005**, *1*, 70–77.

2. Reactivity of Biarylazacyclooctynones in Copper-Free Click Chemistry

Introduction

Since its initial introduction as a bioorthogonal reaction, the strain promoted 1,3-dipolar cycloaddition between cyclooctynes and azides (Figure 8a) has been utilized in a range of biological studies.¹ The reaction was developed in response to the dearth of tools available for the study of biomolecules in their native environments, and was designed to proceed rapidly and selectively *in vivo* without perturbing native biochemical functionality. Due to the strain activation inherent to cyclooctynes,² the reaction proceeds at a rate that is sufficient for *in vivo* labeling while avoiding the use of the toxic copper(I) catalysts traditionally employed in “click chemistry” with terminal alkynes.^{3,4} As a result, the reaction between cyclooctynes and azides is often referred to as “copper-free click chemistry.”

In an effort to further enhance the utility of the strain-promoted reaction, several groups have contributed to a series of structurally varied cyclooctyne scaffolds that display differential reactivities towards the azide. A selection of these compounds is shown in Figures 8b–d. All were designed based on the assumption that one can alter the reactivity of a cyclooctyne through modulation either of strain or electronics. Cyclooctyne **1** (also called “Oct”, Figure 8b), the first cyclooctyne developed specifically as a bioorthogonal reagent, displays a second-order rate constant of $2.4 \times 10^{-3} \text{ M}^{-1} \text{ s}^{-1}$ for the reaction with benzyl azide.^{5,6} It was later shown that this rate can be enhanced through installation of fluorine atoms at the propargylic position. Monofluorinated cyclooctyne (MOFO, **2**) displays a second-order rate constant of $4.3 \times 10^{-3} \text{ M}^{-1} \text{ s}^{-1}$, whereas difluorinated cyclooctyne (DIFO, **3**) reacts with a rate constant of $7.6 \times 10^{-2} \text{ M}^{-1} \text{ s}^{-1}$ (1.8-fold and 32-fold faster than Oct, respectively).^{3a,6} The rate enhancing effects of strain were subsequently demonstrated in the context of dibenzocyclooctyne (DIBO, **4**),^{7a,b} dibenzoazacyclooctyne (DIBAC, **5**),^{7c} and biarylazacyclooctynone (BARAC, **6**),^{7d} which react with azides 24-fold to 375-fold faster than is observed for Oct (Figure 8d).

The intention implicit in the design of compounds **4–6** was to increase strain by adding sp^2 centers to the cyclooctyne ring. However, there may be more subtle consequences of these compounds' structural modifications that actually oppose the desired reactivity outcome. For example, while aryl ring fusion may enhance strain, the “flagpole” hydrogen atoms *ortho* to the aryl/cyclooctyne ring junction were predicted by Goddard and coworkers to decrease reactivity by steric interference with the azide in the transition state.^{8a} The experimentally observed reactivity of biaryl cyclooctynes likely reflects a balance of these rate enhancing and diminishing effects. This example underscores the difficulty inherent to rational design of new cyclooctynes with tailored kinetic properties. Many structural perturbations affect more than one contributor to reactivity, e.g., strain, sterics and electronics. Without a better understanding of their relative influence on the transition state activation energies, these parameters cannot be readily optimized to achieve a desired outcome. In principle, one might derive a set of rules that link structure and

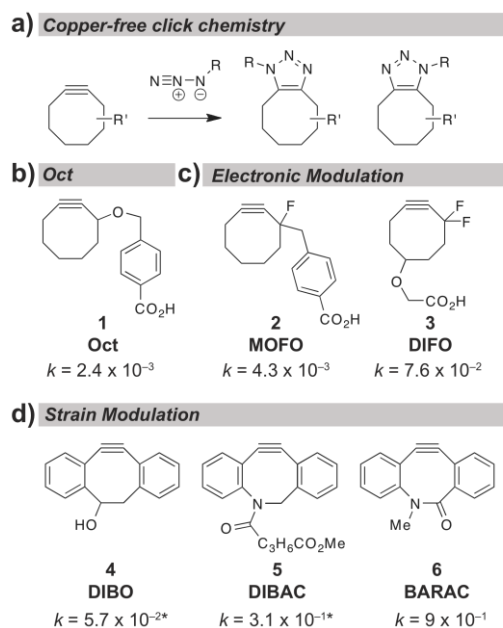


Figure 8. Reagent development for copper-free click chemistry. **a.** The 1,3-dipolar cycloaddition between azides and cyclooctynes. **b.** Oct, the first cyclooctyne developed as a bioorthogonal reagent, and its corresponding second-order rate constant for the reaction with benzyl az-

ide.^{5,6} The reactivity of a cyclooctyne can be altered through **c.** electronic^{6,3a} and **d.** strain modulation.⁷ All rate constants are second order ($M^{-1}s^{-1}$), and were measured at room temperature in CD_3CN except for values noted with an asterisk (*), which were measured in CD_3OD .

reactivity based solely on empirical data. But, cyclooctynes are generally challenging synthetic targets that do not lend themselves to extensive analoging.

In previous work, density functional theory (DFT) models have been employed to analyze reactions of cyclooctynes with azides and have proven to be useful predictors of relative transition state activation energies.⁸ Here we performed a systematic analysis of the effects of strain and electronics on the reactivity of cyclooctynes with azides, using both empirical data and a DFT-based distortion/interaction transition state model.^{8b-c} We focused our analysis on a series of differentially substituted BARAC analogs, comparing their second-order rate constants in the cycloaddition reaction with benzyl azide to those predicted by DFT calculations. We also investigated the relationship between alkyne bond angles and reactivity, and determined the conformation of BARAC's central lactam, which has significant energetic consequences. The results herein provide a framework for understanding and predicting cycloaddition kinetics.

Distortion/Interaction Model

The distortion/interaction model deconstructs the activation energy of a reaction into two components: the distortion energy, which is dependent on ground state strain, and the interaction energy, which is governed by transition state electronics.^{8b-c} In this model, the transition state energy (ΔE^\ddagger) of a reaction is defined as the sum of distortion energy (ΔE^\ddagger_d), the energy required to distort the alkyne and azide into their preferred transition state conformations, and interaction energy (ΔE^\ddagger_i), the energy lowering upon favorable orbital overlap between the azide and the alkyne ($\Delta E^\ddagger = \Delta E^\ddagger_d + \Delta E^\ddagger_i$). Thus, the activation energy of a reaction can be altered by changing either the distortion energy or the interaction energy required to reach the transition state.

In the case of the 1,3-dipolar cycloaddition of 2-butyne with methyl azide (Figure 9a), our calculations indicate that 29.9 kcal/mol energy is required to distort the ground state substrates into their preferred transition state conformations. Upon distortion, the alkyne and azide interact, lowering the energy of the overall system by -9.0 kcal/mol through a favorable orbital overlap that can only be achieved via the geometry of the distorted state. Combining the effects of distortion and interaction, we calculate an overall transition state activation energy of 20.9 kcal/mol ($\Delta E^\ddagger = \Delta E^\ddagger_d + \Delta E^\ddagger_i$). In reality, distortion and interaction are not independent processes, but instead occur simultaneously to bring reactants directly to their transition state geometries. However, this model breaks up activation energy into two imaginary distortion and interaction processes to allow a more detailed analysis of reaction strain and electronics.

An example of how electronic perturbation can affect interaction and distortion energies is illustrated by comparing the above reaction coordinate to that for the reaction of 1,1,1,4,4,4-hexafluoro-2-butyne with methyl azide (Figure 9b). In this case, the interaction energy is more negative than that calculated for 2-butyne ($\Delta E^\ddagger_{i,\text{hexafluoroalkyne}} = -12.2$ kcal/mol versus $\Delta E^\ddagger_{i,2\text{-butyne}} = -9.0$ kcal/mol). This change results from electronic perturbation of the alkyne LUMO energy via mixing of the alkyne π -system with $\sigma^*_{\text{C-F}}$. Alabugin and co-workers have shown that the observed acceleration results from hyperconjugative stabilization of the cycloaddition transition state via electron donation from the in-plane alkyne π -orbital to the $\sigma^*_{\text{C-F}}$ orbital.⁹

As both 1,1,1,4,4,4-hexafluoro-2-butyne and 2-butyne are relatively unstrained molecules, we would expect their distortion energies to be similar for the reaction with methyl azide. However, calculations indicate a larger total distortion energy for the reaction of 2-butyne by 5.3 kcal/mol ($\Delta E^\ddagger_{d,\text{total},2\text{-butyne}} = 29.9$ kcal/mol and $\Delta E^\ddagger_{d,\text{total},\text{hexafluoroalkyne}} = 24.6$ kcal/mol). The data in Figures 9a and b indicate that this difference results both from a change in alkyne transition state distortion energy upon perfluorination as well as from a decrease in azide distortion energy. That both the

alkyne and azide undergo shifts in distortion energy in the perfluorinated case indicates that the transition state occurs at an earlier point on the reaction coordinate. Calculated azide bond angles provide further evidence for an early transition state upon perfluorination. Whereas the azide is bent to 137° in the transition state of the 2-butyne reaction, it is only bent to 143° in the transition state of the perfluorinated-alkyne reaction (Figure 9). Thus, the effect of propargylic fluorination is two-fold when considering the distortion/interaction model; the fluorine atoms enhance transition state interaction energies, which facilitates an early transition state where less distortion is required for both reactants.

The effects of distortion energy modulation in the context of the cyclooctyne have previously been discussed^{8b,c} and are summarized in Figure 9c. The alkyne bond angles in

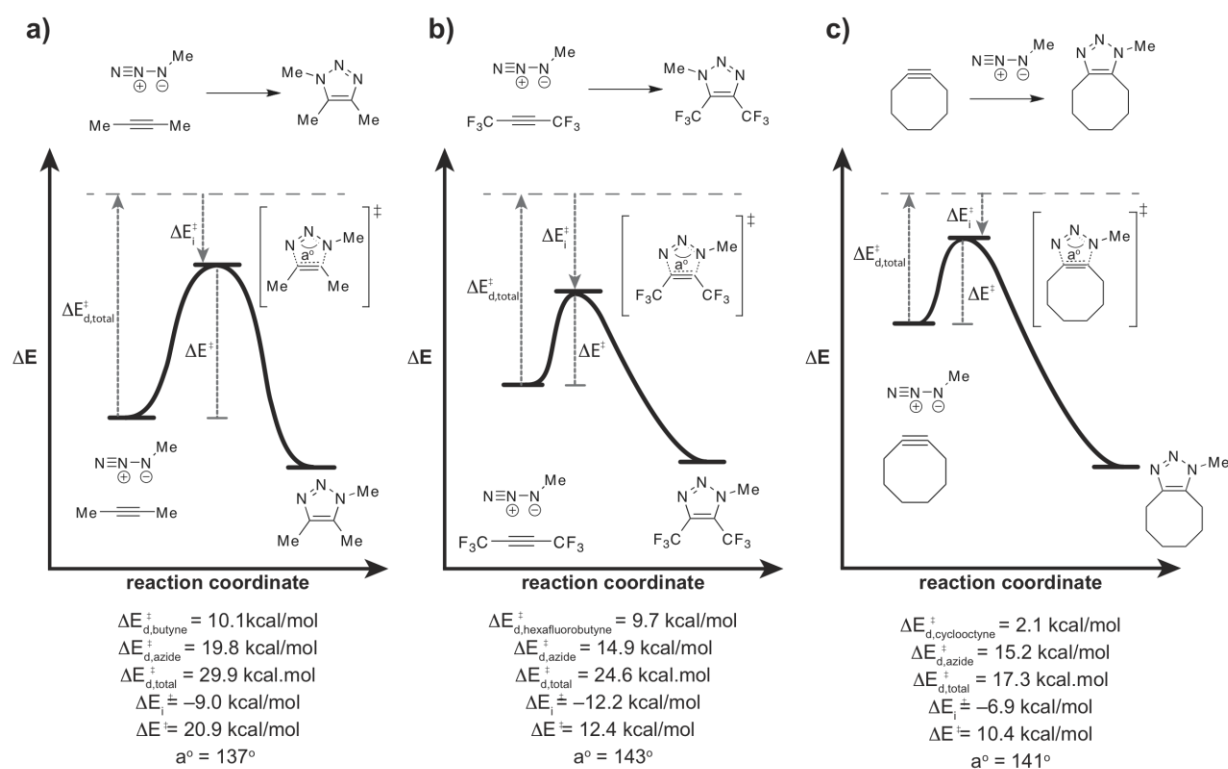


Figure 9. The distortion/interaction model. a. The activation energy (ΔE^{\ddagger}) for the reaction between 2-butyne and methyl azide is the sum of distortion energy (ΔE_d^{\ddagger}) and interaction energy (ΔE_i^{\ddagger}). **b.** Perfluorination of the alkyne reduces ΔE^{\ddagger} of the reaction by increasing the magnitude of stabilizing interactions in the transition state and decreasing distortion energy. **c.** Constraining

the alkyne into an eight membered ring reduces ΔE^\ddagger by decreasing the distortion energy required to bend the starting materials into their preferred transition state conformations. For a–c, calculated values are electronic energies, the potential energy of the molecule on a vibrationless potential energy surface. As all reactions are represented on separate energy diagrams, the depictions are only intended to facilitate comparisons of ΔE^\ddagger , ΔE^\ddagger_a , and ΔE^\ddagger_i values and not the overall energies of starting materials or triazole products. Calculations were performed using B3LYP/6-31G(d).

cyclooctyne are bent from linearity and the molecule is therefore destabilized relative to a linear isomer. Because it is already distorted towards the transition state geometry, the cyclooctyne requires less distortion energy to reach its preferred transition state geometry than does a linear alkyne ($\Delta E^\ddagger_{d,2\text{-butyne}} = 10.1$ kcal/mol and $\Delta E^\ddagger_{d,\text{cyclooctyne}} = 2.1$ kcal/mol). In addition, calculations show that the distortion energy of methyl azide is lower for the reaction with cyclooctyne than it is for the reaction with 2-butyne. We again attribute this difference to the position of the transition state along the reaction coordinate – here, ground state destabilization of the strained cyclooctyne generates an early transition state, thereby reducing the distortion required for the azide to reach its transition state geometry. This shift in the position of the transition state in response to the greater exothermicity of the strained alkyne reaction is also consistent with the Hammond Postulate. As a result of this significant reduction in distortion energy, cyclooctyne displays a lower overall activation energy for the cycloaddition reaction than does 2-butyne. In this way, strain (i.e., distortion) promotes the cycloaddition.

Because this model is capable of distinguishing the effects of strain and electronics on transition state energies, we chose to apply it to the study of cyclooctyne reactivity. We began by preparing a series of substituted BARAC analogs and analyzing their reactivities experimentally and computationally.

Reactivity of BARAC and analogs

The modular nature of BARAC's synthesis^{7d} rendered this scaffold amenable to derivatization with aryl ring substituents. Previous analyses of the difluorinated cyclooctyne DIFO

(**3**, Figure 8c) suggested that addition of fluorine atoms at the propargylic position enhances reaction rates by increasing interaction energies and decreasing distortion energies in the transition state.^{8b,c} We were curious as to whether comparable interaction energy changes might be affected through installation of fluorine atoms on BARAC's aryl rings, and, alternatively, whether electron donating methoxy groups would affect reaction kinetics in an opposite manner. As well, we sought to analyze the steric effects of flagpole methyl substituents on the rate of the reaction. Accordingly, compounds **7–16** (Figure. 10a) were selected as the targets for our study. Compounds **7–10** possess a single fluorine atom variously positioned around BARAC's two aryl rings. Compound **11** is doubly fluorinated. On the other end of the spectrum, compounds **12** and **13** have single methoxy groups on the aryl rings. Compound **14** is monofluorinated at the flagpole

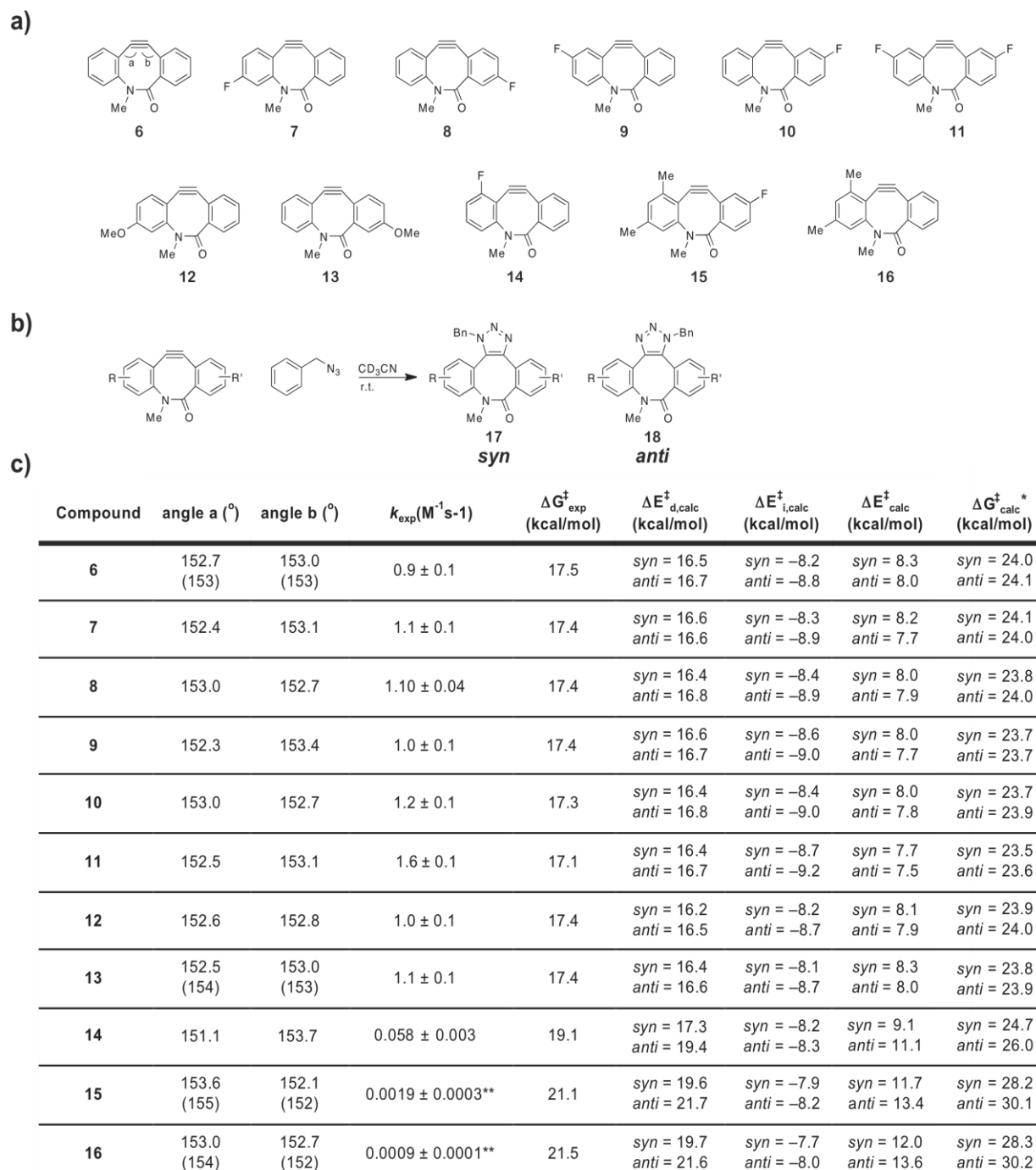


Figure 10. Bond angles and reactivities of BARAC analogs. **a.** BARAC analogs targeted for our initial study of distortion/interaction modulation. **b.** Reactivity was probed empirically by measuring the second-order rate constant for the reaction of each analog with benzyl azide in CD_3CN at rt by ^1H NMR spectroscopy. **c.** Table shows both calculated and measured (X-ray crystallography data shown in parentheses) alkyne bond angles for compounds **6–16** as well as

measured second-order rate constants and activation free energies ($\Delta G^{\ddagger}_{\text{exp}}$) for the model reaction with benzyl azide. Also shown are calculated interaction ($\Delta E^{\ddagger}_{\text{i,calc}}$) and total distortion energies ($\Delta E^{\ddagger}_{\text{d,calc}} = \Delta E^{\ddagger}_{\text{d,calc, azide}} + \Delta E^{\ddagger}_{\text{d,calc, alkyne}}$) as well as overall electronic energies of activation ($\Delta E^{\ddagger}_{\text{calc}}$) and free energies of activation ($\Delta G^{\ddagger}_{\text{calc}}$) for the reaction of each analog with methyl azide. All computational data provided for compounds **6–16** are for the *trans*-BARAC isomer.

*Free energies were calculated for the reaction in acetonitrile. **The second-order rate constants shown for **15** and **16** were measured in CDCl_3 due to the limited solubility of **15** in CD_3CN .

position, potentially generating steric hindrance in the transition state. Finally, compounds **15** and **16** possess methyl substituents at the flagpole position. These compounds were synthesized according to the route published by Jewett *et al.*^{7d} Details are provided in the supporting information.

As a platform for computational studies, we first analyzed the bond angles and conformation of the parent compound BARAC using X-ray crystallography and DFT calculations.

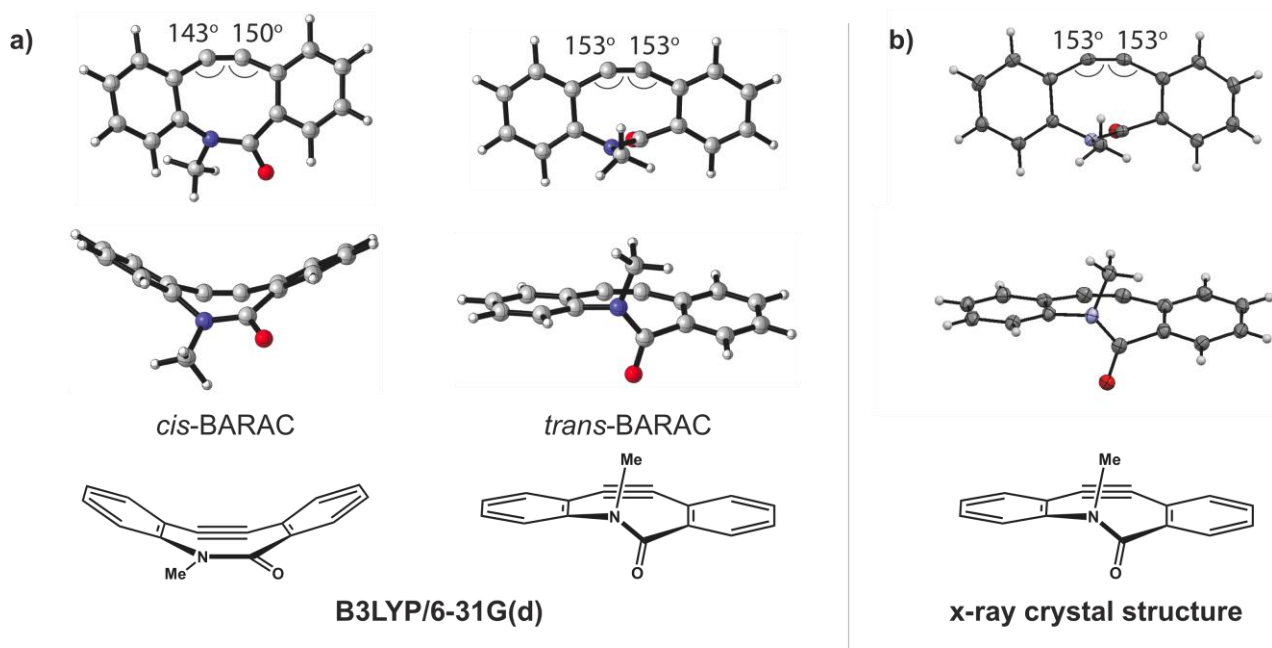


Figure 11. Structural analysis of BARAC. a. DFT calculations (B3LYP/6-31G(d)) of *cis* and *trans* BARAC. b. Front and side view of BARAC obtained via X-ray crystallography. Crystalline BARAC exists as the *trans* conformer.

Figure 11a shows DFT geometry optimizations performed with B3LYP and the 6-31G(d) basis set. The results indicate that the *trans* conformation of the central amide bond is preferred to the *cis* conformation by $\Delta\Delta G_{\text{solv}} = 9.4$ kcal/mol in acetonitrile. X-ray data support this model, indicating that in crystal form, BARAC preferentially occupies the *trans* conformation (Figure 11b).

Interestingly, DFT calculations show that the conformation of the amide functionality dramatically influences BARAC's alkyne bond angles. As shown in Figure 11a, both alkyne angles in *trans*-BARAC are 153° , whereas in *cis*-BARAC the angles are compressed to 143° and 150° . These results suggest that *cis*-BARAC is higher in energy than *trans*-BARAC due to increased alkyne distortion, and also imply that *cis*-BARAC would display enhanced reactivity relative to *trans*-BARAC in the cycloaddition reaction with azides. DFT calculations of free energies of activation in acetonitrile ($\Delta G_{\text{solv}}^\ddagger$) for this reaction support our hypothesis. *Trans*-BARAC has a $\Delta G_{\text{solv}}^\ddagger$ of 24.0 kcal/mol whereas *cis*-BARAC has a $\Delta G_{\text{solv}}^\ddagger$ of 18.0 kcal/mol.

We performed energy optimization calculations on substituted BARAC analogs **7–16** as well, and the results also indicated that the *trans* conformation is preferred to the *cis* conformation by $\Delta\Delta G_{\text{solv}} = 9.1\text{--}9.7$ kcal/mol (Supporting Information). We then calculated $\Delta G_{\text{solv}}^\ddagger$ values for the reactions of compounds **7–16** with methyl azide, and results indicate that for compounds **7–13**, reaction of the *trans* conformer is a lower energy process by 3.0–4.5 kcal/mol than is isomerization to the *cis* conformer followed by reaction to form the triazole. These results suggest that compounds **7–13** react predominantly as the *trans* conformer. Thus, we focus the remainder of the calculations in this section on *trans*-BARAC. As discussed later, $\Delta G_{\text{solv}}^\ddagger$ for reaction of the *cis*- and *trans*- conformers are similar in energy for compounds **14–16**, suggesting a Curtin-Hammett controlled reaction.

The table shown in Figure 10c shows the results of DFT calculations of alkyne bond angles as well as empirical bond angle measurements obtained by X-ray crystallography (shown in

parentheses) for select compounds in the *trans* conformation. We conclude from these data that aryl substitution does not impose significant structural changes, as all compounds exhibit alkyne bond angles close to 153°.

We next measured the second-order rate constants of the reactions of **6–16** with benzyl azide (Figure. 10b). Compounds **7–10** and **12–13** exhibited rate constants between 0.9 and 1.2 M⁻¹ s⁻¹, with differences that do not lie outside the range of experimental error.^{10, 11} Compound **11**, however, showed a roughly 75% increase in reactivity relative to **6** ($k_{11} = 1.6 \pm 0.1 \text{ M}^{-1} \text{ s}^{-1}$ versus $k_6 = 0.9 \pm 0.1 \text{ M}^{-1} \text{ s}^{-1}$). Given the similar reactivities of **6–10**, **12** and **13**, we expected these compounds to display transition state distortion and interaction energies of similar magnitude. DFT calculations were used to model the reaction of each analog with methyl azide, as calculations show that methyl azide behaves similarly to benzyl azide for the reaction with **6** (data provided in the Supporting Information). In discussing the results of these calculations, we define triazole **17** (Figure 10b) as the *syn* regioisomer and triazole **18** (Figure. 10b) as the *anti* regioisomer.

Computational data indicate that compounds **6–10**, **12** and **13** do in fact exhibit similar energetics in their transition states, with distortion energies for all seven compounds lying between 16.2 and 16.6 kcal/mol for the *syn* regioisomer and between 16.5 and 16.8 kcal/mol for the *anti* regioisomer. These data are consistent with both empirical and computational data indicating that the compounds have nearly identical alkyne bond angles (additional structural data are provided in the Supporting Information). Similarly, calculated interaction energies were alike for these compounds with values between -8.1 and -8.6 kcal/mol for the *syn* regioisomer and

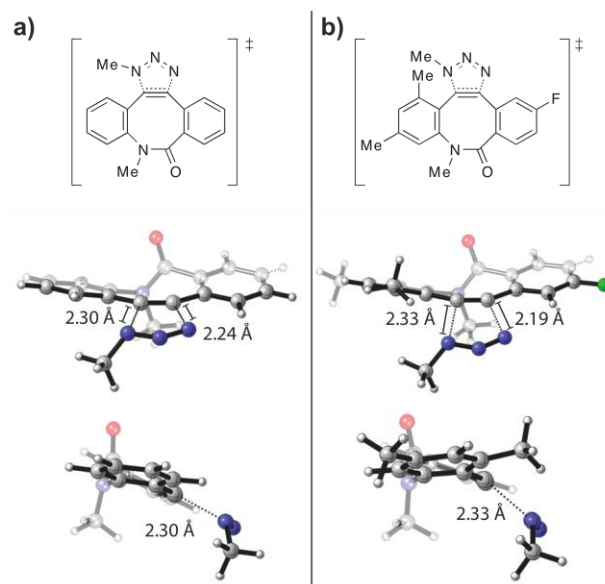


Figure 12. Flagpole methyl substituents sterically hinder the transition state. a. Front and side views of the transition state of the reaction of **6** with methyl azide. **b.** Front and side views of the transition state of the reaction of **15** with methyl azide.

between -8.7 and -9.0 kcal/mol for the *anti* regioisomer. As a result, overall energies of activation ($\Delta E^\ddagger = \Delta E^\ddagger_d + \Delta E^\ddagger_i$) for these compounds are quite comparable, falling within the range of 8.0 – 8.3 kcal/mol for the *syn* regioisomer and between 7.7 – 8.0 kcal/mol for the *anti* regioisomer.

Calculated free energies of activation in acetonitrile ($\Delta G^\ddagger_{\text{calc}}$) are also similar for compounds **6**–**10**, **12** and **13**. For both the *syn* and *anti* regioisomers, $\Delta G^\ddagger_{\text{calc}}$ lies between 23.7 and 24.1 kcal/mol. These calculations systematically overestimate the true free energies of activation by about 6.5 kcal/mol. This error has been previously noted in applications of B3LYP to cycloaddition reactions.^{12, 13} Such calculations also overestimate the entropic penalty associated with the transition states of bimolecular reactions.

Compound **11** was the only analog with substantially increased reactivity compared to BARAC, and accordingly, its transition state interaction energies ($\Delta E^\ddagger_{i,\text{calc}}$ values of -8.7 kcal/mol (*syn*) and -9.2 kcal/mol (*anti*)) were the largest measured in this study. Interestingly, we found that the transition state distortion energies for this analog lie within the range of those calculated

for the other compounds ($\Delta E_{d,calc}^{\ddagger} = 16.4$ kcal/mol (*syn*) and $\Delta E_{d,calc}^{\ddagger} = 16.7$ kcal/mol (*anti*)). As a result, combined activation energies for compound **11** are lower than those observed for the other analogs ($\Delta E_{calc}^{\ddagger} = 7.7$ kcal/mol (*syn*) and $\Delta E_{calc}^{\ddagger} = 7.5$ kcal/mol (*anti*)). The calculated free energies of activation in acetonitrile ($\Delta G_{calc}^{\ddagger}$) for compound **11** follow a similar trend (Figure 10c). These data indicate that the enhanced reaction rate observed for **11** is a result of electronic modulation that generates enhanced stabilizing interactions in the transition state. Modulation of strain and distortion energy does not appear to play a significant role in the rate enhancement.

Our experimental results also provide insight into the effects of sterics on cyclooctyne reactivity. We were surprised to find that compounds **14–16**, which all contain a flagpole substituent *ortho* to the alkyne, exhibit dramatic decreases in their rates relative to the parent cyclooctyne ($k_{14} = 0.058 \pm 0.003$ M⁻¹ s⁻¹ in CD₃CN, $k_{15} = 1.9 \times 10^{-3} \pm 0.0003$ M⁻¹ s⁻¹ in CDCl₃, and $k_{16} = 0.9 \times 10^{-3} \pm 0.0001$ M⁻¹ s⁻¹ in CDCl₃). Calculations show that these three compounds display corresponding increases in transition state distortion energies relative to analogs **6–13**. This enhanced distortion is due to the close proximity of the substituent to the alkyne and its orientation directly toward the path of the incoming azide, requiring both the azide and the alkyne to distort to a higher degree in the transition state. Figure 12 gives both a front and side view of the transition state of the reaction of compounds **6** and **15** with methyl azide, and it is clear that the methyl group is causing disfavorable steric interactions. Even a relatively small fluorine atom in this position, as in compound **14**, causes a significant increase in transition state distortion energy (Figure 10c). By contrast, the transition state interaction energies of compounds **14–16** are similar to those of the other BARAC analogs. As a result, **14–16** have higher activation barriers than do the other analogs tested, resulting in the observed orders of magnitude decrease in reactivity.

Overall, our analyses of compounds **6–16** indicate that aryl substitution can affect minor reactivity changes by altering transition state interaction energies (e.g., compound **11**) and

substantial rate changes by increasing steric hindrance in the transition state (e.g., compounds **14–16**). For compounds **6–13**, we did not observe any changes in reactivity due to modulation of transition state distortion energies, and we hypothesize that the enhanced distortion energies observed for **14–16** are a result of sterics rather than alkyne strain.

Alkyne bond angles as a measure of reactivity

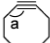
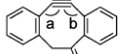
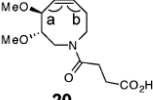
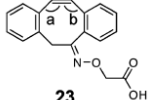
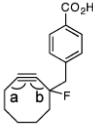
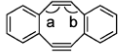

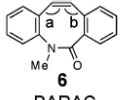
Compounds **6–13**, which share similar reactivities and transition state distortion energies, also possess similar structures with alkyne bond angles close to 153° (Figure 10c). This observation led us to hypothesize that alkyne bond angles may correlate with transition state activation energies for the cycloaddition with organic azides. If so, one may be able to predict the reactivity of a given cyclooctyne by determining its alkyne bond angles either through x-ray crystallography or DFT geometry optimizations.

Table 1 shows compiled x-ray structural data for a series of cyclooctynes as well as second-order rate constants for the reaction of each compound with benzyl azide (complete crystallographic data sets for compounds **2**, **6**, **20**, and **21** are in the Supporting Information; crystallographic or electron diffraction data for the other compounds are referenced in Table 1). Although kinetic parameters for the reaction of cyclooctyne itself (**19**) with organic azides have not been reported, we include the average bond angle of cyclooctyne¹⁴ in Table 1 as a point of comparison.

The data in Table 1 indicate a general correlation between alkyne bond angle distortion and cyclooctyne reactivity. Dimethoxyazacyclooctyne (DIMAC¹⁵, **20**) exhibits bond angles of 158° and 157° , structural deviations of only 1° and 2° , respectively, from the parent cyclooctyne **19**. Thus, neither DIMAC's endocyclic nitrogen nor its exocyclic substituents distort the alkyne bond angles to a significant extent. Installation of a fluorine atom at the propargylic position in MOFO⁶

(2) slightly enhances alkyne distortion at angle b through a bond polarization mechanism that has been extensively documented in substituted arynes.¹⁶ Angle b in MOFO is 4° more distorted than

Table 1. Reactivity and alkyne bond angles. Cyclooctyne bond angles and second-order rate constants for the reaction with benzyl azide in acetonitrile at rt. All bond angles were measured via X-ray crystallography with the exception of compound **19**, which was analyzed by electron diffraction in the gas phase. All data are referenced in the table, and details of the measurements first reported in this publication are located in the supporting information (SI). *Rate was measured for the acid form of DIFO2. **Rate constant measured in methanol. N/A = data not available.

cyclooctyne	a (°)	b (°)	rate constant (M ⁻¹ s ⁻¹)	ref.	cyclooctyne	a (°)	b (°)	rate constant (M ⁻¹ s ⁻¹)	ref.
 19 cyclooctyne	159	N/A	N/A	14	 22	152	157	N/A	18
 20 DIMAC	158	157	3.0 x 10 ⁻³	15, SI	 23	N/A	N/A	6.1 x 10 ^{-2**}	7b
 2 MOFO	160	155	4.3 x 10 ⁻³	6, SI	 24	156	155	6.3 x 10 ^{-2**}	14, 19
 21 DIFO2	162	151	4.2 x 10 ^{-2*}	17, SI	 6 BARAC	153	153	9 x 10 ⁻¹	7d, SI

the average bond angle in cyclooctyne (155° versus 159°, respectively). Conversely, angle a is less distorted in MOFO (160° versus 159°). Overall, the structural differences between MOFO and DIMAC are small, and, correspondingly only minor reactivity differences between the two are observed ($k_{\text{MOFO}} = 4.3 \times 10^{-3} \text{ M}^{-1} \text{ s}^{-1}$ and $k_{\text{DIMAC}} = 3.0 \times 10^{-3} \text{ M}^{-1} \text{ s}^{-1}$).^{6, 15}

As previously mentioned, installation of an additional fluorine atom at the propargylic position as in DIFO2¹⁷ (**21**) further enhances alkyne distortion at angle b (151°) through bond polarization. This additional bending at angle b is accompanied by a reduction in distortion at angle a (162° for DIFO2 versus 160° for MOFO). Despite strain reduction at angle a, however, the data suggest that the highly distorted nature of angle b in DIFO2 may contribute to the order of magnitude rate enhancement observed for this compound relative to MOFO ($k_{\text{DIFO2}} = 4.2 \times 10^{-2} \text{ M}^{-1} \text{ s}^{-1}$ versus $k_{\text{MOFO}} = 4.3 \times 10^{-3} \text{ M}^{-1} \text{ s}^{-1}$).^{6,17} The structure/reactivity trend observed for DIMAC, MOFO, and DIFO2 is also evident in the biarylcyclooctyne series.

Dibenzocyclooctyne **22**, reported by Kornmayer *et al.*, exhibits bond angles of 152° and 157°, and therefore is only slightly less distorted than DIFO2 at one angle but significantly more distorted than DIFO2 at the other.¹⁸ Although rate data are not available for this particular compound, a related oxime-substituted dibenzocyclooctyne (**23**) has been reported by Boons and coworkers to display a second-order rate constant of $k = 6.1 \times 10^{-2} \text{ M}^{-1} \text{ s}^{-1}$ for the reaction with benzyl azide in methanol.^{7b} The enhanced alkyne distortion observed at *both* alkyne angles in compound **22** (versus just one alkyne bond angle in DIFO2) may contribute to its heightened reactivity. Dibenzocyclooctadiyne **24**, with alkyne bond angles of 156° and 155°,^{14, 19} seems to distribute alkyne distortion more symmetrically across the bond but overall is not significantly more distorted than **23**. The reaction of compound **24** with benzyl azide was reported by Kii *et al.* to proceed with a second-order rate constant of $k = 6.3 \times 10^{-2} \text{ M}^{-1} \text{ s}^{-1}$.^{19b} As expected given their similar degrees of overall alkyne distortion, the reactivity of compound **24** is similar in magnitude to that measured for compound **23** ($k = 6.1 \times 10^{-2} \text{ M}^{-1} \text{ s}^{-1}$).

Relative to compounds **23** and **24**, BARAC (**6**) is significantly more distorted. With both alkyne bond angles at 153°, BARAC's structure exhibits the greatest overall deviation from cyclooctyne (159°). Accordingly, BARAC exhibits a second-order rate constant that is an order of

magnitude greater than compound **24** ($k_{\text{BARAC}} = 9 \times 10^{-1} \text{ M}^{-1} \text{ s}^{-1}$ versus $k_{24} = 6.3 \times 10^{-2} \text{ M}^{-1} \text{ s}^{-1}$).^{19b}

In summary, compounds **6** and **22–24** follow the same distortion/reactivity trend observed for

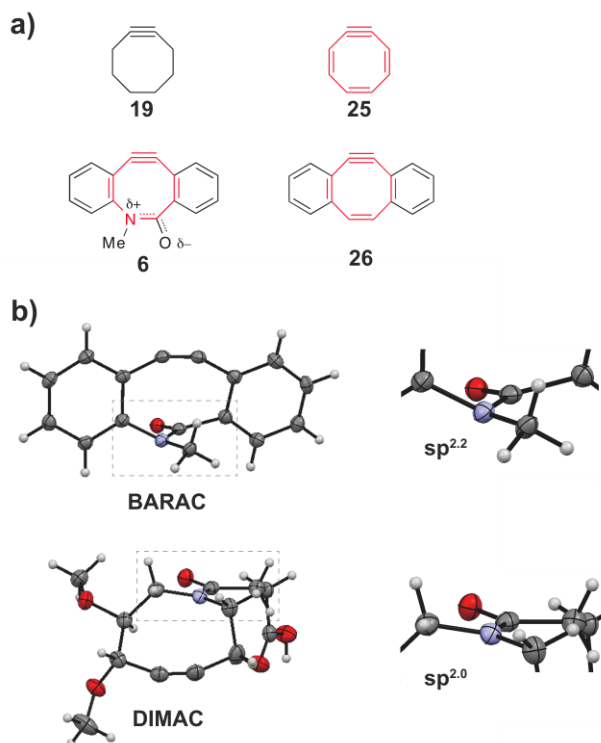


Figure 13. Strain modulation through rehybridization. **a.** Ring strain in cyclooctynes increases with increased unsaturation. We hypothesize that BARAC's fused aryl rings and central lactam contribute significantly to the compound's ring strain. **b.** X-ray crystal structures show that the nitrogen atom of BARAC's central lactam is $sp^{2.2}$ hybridized whereas DIMAC's amide nitrogen atom is sp^2 hybridized.

DIMAC, MOFO and DIFO2, with increased overall alkyne bond angle distortion correlating with increased reactivity.

Effects of BARAC's amide bond structure on reactivity and regioselectivity

The extreme distortion of BARAC's alkyne bond angles compared to other dibenzocyclooctynes may reflect adjustments of the cyclooctyne ring geometry to accommodate the lactam functionality. We speculate that BARAC's endocyclic amide bond enhances the overall ring strain of the compound by contributing some partial double bond character to the position

directly opposite the alkyne. Semi-empirical calculations by Meier *et al.* predict that the fully unsaturated cyclooctyne **25** (Figure 13a) would possess almost 3-fold more ring strain than the parent cyclooctyne **19**.^{2b} A related dibenzocyclooctenyne (**26**, Figure 13a) has been synthesized but is not bench-stable,¹⁴ consistent with the notion that ring strain increases with cyclooctyne unsaturation. BARAC shares structural features with compounds **25** and **26** but is relatively stable, prompting us to investigate the properties of BARAC's central amide bond.

An interesting comparison can be made between the hybridization indices of the nitrogen atoms in BARAC's and DIMAC's (**20**, Table 1) amide bonds, which we calculated using the sum of the bond angles surrounding the atom.²⁰ Whereas the amide nitrogen of DIMAC displays the expected sp^2 hybridization, that of BARAC is slightly pyramidalized with an $sp^{2.2}$ hybridization index. Though deviation from sp^2 hybridization in amides is generally thermodynamically disfavored, such distortion may reduce BARAC's overall ring strain by diminishing the double bond character and planarity of the lactam. This structural flexibility allows BARAC to balance reactivity and stability through amide nitrogen rehybridization.

Another notable feature of BARAC's amide bond is that its conformational state appears to impact regioselectivity in the alkyne-azide cycloaddition reaction. Whereas parent compound **6** reacts with benzyl azide to give a 1:1 mixture of *syn* and *anti* triazole products, analogs **15** and **16** generate *syn:anti* triazole product ratios of 3:1 and 2:1, respectively, wherein the favored product reflects the more sterically hindered transition state. Though counterintuitive on its face, this observation follows the general trend predicted using the distortion/interaction model.²¹ However, the magnitude of the regioisomeric preference is strongly affected by the conformation of BARAC's lactam in the ground state. For both **15** and **16**, our calculations predict a 25:1 preference for the *syn* regioisomer when BARAC reacts through its lowest energy *trans* conformer. But when the calculation was performed using *cis* BARAC as a substrate, the

predicted product ratio was 1.2:1 *syn/anti* for **15** and 0.8:1 *syn/anti* for **16**. Our experimentally observed product ratio may therefore reflect the presence of both conformers in solution, which, if interconvertible, would generate a Curtin-Hammett-controlled product distribution.

We calculated the barrier to amide bond isomerization for BARAC (**6**) and analogs **15** and **16** (Figures 14a and b). For BARAC, the barrier to *cis/trans* isomerization is 15.9 kcal/mol. With the energy of *trans* BARAC set to 0 kcal/mol, reaction of the *trans* conformer with methyl azide has an energetic barrier of 24.0 or 24.1 kcal/mol for formation of the *syn* and *anti* regioisomers respectively. Isomerization to and reaction of the *cis* conformer has barriers of 27.4 (*anti*) or 27.6 (*syn*) kcal/mol. Because the energetic barrier to isomerization is significantly lower than the barrier to reaction, we hypothesize that BARAC isomerizes during the course of the cycloaddition. However, because the activation energy for reaction of the *trans* isomer is lower than the activation energy for isomerization to and reaction of the *cis* isomer, we conclude that BARAC (**6**) reacts mainly through the *trans* isomer. As a result, the energetic barriers shown in Figure 14a, which predict a roughly 1:1 ratio of regioisomeric products, accurately predict the experimentally observed ratio of regioisomers (also 1:1).

The calculated barriers to *cis/trans* isomerization for both compounds **15** and **16** are about 16 kcal/mol, on par with that observed for the parent BARAC. Interestingly, however, for **15**, the transition state energies of the *trans* and *cis* isomers are much closer in energy than they are for the parent compound. Reaction of the *trans* isomer of **15** displays activation energies of 28.2 (*syn*) and 30.1 (*anti*) kcal/mol, and reaction of the *cis* isomer displays similar activation energies of 28.7 (*anti*) and 28.8 (*syn*) kcal/mol. Because the transition state energies of the *cis* and *trans* isomers are similar, we hypothesize that **15** may undergo the 1,3-dipolar cycloaddition with methyl azide by reacting through both the *cis* and the *trans* pathways. Based on this hypothesis and the aforementioned transition state energies, we calculate a *syn/anti* product ratio of 3:1 for **15**.

Compound **16** also showed similar *trans* and *cis* transition state energetics, and gave a calculated *syn/anti* product ratio of 5:1. These values are close to the observed product ratios (3:1 and 2:1 *syn:anti* for **15** and **16**, respectively).

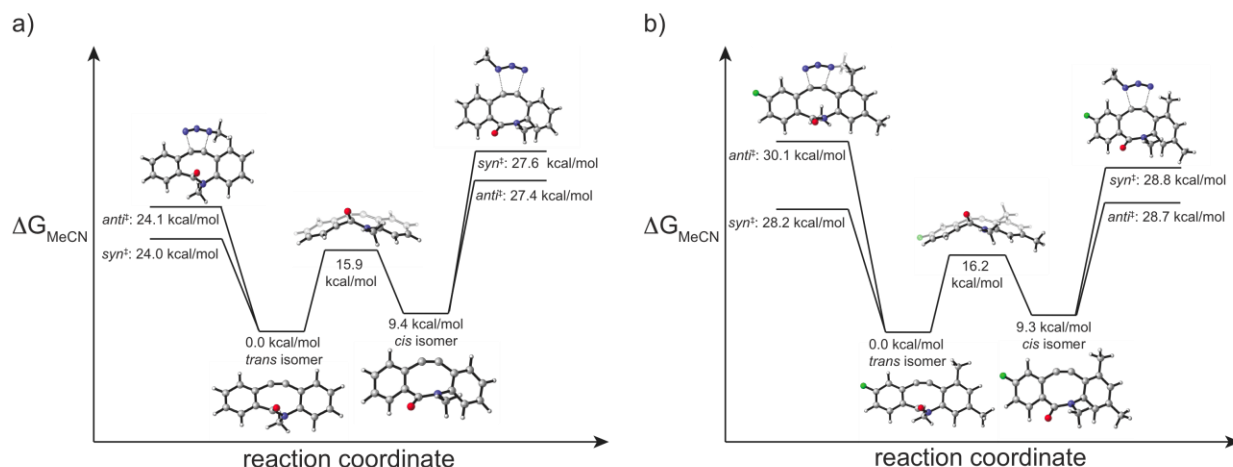


Figure 14. Under Curtin-Hammett conditions, BARAC's amide conformation influences reactivity and regioselectivity. **a.** The reaction coordinate diagram displays calculated activation free energies for reaction of the parent BARAC compound **6** with methyl azide in acetonitrile. Also shown are the relative energies of *cis-6* and *trans-6* and the barrier to *cis/trans* interconversion. Transition state images show only the lowest energy regioisomers. **b.** Calculated values for the reaction and interconversion of analog **15** with methyl azide in acetonitrile. Transition state images show only the lowest energy regioisomers.

Conclusion

We have performed a systematic analysis of the effects of strain and electronics on the reactivities of various cy-clooctynes using the distortion/interaction model. We found that aryl ring substitution with electron withdrawing and donating groups produces only minor alterations in reactivity. The majority of the analogs tested did not display significant rate changes relative to the parent compound **6** for the reaction with benzyl azide. However, we did see a ~75% increase in reactivity for the difluorinated analog **11**, which subsequent DFT calculations attributed to increased stabilizing interaction energy in the transition state of the reaction.

We observed more significant rate changes upon aryl substitution with groups capable of imposing steric hindrance in the transition state. Methyl substituted analogs **15** and **16** and fluorine-substituted analog **14**, which possess substituents at the flagpole position (*ortho* to the alkyne) displayed second-order rate constants between 2 and 3 orders of magnitude lower than that observed for parent BARAC. DFT data confirmed significantly increased transition state distortion energies for the reactions of these compounds with methyl azide. We also identified a correlation between total alkyne bond angle distortion and reactivity for the series of cyclooctynes shown in Table 1. Thus, computed alkyne bond angles as well as transition state distortion and interaction energies may be used in the informed design of cyclooctynes with tailored reactivity.

Analysis of BARAC's amide bond structure provided insight into its reactivity and regioselectivity with azides. X-ray structures of BARAC analogs provided evidence that BARAC is able to modulate stability through amide bond rehybridization. As well, we found that BARAC's lactam has the *trans* configuration in crystal form. Computations confirmed that the *trans* conformation is energetically preferred to the *cis* conformation by 9.4 kcal/mol in acetonitrile, and that this significant energetic difference may be in part a result of enhanced alkyne distortion upon isomerization to the *cis* conformer (Figure 11). These data suggest that a *cis*-constrained BARAC analog may display enhanced reactivity towards the azide as a result of enhanced strain.

Overall, our results show that DFT calculations can be a valuable resource in predicting the reactivity of potential new cyclooctynes. Accordingly, tools and trends summarized here should be useful for crafting new bioorthogonal reagents.

Acknowledgment. We thank Dr. A. DiPasquale for solving crystal structures and Dr. C. Canlas for help with NMR kinetics experiments.

Supporting Information Available. Details of the syntheses of compounds **6–16**, full characterizations of **6–16**, kinetics data for the reactions of **6–16** with benzyl azide, computational (DFT) details, and X-ray crystallography data for **2**, **6**, **20**, and **21** are found in the supporting information. This material is available free of charge via the Internet at <http://pubs.acs.org>.

References

- (1) For reviews, see: (a) Sletten, E. M.; Bertozzi, C. R. *Angew. Chem., Int. Ed.* **2009**, *48*, 6974-6998. (b) Jewett, J. C.; Bertozzi, C. R. *Chem. Soc. Rev.* **2010**, *39*, 1272-1279. (c) Debets, M. F.; Van Berkel, S. S.; Dommerholt, J.; Dirks, A. J.; Rutjes, F. P. J. T.; Van Delft, F. L. *Acc. Chem. Res.* **2011**, *44*, 805-815. (d) Sletten, E. M.; Bertozzi, C. R. *Acc. Chem. Res.* **2011**, *44*, 666-676. (e) Debets, M. F.; Van der Dolen, C. W. J.; Rutjes, F. P. J. T.; Van Delft, F. L. *ChemBioChem.* **2010**, *11*, 1168-1184.
- (2) (a) Bach, R. D. *J. Am. Chem. Soc.* **2009**, *131*, 5233-5243. (b) Meier, H.; Hanold, N.; Molz, T.; Bissinger, H. J.; Kolshorn, H.; Zountsas, J. *Tetrahedron*, **1986**, *42*, 1711-1719. (c) Turner, R. B.; Jarrett, A. D.; Goebel, P.; Mallon, B. J. *J. Am. Chem. Soc.* **1973**, *95*, 790-792. (d) For a summary of the structures/properties of strained alkynes, see Krebs, A.; Wilke, J. *Topics in Current Chemistry*, **1983**, *109*, 189-233.
- (3) (a) Baskin, J. M.; Prescher, J. A.; Laughlin, S. T.; Agard, N. J.; Chang, P. V.; Miller, I. A.; Lo, A.; Codelli, J. A.; Bertozzi, C. R. *Proc. Natl. Acad. Sci. USA.* **2007**, *104*, 16793-16797. (b) Chang, P. V.; Prescher, J. A.; Sletten, E. M.; Baskin, J. M.; Miller, I. A.; Agard, N. J.; Lo, A.; Bertozzi, C. R. *Proc. Natl. Acad. Sci. USA.* **2010**, *107*, 1821-1826. (c) Laughlin, S. T.; Baskin, J. M.; Amacher, S. L.; Bertozzi, C. R. *Science*, **2008**, *320*, 664-667. (d) Dehnert, K. W.; Beahm, B. J.; Huynh, T. T.; Baskin, J. M.; Laughlin, S. T.; Wang, W.; Wu, P.; Amacher, S. L.; Bertozzi, C. R. *ACS Chem. Biol.* **2011**, *6*, 547-552.
- (4) (a) Rostovtsev, V. V.; Green, L. G.; Fokin, V. V.; Sharpless, K. B. *Angew. Chem. Int. Ed.* **2002**, *41*, 2596-2599. (b) Tornøe, C. W.; Christensen, C.; Meldal, M. *J. Org. Chem.* **2002**, *67*, 3057-3064. (c) For a review of click chemistry see: Kolb, H. C.; Finn, M. G.; Sharpless, K. B. *Angew. Chem. Int. Ed.* **2001**, *40*, 2004-2021. For examples of *in vivo* Cu(I) catalysis see: (d) Hong, V.; Steinmetz, N. F.; Manchester, M.; Finn, M. G. *Bioconjugate Chem.* **2010**, *21*, 1912-1916. (e) Soriano del Amo, D.; Wang, W.; Jiang, H.; Besanceney, C.; Yan, A. C.; Levy, M.; Liu, Y.; Marlow, F. L.; Wu, P. *J. Am. Chem. Soc.* **2010**, *132*, 16893-16899. (f) Besanceney-Webler, C.; Jiang, H.; Zheng, T.; Feng, L.; Soriano del Amo, D.; Wang, W.; Klivansky, L. M.; Marlow, F. L.; Liu, Y.; Wu, P. *Angew. Chem. Int. Ed.* **2011**, *50*, 8051-8056.
- (5) Agard, N. J.; Prescher, J. A.; Bertozzi, C. R. *J. Am. Chem. Soc.* **2004**, *126*, 15046-15047.
- (6) Agard, N. J.; Baskin, J. M.; Prescher, J. A.; Lo, A.; Bertozzi, C. R. *ACS Chem. Biol.* **2006**, *1*, 644-648.
- (7) (a) Ning, X.; Guo, J.; Wolfert, M. A.; Boons, G. J. *Angew. Chem. Int. Ed.* **2008**, *47*, 2253-2255. (b) Mbua, N. E.; Guo, J.; Wolfert, M. A.; Steet, R.; Boons, G. J. *ChemBioChem*, **2011**, *12*, 1912-1921. (c) Debets, M. F.; Van Berkel, S. S.; Schoffelen, S.; Rutjes, F. P. J. T.; Van Hest, J. C. M.;

Van Delft, F. L. *Chem. Comm.* **2010**, *46*, 97-99. (d) Jewett, J. C.; Sletten, E. M.; Bertozzi, C. R. *J. Am. Chem. Soc.* **2010**, *132*, 3688-3690.

(8) (a) Chenoweth, K.; Chenoweth, D.; Goddard, W. A. III. *Org. Biomol. Chem.* **2009**, *7*, 5255-5258. (b) Ess, D. H.; Jones, G. O.; Houk, K. N. *Org. Lett.* **2008**, *10*, 1633-1636. (c) Schoenebeck, F.; Ess, D. H.; Jones, G. O.; Houk, K. N. *J. Am. Chem. Soc.* **2009**, *131*, 8121-8133.

(9) Gold, B.; Shevchenko, N. E.; Bonus, N.; Dudley, G. B.; Alabugin, I. V. *J. Org. Chem.* **2012**, *77*, 75-89.

(10) Calculated p-values (two-tailed, unpaired Student's *t*-test) comparing the second order rate constants measured for compounds **7–9**, **12**, and **13** to that measured for **6** are $0.5 > p > 0.001$. The p-value calculated for compound **10** is $p = 0.0001$. P-values calculated for compounds **11** and **14–16** are $p < 0.0001$.

(11) A di-substituted BARAC analog with a fluorine atom at the position shown in compound **8** and a methoxy group at the position shown in compound **12** was synthesized and its kinetics analyzed to determine the combined effects of electron withdrawing and donating groups on cyclooctyne reactivity. The calculated second order rate constant was $k = 1.1 \pm 0.1 \text{ M}^{-1} \text{ s}^{-1}$ for the reaction with benzyl azide in CD₃CN at rt – on par with rate constants observed for compounds **6–10**, **12**, and **13**.

(12) During the course of this work, a more extensive benchmarking of 1,3-dipolar cycloadditions to ethylene and acetylene was performed, see Lan, Y.; Zou, L.; Cao, Y.; Houk, K. N. *J. Phys. Chem. A.* **2011**, *115*, 13906–13920. Through this work, more accurate methods and addition functionals for modeling these reactions were identified. The M06-2X functional was found to provide activation barriers that more closely matched higher accuracy calculations. As a result, in addition to the B3LYP results in Figure 10c, M06-2X calculations have been performed on BARAC compounds **6** and **14–16** and are given in the SI. These activation energies deviate by 1.3–4.6 kcal/mol from energies calculated using the B3LYP functional. The conclusions are the same, except that M06-2X predicts all reactions to involve only the *trans* isomer.

(13) Ess, D. H.; Houk, K. N. *J. Phys. Chem. A.* **2005**, *109*, 9542-9553.

(14) De Graff, R. A. G.; Gorter, S.; Romers, C.; Wong, H. N. C.; Sondheimer, F. *J.C.S. Perkin II*, **1981**, 478-480.

(15) Sletten, E. M.; Bertozzi, C. R. *Org. Lett.* **2008**, *10*, 3097-3099.

(16) (a) Cheong, P. H.-Y.; Paton, R. S.; Bronner, S. M.; Im, G.-Y. J.; Garg, N. K.; Houk, K. N. *J. Am. Chem. Soc.* **2010**, *132*, 1267-1269. (b) Im, G.-Y. J.; Bronner, A. M.; Goetz, A. E.; Paton R. S.; Cheong, P. H.-Y.; Houk, K. N.; Garg, N. K. *J. Am. Chem. Soc.* **2010**, *132*, 17933-17944.

(17) Codelli, J. A.; Baskin, J. M.; Agard, N. J.; Bertozzi, C. R. *J. Am. Chem. Soc.* **2008**, *130*, 11486-11493.

(18) Kornmayer, S. C.; Rominger, F.; Gleiter, R. *Synthesis*, **2006**, *15*, 2547-2552.

(19) (a) Destro, R.; Pilati, T.; Simonetta, M. *J. Am. Chem. Soc.* **1975**, *97*, 658-659. (b) Kii, I.; Shiraishi, A.; Hiramatsu, T.; Matsushita, T.; Uekusa, H.; Yoshida, S.; Yamamoto, M.; Kudo, A.; Hagiwara, M.; Hosoya, T. *Org. Biomol. Chem.* **2010**, *8*, 4051-4055.

(20) $1 + i \cos \theta = 0$ where i = hybridization index. Anslyn, E. V.; Dougherty D. A. In *Modern Physical Organic Chemistry*; University Science Books, 2006; p 10.

(21) Notably, Yoshida *et al.* recently reported that sterically hindered azides react more rapidly with cyclooctynes than unhindered azides. Their explanation for the energetic origins of this observation may also apply to our system. Yoshida, S.; Shiraishi, A.; Kanno, K.; Matsushita, T.; Johmoto, K.; Uekusa, H.; Hosoya, T. *Sci. Rep.* **2011**, 1:82.

3. Steric Effects Compete with Aryne Distortion to Control Regioselectivities of Nucleophilic Additions to 3-Silylarynes

Introduction

Despite once being a subject of controversy,¹ arynes are now a thriving area of chemical discovery.² Modern methods of aryne generation have led to greater control of reactivity, thus enabling the use of arynes in a host of synthetic applications.³ Nonetheless, the control and understanding of regioselectivity in reactions of unsymmetrical arynes remains an important area of research.²

The aryne distortion model, reported by our laboratories in 2010,⁴ shows that regioselectivity in nucleophilic additions and cycloadditions of arynes is governed by the inherent distortion present in unsymmetrical arynes and transition state distortion energies.⁵ The model allows for reliable regioselectivity predictions to be made using simple computations, and has been validated for ring-fused arynes and arynes that possess neighboring inductively withdrawing substituents.^{4,6} In the case of 3-methoxybenzyne,⁷ the aryne is pre-distorted as suggested in Figure 15. Addition of the nucleophile occurs at the more electrophilic site, with flattening at the carbon undergoing attack, to give *meta*-substituted products.^{8,9} As a means to further probe the aryne distortion model, we examined the influence of inductively donating silyl substituents on aryne regioselectivities.¹⁰ Our experimental and computational study demonstrates that the sense of regioselectivity in silylaryne reactions is variable, but aryne distortion can play a significant role. Computations correctly predict the preferred site of attack observed in both nucleophilic addition and cycloaddition experiments.

Geometry optimization of 3-triethylsilylbenzyne was conducted using DFT methods (B3LYP/6-311+G(d,p)).¹¹ The silyl group severely distorts the aryne, such that the internal

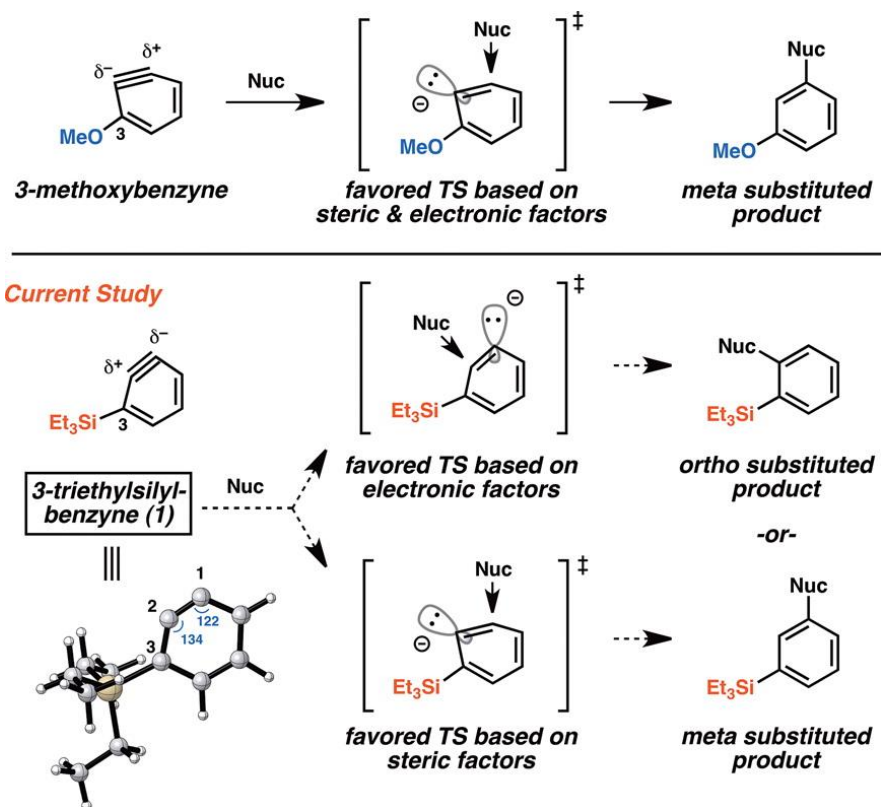


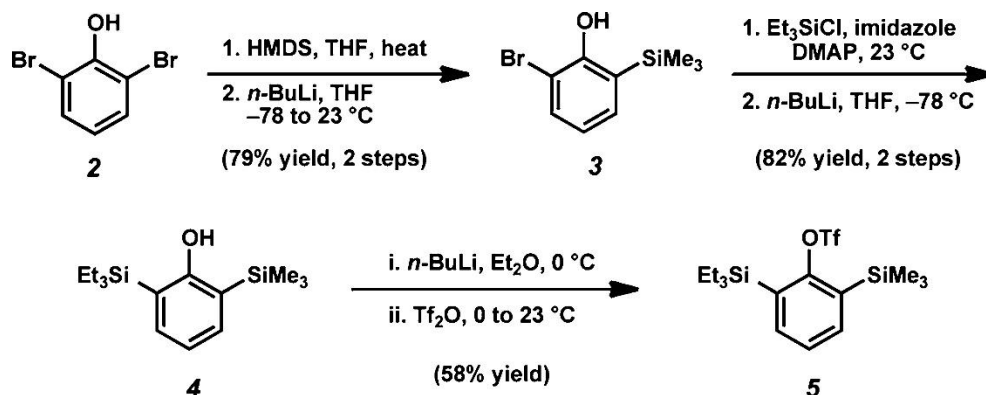
Figure 15. Influence of 3-methoxy and 3-silyl substituents on aryne regioselectivity.

angles at C2 and C1 are 134° and 122° , respectively.¹² Following the aryne distortion model, nucleophilic addition at C2, the more electropositive terminus of the aryne, is favored electronically; however, *meta* substitution should be preferred based on steric factors. Only few examples of silylaryne reactions have been reported, but it should be noted that additions of organolithium reagents to silylarynes occur with *meta*-selectivity,^{10a,b,c} whereas additions of amines are primarily *ortho*-selective.^{10g,13}

With the aim of studying regioselectivity patterns of silylarynes in a variety of nucleophilic addition and cycloaddition reactions, we prepared bis(silyl)triflate **5**, which was envisioned to be a suitable precursor to triethylsilylbenzyne **1** (Scheme 5).¹⁴ Commercially available dibromophenol **2** was elaborated to known compound **3**¹⁵ via a two-step procedure involving *O*-silylation followed by halogen-metal exchange-mediated *O* to *C* migration of the silyl substituent.¹⁶ Next, an

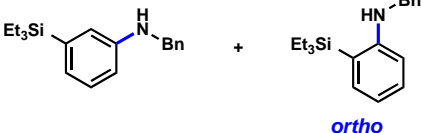
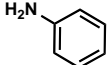
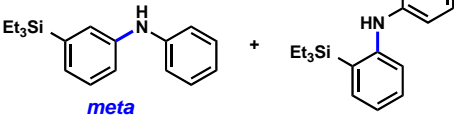
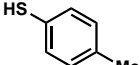
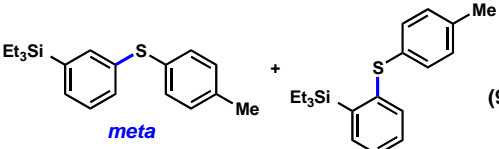
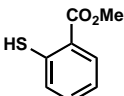
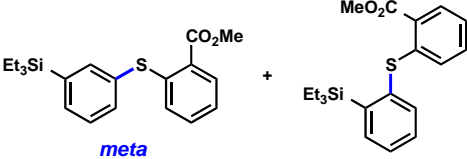
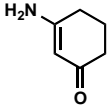
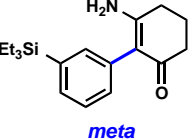
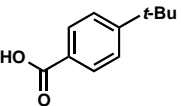
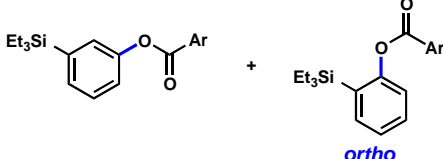
analogous sequence was employed to install the triethylsilyl group, thus providing **4**.¹⁷ Triflation of **4** afforded the desired bis(silyl)triflate **5**.¹⁸

Scheme 5. Synthetic route to triethylsilylbenzynes



A comparative regioselectivity study was performed, where triethylsilylbenzynes **1** was generated in situ upon treatment of **5** with CsF in acetonitrile, in the presence of a variety of nucleophiles (Table 2).^{19,20} Upon trapping of the aryne with benzylamine, reaction occurred to give a 1:2 ratio of products favoring *ortho* substitution (entry 1). However, when aniline was employed, the regioselective preference switched to favor *meta* addition (entry 2), which is consistent with the observations reported by Akai.^{10g} Other trapping agents that have not been used with silylbenzynes previously were also tested. Thiophenol based reagents also gave products of *meta* substitution predominantly (entries 3 and 4); in the later case, selectivity was 10:1. An enamine reagent, which functions as a carbon nucleophile, exclusively yielded the *meta*-substituted product (entry 5). Use of 4-*t*-Bu-benzoic acid, however, gave 1:3 selectivity, favoring *ortho* addition (entry 6).

Table 2. Nucleophilic additions to triethylsilylbenzyne 1^a

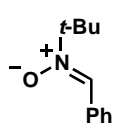
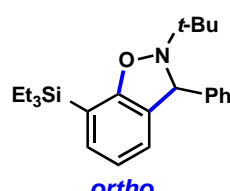
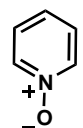
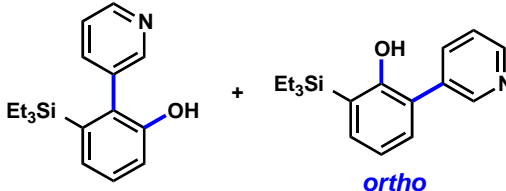
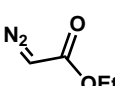
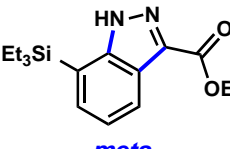
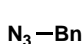
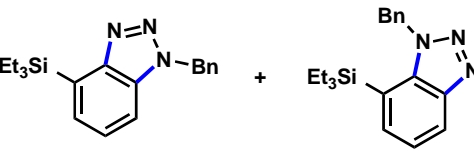
entry	trapping agent	product(s)	ratio (yield ^b)
1	H ₂ N-Bn		1:2 (81% yield)
2			2:1 (99% yield)
3			4:1 (91% yield)
4			10:1 (77% yield)
5			(52% yield)
6			1:3 (53% yield)

^a See Supporting Information for experimental details. ^b Yields determined by ¹H NMR analysis with external standard.

Triethylsilylaryne **1** was next evaluated in a series of cycloaddition reactions. As shown in Table 3, the selectivity patterns varied as a function of the trapping agent employed. A nitrene cycloaddition gave a 73% yield of a single regioisomer of product (entry 1), suggestive of *ortho* attack, as seen in previous nitrene cycloadditions of silylarynes.^{10d} Trapping of the silylaryne with

pyridine *N*-oxide²¹ also proceeded with a significant preference for *ortho* addition (entry 2). Conversely, cycloaddition with a diazoester²² exclusively afforded the product resulting from initial *meta* attack (entry 3). Reaction with benzyl azide²³ gave a 6:1 ratio of products, favoring initial *meta* addition (entry 4). Despite variations in the initial site of nucleophilic attack, the major regioisomer observed in each cycloaddition is presumably that which arises from the least sterically encumbered transition state.

Table 3. Cycloaddition reactions with triethylsilylbenzyne 1^a

entry	trapping agent	product(s)	ratio (yield ^b)
1		 <i>ortho</i>	(73% yield)
2		 <i>ortho</i>	1:9 (60% yield)
3		 <i>meta</i>	(65% yield)
4		 <i>meta</i>	6:1 (85% yield)

^a See Supporting Information for experimental details. ^b Yields determined by ¹H NMR analysis with external standard.

These results demonstrate that nucleophilic additions and cycloadditions of 3-triethylsilylbenzyne do occur with significant regioselectivities, but the orientation of attack varies as a function of the trapping agent. DFT calculations were carried out to provide additional insights into

the origins of these observations. All geometry optimizations were performed using Gaussian 09²⁴ using the B3LYP density functional and the 6-311+g(d,p) basis set. A frequency calculation was performed on all reactants and transition states to verify minima and first order saddle points, respectively, and an ultra-fine grid was used for all numerical integration. Unscaled zero-point energies were used, and Truhlar's anharmonic correction was applied to frequencies that are less than 100 cm⁻¹.²⁵ Trimethylsilylbenzene was used as a model for triethylsilylbenzyne.²⁶

Figure 16 shows optimized transition states for the nucleophilic additions of benzylamine and aniline to 3-trimethylsilylbenzyne. The barrier for attack of benzylamine at C2 is predicted to be 0.7 kcal/mol lower than for attack at C1. Addition at C2 is favored because the aryne's pre-distorted bond angles favor nucleophilic attack at the flatter, more electrophilic carbon, which is C2 in this case. During the attack, the aryne has to undergo geometric changes, including an increase of the CCC angle at the site of attack and compression of the other terminus of the aryne. The larger angle, like C2 in triethylsilylbenzyne, will be attacked preferentially. In contrast, for aniline, attack is predicted to be favored at C1 rather than C2 by 3.7 kcal/mol. Because aniline is a more bulky nucleophile, it suffers from more steric hindrance with the silyl group of the benzyne. As shown in Figure 16, the H–H distance of the two closest hydrogens in the C2 attack of aniline are very close at 2.13 Å. In the case of benzylamine the closest H–H distance is 2.52 Å. This steric interaction is overriding the aryne distortion preference for attack at C2. Although the magnitude of selectivity is exaggerated, computations correctly predict experimental regioselectivities.²⁷

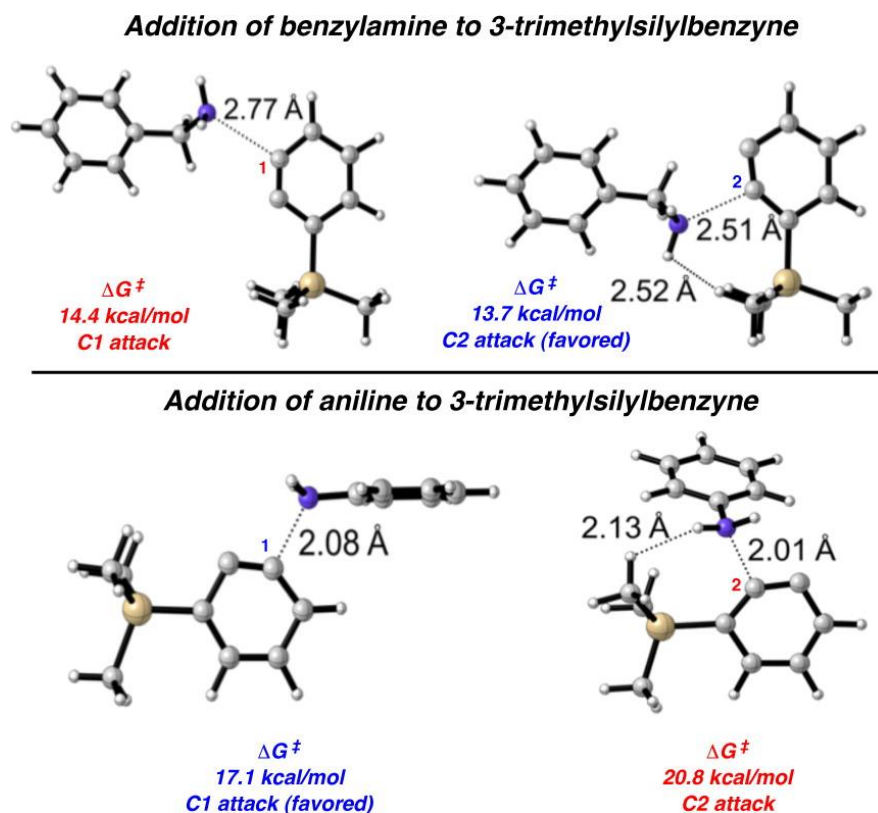


Figure 16. Transition states for nucleophilic additions of benzylamine and aniline to 3-trimethylsilylbenzyne.

The cycloaddition of methylazide with 3-trimethylsilylbenzyne was also examined computationally, with methylazide serving as a model for benzylazide. Transition states are shown in Figure 17. C1 attack is favored, which is consistent with experimental results, by 0.7 kcal/mol. Aryne distortion would favor attack of the nucleophilic substituted terminus at C2, but steric hindrance overrides this electronic preference leading to preferential attack at C1.

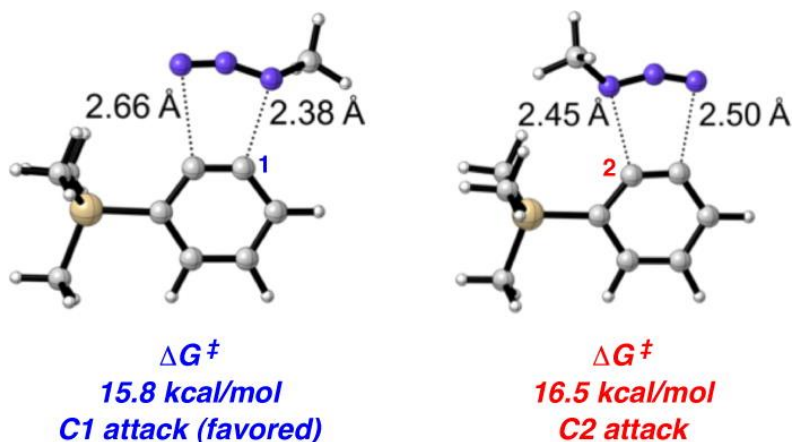


Figure 17. Cycloaddition of methylazide with 3-trimethylsilylbenzene.

For comparison, we studied 3-*t*-butylbenzene (**6**),²⁸ which is sterically similar to 3-triethylsilylbenzene (**1**), but varies electronically (Figure 18). The geometry optimized structure of **6** (B3LYP/6-311+G(d,p)) revealed internal angles of 129° and 127° at C2 and C1, respectively. Given the minimal distortion present, **6** was predicted to undergo sterically-guided attack at C1 to give *meta*-substituted products.

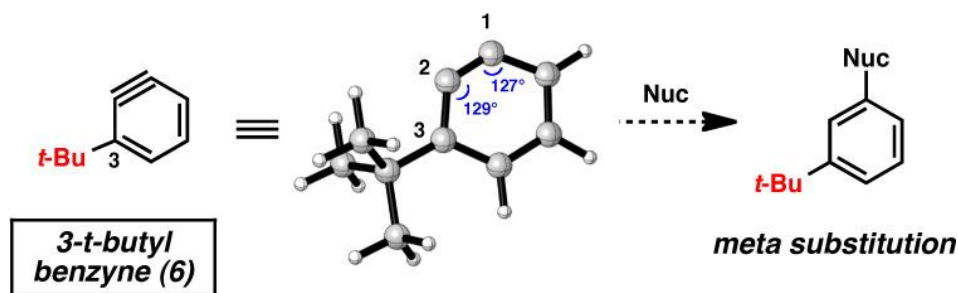
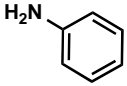
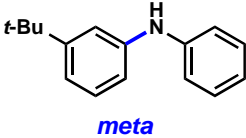
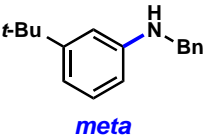
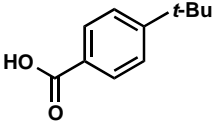
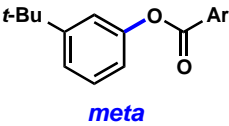


Figure 18. Geometry optimized structure of 3-*t*-butylbenzyne **6 and predicted regioselectivity.**

A silyltriflate precursor to aryne **6** was prepared from *o*-*t*-Bu-phenol and examined in nucleophilic addition reactions (Table 4).²⁹ When aniline was used as the trapping agent, formation of the *meta*-substituted product was preferred (entry 1), similar to the trend observed in the reaction of 3-triethylsilylbenzyne. Benzylamine and 4-*t*-Bu-benzoic acid were also tested with aryne **6**. In contrast to the outcome seen in reactions of **1**, only *meta* substitution was observed (entries 2

and 3). These results support the notion that aryne distortion plays a significant role in reactions of 3-silylaryne **1**. Quantum chemical calculations were performed for the reaction of **6** with aniline and benzylamine, and in both cases the attack at C1 was strongly favored.²⁹

Table 4. Nucleophilic additions to *t*-butylbenzyne **6^a**

entry	trapping agent	product ^b	ratio (yield ^c)
1		 <i>meta</i>	(66% yield)
2	H ₂ N-Bn	 <i>meta</i>	(61% yield)
3		 <i>meta</i>	(50% yield)

^a See Supporting Information for experimental details. ^b *ortho*-Substituted products were not observed. ^c Yields determined by ¹H NMR analysis with external standard.

The effects of the inductively donating silyl group on arynes have been studied both experimentally and computationally. It has been shown that if the incoming nucleophile is not bulky, the aryne distortion model holds true and the flatter terminus of the aryne is the site of attack. If however, there is sufficient steric bulk on the nucleophile, then attack on the more accessible carbon of the aryne is favored. When the substituent adjacent to the aryne is an alkyl group, steric effects dominate, since there is no significant differential distortion of the aryne bond angles.

Acknowledgment. The authors are grateful to the NIH-NIGMS (R01 GM090007), Boehringer Ingelheim, DuPont, Eli Lilly, Amgen, AstraZeneca, the Foote Fellowship (S.M.B.), the Stauffer Charitable Trust (S.M.B.) and the University of California, Los Angeles, for financial support. We thank Joshua Melamed (UCLA) for experimental assistance, and Dr. John Greaves (UC Irvine) for mass spectra. We are grateful to the National Science Foundation (CHE-0548209 to

K.N.H.) for financial support. Computer time was provided in part by the UCLA Institute for Digital Research and Education (IDRE) and the XSEDE supercomputers Trestles and Gordon at San Diego Supercomputer Center. These studies were supported by shared instrumentation grants from the NSF (CHE-1048804) and the National Center for Research Resources (S10RR025631).

Supporting Information Available: Detailed experimental procedures and compound characterization data (PDF). This material is available free of charge via the Internet at <http://pubs.acs.org>.

References

- (1) Reinecke, M. G. *Tetrahedron* **1982**, *38*, 427.
- (2) a) Pellissier, H.; Santelli, M. *Tetrahedron* **2003**, *59*, 701. b) Wenk, H. H.; Winkler, M.; Sander, W. *Angew. Chem. Int. Ed.* **2003**, *42*, 502. c) Sanz, R. *Org. Prep. Proced. Int.* **2008**, *40*, 215. d) Chen, Y.; Larock, R. C. Arylation Reactions Involving the Formation of Arynes. In *Modern Arylation Methods*; Ackermann, L., Ed.; Wiley–VCH: Weinheim, 2009; pp 401–473.
- (3) Tadross, P. M.; Stoltz, B. M. *Chem. Rev.* **2012**, *112*, 3550.
- (4) a) Cheong, P. H.-Y.; Paton, R. S.; Bronner, S. M.; Im, G.-Y.; Garg, N. K.; Houk, K. N. *J. Am. Chem. Soc.* **2010**, *132*, 1267. b) Im, G.-Y.; Bronner, S. M.; Goetz, A. E.; Paton, R. S.; Cheong, P. H.-Y.; Houk, K. N.; Garg, N. K. *J. Am. Chem. Soc.* **2010**, *132*, 17933.
- (5) For the application of distortion energies to regioselectivity of cycloaddition reactions, see: a) Ess, D. H.; Houk, K. N. *J. Am. Chem. Soc.* **2007**, *129*, 10646. b) Ess, D. H.; Houk, K. N. *J. Am. Chem. Soc.* **2008**, *130*, 10187. c) Lam, Y.-h.; Cheong, P. H.-Y.; Blasco Mata, J. M.; Stanway, S. J.; Gouverneur, V.; Houk, K. N. *J. Am. Chem. Soc.* **2009**, *131*, 1947. d) Hayden, A. E.; Houk, K. N. *J. Am. Chem. Soc.* **2009**, *131*, 4084. e) Schoenebeck, F.; Ess, D. H.; Jones, G. O.; Houk, K. N. *J. Am. Chem. Soc.* **2009**, *131*, 8121. For the application of distortion energies to regioselectivity of palladium-catalyzed cross-coupling reactions, see: f) Legault, C. Y.; Garcia, Y.; Merlic, C. A.; Houk, K. N. *J. Am. Chem. Soc.* **2007**, *129*, 12664. g) Garcia, Y.; Schoenebeck, F.; Legault, C. Y.; Merlic, C. A.; Houk, K. N. *J. Am. Chem. Soc.* **2009**, *131*, 6632. For a discussion of activation strain theory, see: h) van Zeist, W.-J.; Bickelhaupt, F. M. *Org. Biomol. Chem.* **2010**, *8*, 3118. For a discussion of the application of distortion/interaction theory to stereoselectivity, see: i) Kolakowski, R. V.; Williams, L. J. *Nat. Chem.* **2010**, *2*, 303.
- (6) Bronner, S. M.; Goetz, A. E.; Garg, N. K. *J. Am. Chem. Soc.* **2011**, *133*, 3832.
- (7) 3-Alkoxyarynes are known to react regioselectively. For pertinent reviews, see reference 2. For a recent example of alkoxybenzynes undergoing regioselective reactions, see: Tadross, P. M.; Gilmore, C. D.; Bugga, P.; Virgil, S. C.; Stoltz, B. M. *Org. Lett.* **2010**, *12*, 1224; see also references therein.

(8) 3-Haloarynes react in a similar sense; for examples, see reference 6 and the following: a) Biehl, E. R.; Nieh, E.; Hsu, K. C. *J. Org. Chem.* **1969**, *34*, 3595. b) Moreau–Hochu, M. F. *Tetrahedron* **1977**, *33*, 955. c) Ghosh, T.; Hart, H. *J. Org. Chem.* **1988**, *53*, 3555. d) Hart, H.; Ghosh, T. *Tetrahedron Lett.* **1988**, *29*, 881. e) Wickham, P. P.; Reuter, K. H.; Senanyake, D.; Guo, H.; Zalesky, M.; Scott, W. J. *Tetrahedron Lett.* **1993**, *34*, 7521. f) Gokhale, A.; Scheiss, R. *Helv. Chem. Acta* **1998**, *81*, 251.

(9) The formation of *meta*-substituted products is also favorable because of steric considerations.

(10) For the addition of organolithium species to silylarynes (*meta* preferred), see: a) Heiss, C.; Cottet, F.; Schlosser, M. *Eur. J. Org. Chem.* **2005**, 5236. b) Heiss, C.; Cottet, F.; Schlosser, M. *Eur. J. Org. Chem.* **2005**, 5242. c) Diemer, V.; Begaud, M.; Leroux, F. R.; Colobert, F. *Eur. J. Org. Chem.* **2011**, 341. For nitrene or furan Diels–Alder cycloadditions involving silylarynes (initial *ortho* preferred addition), see: d) Matsumoto, T.; Sohma, T.; Hatazaki, S.; Suzuki, K. *Synlett* **1993**, 843. e) Akai, S.; Ikawa, T.; Takayanagi, S.-i.; Morikawa, Y.; Mohri, S.; Tsubakiyama, M.; Egi, M.; Wada, Y.; Kita, Y. *Angew. Chem. Int. Ed.* **2008**, *47*, 7673. f) Dai, M.; Wang, Z.; Danishefsky, S. J. *Tetrahedron Lett.* **2008**, *49*, 6613. For the addition of amine nucleophiles to silylarynes, see: g) Ikawa, T.; Nishiyama, T.; Shigeta, T.; Mohri, S.; Morita, S.; Takayanagi, S.-i.; Terauchi, Y.; Morikawa, Y.; Takagi, A.; Ishikawa, Y.; Fujii, S.; Kita, Y.; Akai, S. *Angew. Chem. Int. Ed.* **2011**, *50*, 5674.

(11) The trimethylsilyl derivative was studied initially, but competitive product desilylation complicated regioselectivity analysis.

(12) For ring-fused aryne or those that possess inductively withdrawing groups, angle differences of >4 degrees between the two aryne termini generally give synthetically useful regioselectivities, regardless of the trapping agent employed.

(13) The *ortho*-selectivity for the addition of amines has previously been rationalized by the presumed formation of a pentavalent fluorosilicate, which in turn, perturbs the aryne electronically; see ref 10g.

(14) For Kobayashi's approach to aryne, see: Himeshima, Y.; Sonoda, T.; Kobayashi, H. *Chem. Lett.* **1983**, 1211.

(15) Booker, J. E. M.; Boto, A.; Churchill, G. H.; Green, C. P.; Ling, M.; Meek, G.; Prabhakaran, J.; Sinclair, D.; Blake, A. J.; Pattenden, G. *Org. Biomol. Chem.* **2006**, *4*, 4193.

(16) Díaz, M.; Cobas, A.; Guitián, E.; Castedo, L. *Eur. J. Org. Chem.* **2001**, 4543. Also see reference 9g.

(17) Peterson, E. A.; Jacobsen, E. N. *Angew. Chem. Int. Ed.* **2009**, *48*, 6328.

(18) Shimizu, M.; Mochida, K.; Hiyama, T. *Angew. Chem. Int. Ed.* **2008**, *47*, 9760.

(19) Liu, Z.; Larock, R. C. *J. Org. Chem.* **2006**, *71*, 3198.

(20) Ramtohl, Y. K.; Chartrand, A. *Org. Lett.* **2007**, *9*, 1029.

(21) Raminelli, C.; Liu, Z.; Larock, R. C. *J. Org. Chem.* **2006**, *71*, 4689.

(22) Liu, Z.; Shi, F.; Martinez, P. D. G.; Raminelli, C.; Larock, R. C. *J. Org. Chem.* **2008**, *73*, 219.

(23) a) Shi, F.; Waldo, J. P.; Chen, Y.; Larock, R. C. *Org. Lett.* **2008**, *10*, 2409. b) Campbell-Verduyn, L.; Elsinga, P. H.; Mirfeizi, L.; Dierckx, R. A.; Feringa, B. L. *Org. Biomol. Chem.* **2008**, *6*, 3461.

(24) Frisch, M. J. et al. Gaussian 09, revision C.01; Gaussian, Inc.: Wallingford, CT, 2009.

(25) Ribeiro, R. F.; Marenich, A. V.; Cramer, C. J.; Truhlar, D. G. *J. Phys. Chem. B* **2011**, *115*, 14556.

(26) See the SI for comparison of aniline attack at either C1 or C2 of 3-trimethylsilylbenzyne and 3-triethylsilylbenzyne.

(27) This observation is consistent with previous studies of the aryne distortion model; see reference 4a for discussion.

(28) 3,5-di-*t*-Butylbenzyne has been studied in a nitrene cycloaddition (see reference 10d). For other studies involving **6** (or substituted derivatives), see: a) Franck, R. W.; Leser, E. G. *J. Org. Chem.* **1970**, *35*, 3932. b) Yamamoto, G.; Koseki, A.; Sugita, J.; Mochida, H.; Minoura, M. *Bull. Chem. Soc. Jpn.* **2006**, *79*, 1585. c) Cadogan, J. I. G.; Cook, J.; Harger, M. J. P.; Hibbert, P. G.; Sharp, J. T. *J. Chem. Soc. B* **1971**, 595. d) Franck, R. W.; Yanagi, K. *J. Am. Chem. Soc.* **1968**, *90*, 5814.

(29) See the Supporting Information.

4. The Role of Aryne Distortions, Steric Effects, and Charges on Regioselectivities of Aryne Reactions

Introduction

The fundamental understanding of molecular reactivity continues to fuel countless aspects of scientific discovery. One model for understanding reactivity that has recently received great attention is the distortion / interaction model.^{1,2,3,4,5,6} The premise of this model, which is also known as the activation–strain model according to Bickelhaupt,⁷ divides the activation energy of a bimolecular process into two components: the energy needed to distort reactants to the transition state geometry and the energy of interaction between the distorted fragments. The distortion / interaction model has provided fundamental new insight into chemical reactivity, and has been used to understand and predict reactivities and selectivities in an array of chemical processes, including Diels–Alder, 1,3-dipolar and bioorthogonal cycloadditions,¹ palladium-catalyzed cross-couplings,² C–H functionalizations,³ and epoxidation reactions.⁴

We have recently explored the application of the distortion / interaction model to explain regioselectivity patterns observed in the reactions of certain arynes, especially heterocyclic arynes such as indolynes.^{5,6} Although historically avoided because of their high reactivities, a revival of interest in the chemistry of benzyne has occurred in recent decades and benzyne itself may now be exploited in a variety of efficient transformations.⁸ Garnering an improved understanding of the reactivity of substituted benzyne should not only facilitate their use in complexity-generating reactions, but may also explain reactivity trends observed over several decades of prior study.

One particular class of substituted benzyne known to react with significant regioselectivities are 3-substituted benzyne (**1**, Figure 19).^{8,9} More specifically, when X is an inductively electron-withdrawing group (e.g., methoxy or halide), nucleophilic attack at C1 is preferred.¹⁰ This leads to the formation of *meta*-substituted products **2** rather than *ortho*-

substituted adducts **3**. This has been explained by several models. In the *Charge-Controlled Model*,¹¹ the X group polarizes the triple bond, and nucleophilic addition occurs at the site of greatest positive charge.¹² A related model, based on NBO electron densities of in-plan π -orbitals has been advocated by Ikawa, Akai, and coworkers.^{9c,d} Alternatively, nucleophilic attack at C1 might be dictated by steric effects (*Steric Model*).³ Finally, our groups have shown that the regioselectivities of reactions of hetarynes and other aryne are controlled by *Aryne Distortions*, where a substituent causes a geometrical distortion such that the geometry of the aryne resembles the transition state for nucleophilic attack on one of the carbons.⁵ Each of these models provides a useful mnemonic to predict aryne regioselectivities, but the importance of the different factors emphasized by each of these models has not been unambiguously determined. We report a systematic experimental and theoretical study of 3-substituted aryne **1**, where X = halide or methoxy, which demonstrates that regioselectivities for these aryne are predominantly controlled by aryne distortions. Moreover, we showcase the synthetic utility of 3-haloarynes for the efficient synthesis of heterocyclic compounds using a tandem aryne trapping / cross-coupling sequence.

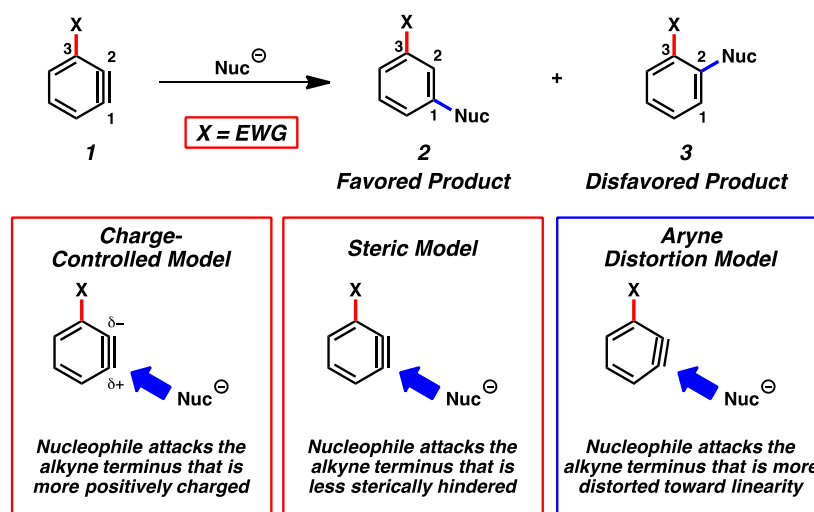


Figure 19. Charge-controlled, steric, and aryne distortion models.

Results and Discussion

Aryne Distortion versus Steric Factors. We first performed computational geometry optimizations of the 3-substituted benzyne **1a–1e** shown in Figure 20. Calculations were carried out using DFT methods (B3LYP/6-311+G(d,p) and LANL2DZ for Br and I atoms). We also studied these arynes and reactants with M06-2X and MP2 and these results are reported and discussed in the SI.^{13,14,15,16} The SI also provides structural and charge information for each substituted benzyne. Methoxybenzyne (**1a**) is well known to react with a high degree of regioselectivity for attack at C1⁸ and serves as a useful point of comparison to the corresponding haloarynes **1b–1e**. Regarding the *Aryne Distortion Model*, a simplified view of this model allows one to make predictions based on an analysis of an optimized geometry of the aryne.^{5b,17} The 3-methoxybenzyne (**1a**) shows significant distortion; there is a 15° difference in internal angles between C1 and C2. Nucleophilic addition is favored at the more linear terminus, C1, as the transition state distortion energy for attack at this site is lowest.⁴ Halobenzyne **1b–1e** are all distorted in a similar manner and are all predicted to undergo preferential attack at C1. The degree of regioselectivity is expected to decrease as a function of the electronegativity of the halide going from 3-fluorobenzyne (**1b**) to 3-iodobenzyne (**1e**), as a consequence of decreased distortion. Although reactions of 3-haloarynes are well known in the literature,^{1,18} a systematic study of reactions involving **1b–1e** has not been performed previously.

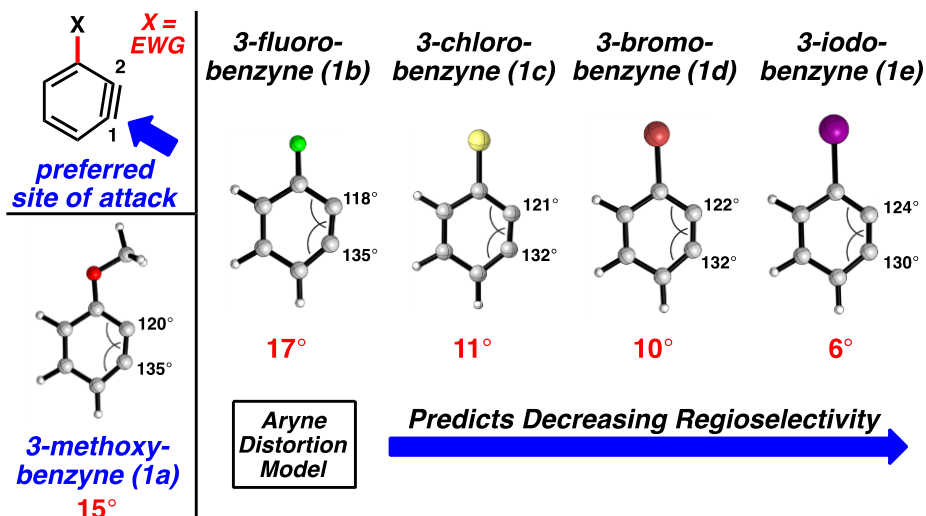


Figure 20. Geometry-optimized structures of 1a–1e (B3LYP) and regioselectivity predictions for nucleophilic attack based on the aryne distortion model.

The regioselectivities of reactions of **1a–1e** using *N*-methylaniline as the trapping agent were determined using both computations and experiments (Table 5). The results vary from exclusive attack at C1 for OMe and F, high selectivity with Cl, and less pronounced selectivity with Br and I. Transition state modeling was performed using DFT calculations (B3LYP) for the addition of *N*-methylaniline to C1 or C2 for each aryne. The $\Delta\Delta G^\ddagger$ values predict that nucleophilic addition to 3-methoxybenzyne (**1a**) and 3-fluorobenzyne (**1b**) should be highly regioselective (entries 1 and 2). Decreased regioselectivity was predicted for **1c–1e** (entries 3–5), consistent with the *Aryne Distortion Model* (see Figure 20). After accessing suitable silyltriflate precursors **4a–4e**,^{19,20} we verified the computational predictions experimentally.²¹ The *Steric Model* was deemed inconsequential based on our results and a comparison to A-values, which are 0.15 (fluoride), 0.43 (chloride), 0.38 (bromide), and 0.43 (iodide).²² The highest selectivity for attack at C1 is observed for the smallest substituent, fluoro **4b**. Consequently steric effects are not dictating regioselectivities in reactions of 3-halobenzyne. Previous studies of 3-silylarynes have also shown that steric effects can be outweighed by other factors (i.e., distortion),^{6,9a,9b} despite the fact that trialkylsilyl groups have A-values greater than 2.

Table 5: Addition of *N*-methylaniline to various benzenes.^a

Entry	4a-e	Computations (ratio 2 : 3)	Yield (ratio 2 : 3) ^b
1 ^a	4a X = OMe	$\Delta\Delta G^\ddagger = 5.2$ kcal/mol (>500 : 1)	94% (2a formed exclusively)
2	4b X = F	$\Delta\Delta G^\ddagger = 4.1$ kcal/mol (>500 : 1)	80% (2b formed exclusively)
3	4c X = Cl	$\Delta\Delta G^\ddagger = 2.4$ kcal/mol (57 : 1)	66% (>20 : 1)
4	4d X = Br	$\Delta\Delta G^\ddagger = 1.4$ kcal/mol (11 : 1)	67% (13 : 1)
5	4e X = I	$\Delta\Delta G^\ddagger = 1.7$ kcal/mol (19 : 1)	57% (9 : 1)

^a Conditions: see supporting information. Computed ratios obtained from Boltzmann factors using B3LYP/6-31G(d) free energies including Conductor-Like Polarizable Continuum Model (CPCM) solvation by MeCN. ^b Experimental yields and ratios are the average of three experiments and were determined by ¹H NMR analysis using hexamethylbenzene as an external standard.

The same conclusion was drawn for the trapping of arynes **1a–1e** in azide cycloaddition reactions (Table 6).²³ Consistent with computational predictions, 3-methoxybenzyne (**1a**) and 3-fluorobenzyne (**1b**) react with high regioselectivity (entries 1 and 2, respectively). A sequential decrease in regioselectivity was observed for reactions of arynes **1c–1e**, as the electron-withdrawing effects of the halide substituents decrease from F to Cl to Br to I (entries 3–5, respectively).²⁴

Table 6: Cycloaddition of benzylazide with various benzyne.^a

Entry	4a-e	Computations (ratio 5 : 6)	Yield (ratio 5 : 6) ^b
1 ^a	4a X = OMe	$\Delta\Delta G^\ddagger = 3.4$ kcal/mol (292 : 1)	94% (5a formed exclusively)
2	4b X = F	$\Delta\Delta G^\ddagger = 2.5$ kcal/mol (71 : 1)	68% (5b formed exclusively)
3	4c X = Cl	$\Delta\Delta G^\ddagger = 1.4$ kcal/mol (10 : 1)	53% (16 : 1)
4	4d X = Br	$\Delta\Delta G^\ddagger = 1.2$ kcal/mol (8 : 1)	45% (12 : 1)
5	4e X = I	$\Delta\Delta G^\ddagger = 0.9$ kcal/mol (5 : 1)	43% (6 : 1)

^a Conditions: see supporting information. Computed ratios obtained from Boltzmann factors using B3LYP/6-31G(d) free energies including CPCM solvation by MeCN; methylazide was used as a model for benzylazide to simplify computational studies. ^b Experimental yields and ratios are the average of three experiments and were determined by ¹H NMR analysis using hexamethylbenzene as an external standard.

The Role of Charges. Having ruled out the importance of the *Steric Model*, we next assessed the role of charges, which have often been used to explain aryne regioselectivities.³ Indeed it is quite natural to think of the greater negative charge at the carbon with the smallest angle because that carbon will have more s character in the orbital involved in the in-plane π bond. However, we will argue here that this charge polarization is insufficient to account for observed regioselectivities.

The charge on an atom is not an observable parameter, and there have been different definitions made of charges on atoms. Each of these depends on the definition of the boundaries separating atoms in molecules. Charges derived from a natural bond orbital analysis have been found to be very useful,²⁵ and we use NBO charges here. Figure 21 shows computed Natural Bond Orbital (NBO) charges of *ortho*-benzyne (**7**), which were obtained computationally using

B3LYP/6-311+G(d,p). The charges found on the triple bond carbons of *ortho*-benzyne (**7**) are +0.02. This charge is negligible, and the high electrophilic reactivity of benzyne is not a result of charge effects. For comparison, NBO charges were computed at the same level of theory for acetone. A charge of 0.57 was found for the electrophilic carbon, in agreement with its polarized double bond. Acetone is, however, much less reactive than the nonpolar benzyne, so the magnitude of charge is not an index of reactivity. We next studied the charges of substituted arynes that might have polarized triple bonds to determine if the charges are related to regioselectivity.

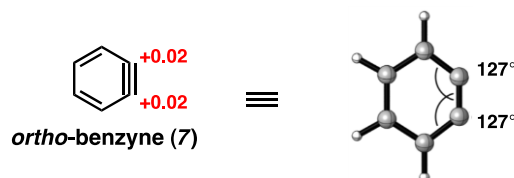
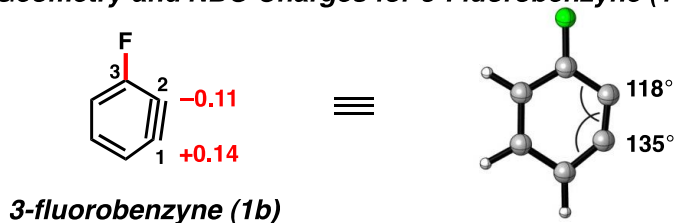


Figure 21. Geometry-optimized structures and NBO charges for benzyne (7) (B3LYP).

Since many authors use charges for qualitative interpretations, it behooves us to provide a quantitative assessment of such a model and not just invoke the view that theoreticians deny the validity of atomic charges. The charges of 3-fluorobenzyne (**1b**) are shown in Figure 22. The geometry-optimized structure reveals NBO charges of +0.14 and -0.11 for C1 and C2 respectively. To determine if this charge polarization could be reasonable for the observed regioselectivities, a simple Coulombic interaction model was devised. A point charge of -1 was placed in the benzyne plane at a distance of 2.4 Å from C1. This model is an exaggeration in the localization of charge, but is the extreme case of an anionic nucleophile. The position of the nucleophile charge bisects the C6-C1-C2 angle at C1. The distance between the point charge and C2 is 3.1 Å in this model. Coulomb's law was used to compute the net interaction energy between the point negative charge and benzyne with these charges.²⁶ This gives an attractive energy of 0.2 kcal/mol at C1 using a dielectric constant of 36, which is appropriate for acetonitrile. The corresponding analysis with a point negative charge 2.4 Å from C2 and a dielectric constant

of 36 gives an interaction energy of 0.0 kcal/mol. The electrostatic energy difference for the two modes of attack differ by 0.2 kcal/mol, whereas moderate to high regioselectivities are observed in reactions of all 3-halobenzyne, in addition to computed energy differences that are typically several kcal/mol. We conclude that electrostatic effects are nearly negligible, and in any case too small to explain the regioselectivities. Furthermore, the explanation of regioselectivities of reactions such as cycloadditions by electrostatic effects have long been discredited.²⁷

Geometry and NBO Charges for 3-Fluorobenzynes (1b)



Point Charges Adjacent to C1 and C2 of 3-Fluorobenzynes (1b)

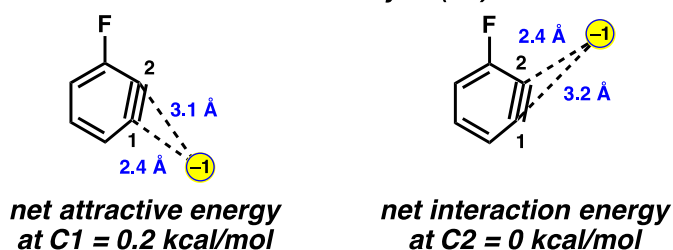


Figure 22. Geometry-optimized structure and NBO charges for 3-fluorobenzynes (1b) (B3LYP) and point charge analysis.

We also calculated the electrostatic potentials for interaction of a charge with the full 3-fluorobenzynes (1b) to compare to our simple Coulombic model, again with a dielectric constant of 36, for acetonitrile. These values are 0.0 kcal/mol at C1 and repulsive by 0.2 kcal/mol at C2. The 0.2 kcal/mol preference for attack at C1 is favored in both models and is not enough to explain the observed regioselectivities. We also performed calculations of this type for 3-chlorobenzynes (1c). While our simple Coulombic model predicts a 0.1–0.2 kcal/mol preference for attack at C1

(with the charge placed anywhere from 2.0-2.4 Å from the carbon being attacked), the full electrostatic potential calculation predicts a modest 0.2–0.3 kcal/mol preference for attack at C1.

Two additional calculations involving **1b** were performed to probe the origin of the small charge polarization shown from NBO charges or electrostatic potentials (Figure 23). First, we replaced the F substituent with H, but maintained the geometry of **1b**. Despite not having the electron-withdrawing substituent, significant charge polarization was observed (+0.10 for C1 and –0.05 for C2) in the distorted molecule. The negative charge is preferred on C2, the carbon with the smaller angle and greater s character in the in-plane π bond. Additionally, calculations were performed on **1b**, but with the geometry restricted to that of benzyne (i.e., 127° internal angle at C1 and C2). Charges of +0.07 and –0.05 for C1 and C2, respectively, were observed. Here the charge polarization due to pure induction without rehybridization is one-half that observed when there is geometrical relaxation. Figure 23 also shows color-coded electrostatic potentials on the isodensity surfaces for benzyne (**7**) and 3-fluorobenzyne (**1b**), in addition to those for benzyne constrained to the 3-fluorobenzyne geometry and for 3-fluorobenzyne constrained to the benzyne geometry. These geometrical constraints have a meaningful influence on the relative electrostatic potential at C1 and C2.

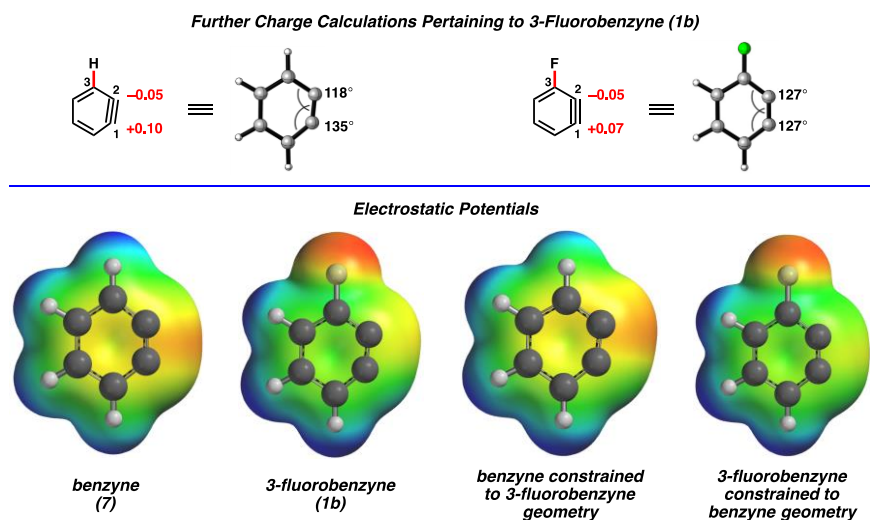


Figure 23. NBO charges for 1b separated based on distortion or inductive effects. Electrostatic potentials of benzyne (**7**) and 3-fluorobenzyne (**1b**). Also shown are electrostatic potentials for benzyne with 3-fluorobenzyne geometry and 3-fluorobenzyne with benzyne geometry (red indicates the lowest electrostatic potential energy, whereas blue indicates the highest).

These findings show that the aryne distortion and inductive effects are synergistic factors contributing to the overall charge polarization. Of course, there is no geometrical distortion until a substituent is added. This geometrical distortion and the small charge polarization are caused by the electronegativity of the substituent. According to Bent's Rule,²⁸ the bond from C2 to C3 of the aryne will involve a hybrid orbital on C2 with more p character than that on C3. This releases electron density to C3 and its attached electronegative atom. This decreases the C2 bond angle from its natural 127° (see Figure 21) toward 90°. The in-plane π orbital between C1 and C2 is polarized toward C2 since C2 will have more s character.

A similar charge analysis was performed for 3-trimethylsilylbenzyne (**8**), as shown in Figure 24.^{6,29} Notably, the distortion and partial charges for **8** are reversed in comparison to 3-haloarynes. The charges at C1 and C2 are -0.04 and +0.09, respectively. By replacing the trimethylsilyl group with H, but maintaining the geometric constraints found in **8**, the charge distribution was found to be similar (-0.03 and +0.07 at C1 and C2, respectively). Most of the

polarization is the result of distortion and rehybridization codified in Bent's rule. Finally, we gauged the electronic influence of the trimethylsilyl group on charge by performing calculations on **8** but with the undistorted geometry of benzyne. Only small charges of -0.01 and $+0.04$ at C1 and C2, respectively, were observed.

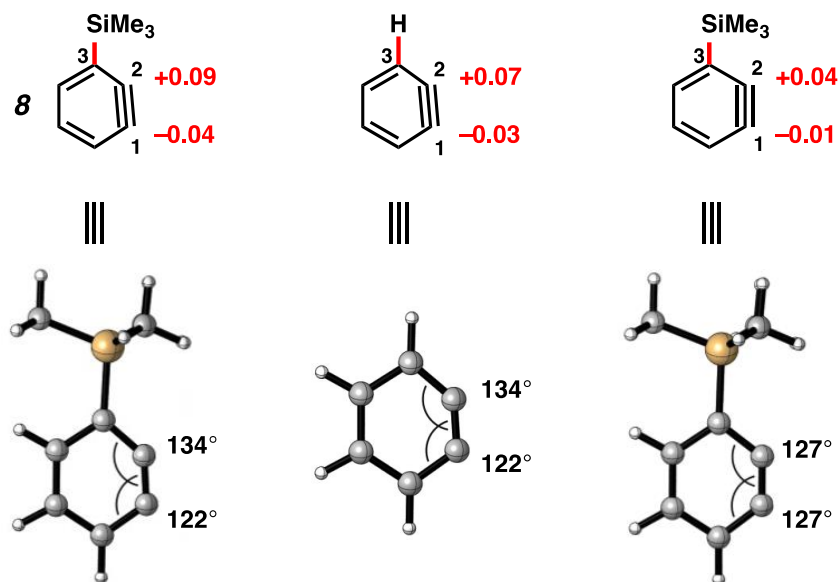


Figure 24. Geometry-optimized structure and NBO charges for 3-trimethylsilylbenzyne (8), in addition to charge distribution due to distortion or inductive effects.

These results underscore that the geometrical distortion present in unsymmetrical arynes, and rehybridization that accompanies this distortion, largely contributes to observed charge polarization. The small degree of charge polarization is not the sole cause of the observed regioselectivities, and we conclude that the *Charge-Controlled Model* is not sufficient to explain the regioselectivities observed in these unsymmetrical aryne reactions, particularly in the case of 3-halobenzenes. It does, of course, give a qualitatively correct prediction about selectivity, and might be considered a useful mnemonic for this reason. However, it is an example of the “right answer for the wrong reason”.

Ikawa, Akai, and coworkers have shown that there is a qualitative correspondence between the NBO electron density of the in-plane aryne π -orbital and the regioselectivity of

nucleophilic attack.^{9c,d} Attack occurs at the site of lower NBO electron density. This is presumably related to the lesser closed-shell repulsion that occurs upon overlap of the occupied orbitals of the nucleophile and aryne.

Transition State Analysis and Aryne Distortion. In previous articles,⁵ we have shown that the reactant distortion controls regioselectivities by influencing the distortion energies for attack at C1 vs C2. Figure 25 shows the geometry of the transition state for methyl azide attack on benzyne (**7**). As described earlier, the nucleophilic attack of N1 of the azide occurs at the relatively more linear angle on the benzyne where the π orbital has more p character. The 131° angle is similar to that in benzyne itself (i.e., 127°). The weaker interaction is at the carbon with the angle of 121°.

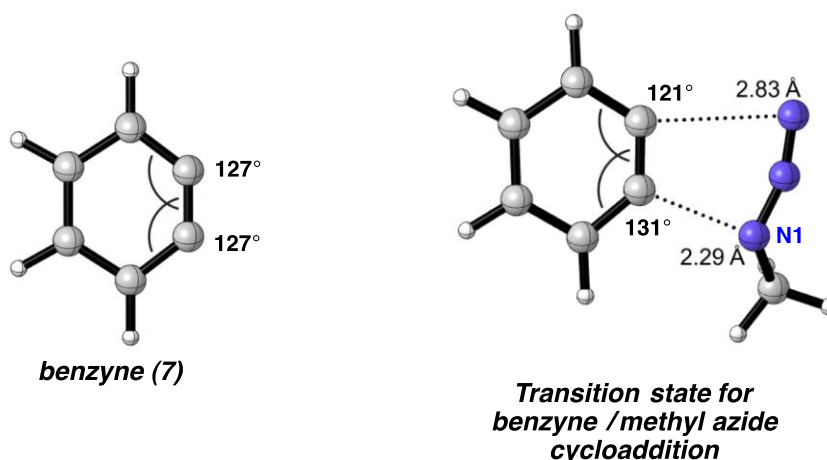


Figure 25. Benzyne internal angles and transition state for methyl azide / benzyne cycloaddition.

The regioselectivity trends for the reactions of halobenzenes are explained by analysis of the competing transition states, as shown in Figure 26 for 3-fluorobenzene (**1b**) and 3-chlorobenzene (**1c**). In the case of 3-fluorobenzene (**1b**), **TS1** and **TS3** are favored over **TS2** and **TS4**, respectively. The aryne distortion⁵ in each of the favored transition states closely resembles the distortion already present in the ground state of aryne **1b**. Initial bond formation occurs at C1;

the π orbital at this site possesses greater p-character due to the aryne distortion. In the preferred transition states **TS1** and **TS3**, the distortion caused by fluorine is slightly increased by the attacking azide, but fluorine and the azide are distorting in conflicting manners for the disfavored transition state, **TS4**.

The reactions involving 3-chlorobenzynes (**1c**) are analogous. **TS5** and **TS7** are favored over **TS6** and **TS8**, respectively due to the distortion present in **1c**. As the atomic radius and A-values for Cl (79 pm and 0.43, respectively) are significantly larger compared to those of F (42 pm and 0.15, respectively), steric effects should be considered as well in the disfavored transition states, **TS6** and **TS8**. Comparisons of **TS2** and **TS6** show that the trajectories for approach of the *N*-Me-aniline nucleophile is nearly identical; additionally, the forming C–N bond distances are nearly the same in both cases (2.12 Å and 2.16 Å, respectively). As such, there is no evidence for steric repulsions by chlorine in **TS2** or **TS6**. The comparison of **TS4** and **TS8** reveal slightly different transition states, but the shorter distance of the forming C–N bond at C2 in **TS8** (2.52 Å in **TS4** vs. and 2.35 Å in **TS8**) suggests that steric effects are not a major controlling factor in the reaction of 3-chlorobenzynes. Moreover, as mentioned earlier, if steric factors were the guiding factor in reactions of 3-halobenzenes, a higher preference for reaction at C1 would be expected in trapping experiments of 3-chlorobenzynes (**1c**) than with 3-fluorobenzynes (**1b**). Experimentally and computationally the opposite trend is observed. We can conclude that although steric factors and charge distribution can make small contributions to the observed regioselectivities, the aryne distortion and the associated transition state distortion play key roles in determining regioselectivity in these trapping experiments.

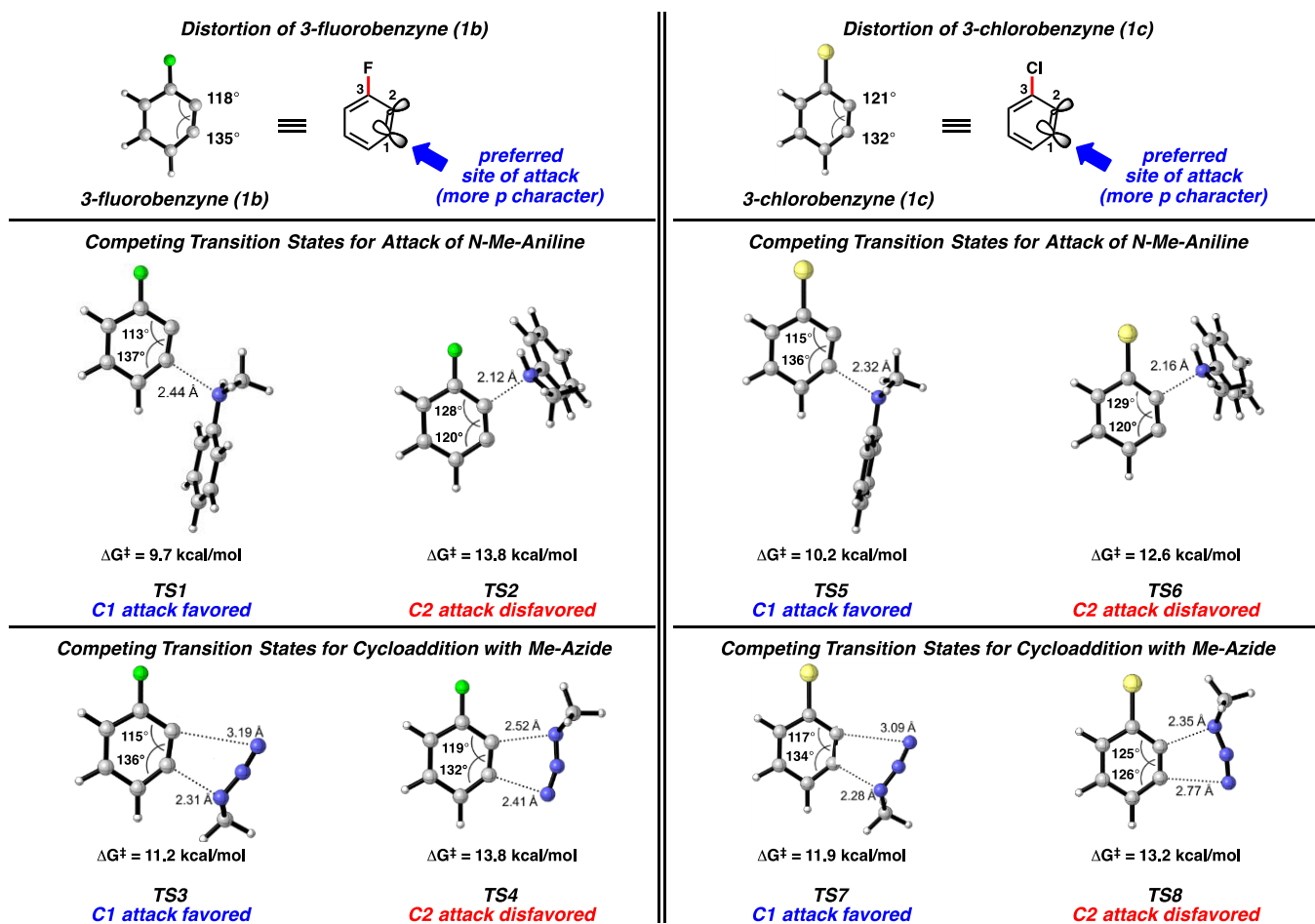


Figure 26. Competing transition states for the addition of *N*-methylaniline and methyl azide to 3-fluorobenzynes (1b) and 3-chlorobenzynes (1c). Transition states were located using B3LYP/6-311+G(d).

Efficient Synthesis of Heterocyclic Scaffolds. Although trapping experiments of 3-haloarynes have been reported,^{8,18} the general synthetic utility of these species has remained underexplored. We hypothesized that 3-halosilyltriflates (and, in turn, the corresponding arynes) could serve as valuable building blocks for the synthesis of functionalized heterocycles. Specifically, it was envisioned that a sequence involving aryne cycloaddition³⁰ and subsequent metal-catalyzed cross-coupling³¹ could allow for the conversion of aryne precursors **4** to decorated heterocycles **10** in just two steps. In this scenario, the halide would first be used to govern aryne distortion; cycloaddition of the aryne would then give rise to a heterocyclic product

9 with regiocontrol. Finally, the halide would be used as a cross-coupling partner to construct a new C–C or C–N bond and deliver products **10**.

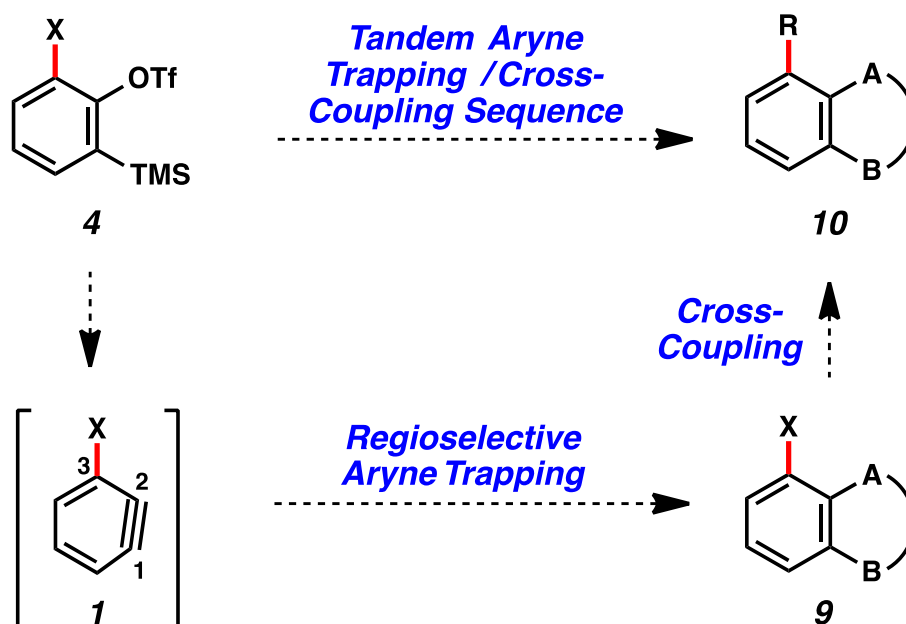


Figure 27. Tandem Aryne Trapping / Cross-Coupling Sequence.

We elected to synthesize C4-substituted benzotriazoles as a means to validate the sequence suggested in Figure 27. C4-substituted benzotriazoles have been studied as drug candidates, for example in the search for JNK1 inhibitors.³² As described earlier, the 3-haloarynes readily undergo cycloaddition with benzylazide to give benzotriazole products bearing halide substituents with significant regioselectivities (see Table 6). As a challenging test for the cross-coupling part of the sequence, we chose chlorobenzotriazole **5c** as the test substrate. Although cross-couplings of aryl chlorides are generally less common compared to couplings of aryl bromides and iodides, conditions for aryl chloride couplings are available. In fact, nickel catalysis can be used for aryl chloride couplings using conventional ligands, including readily available phosphines.³³ As shown in Figure 28, **5c** could be employed in the Ni-catalyzed Suzuki–Miyaura coupling with heteroaryl boronic acids.³⁴ The transformation proceeds in the green solvent 2-Me-THF, and gives products **11a** and **11b** in good yields. Additionally, the Ni-catalyzed amination³⁵

of **5c** proceeded smoothly to produce aminobenzotriazoles **12a** and **12b**, also in synthetically useful yields. It should be emphasized that the Ni-catalyzed C–C and C–N bond formations: a) utilize air-stable precatalysts, and thus are carried out on the benchtop, b) are tolerant of the benzotriazole motif, and c) are tolerant of a variety of other heterocycles, as demonstrated by the formation of products **11a**, **11b**, **12a**, and **12b**. Therefore, our results not only validate the utility of 3-haloarynes for the construction of functionalized heterocycles, but also showcase the growing value of nickel catalysis in modern cross-coupling reactions.³³

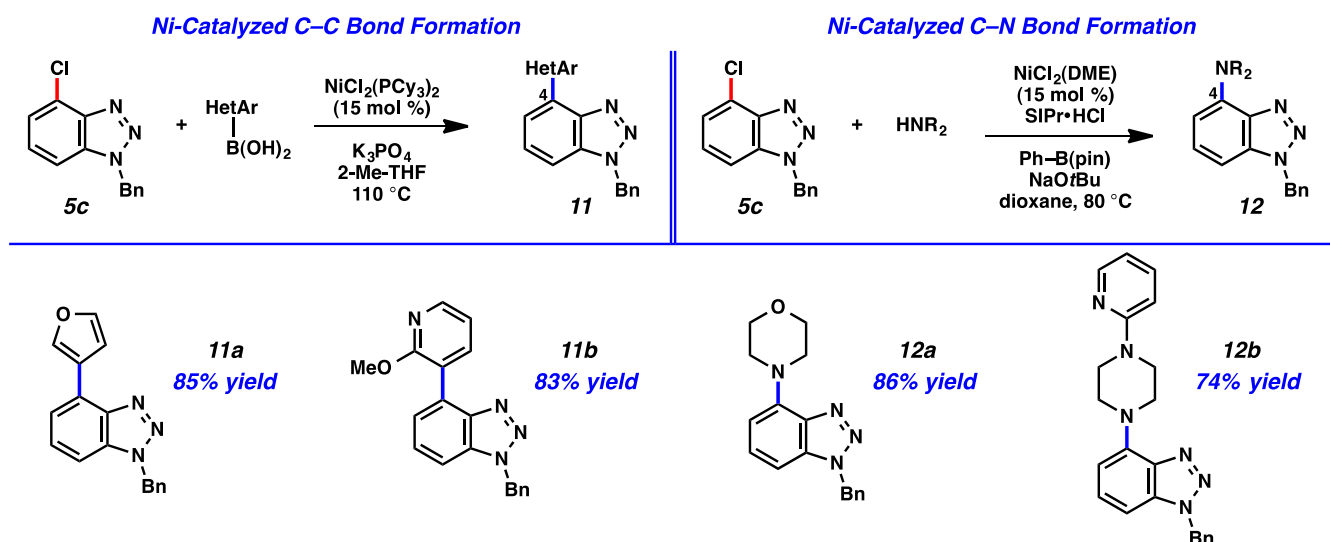


Figure 28. Nickel-catalyzed C–C and C–N bond forming reactions for the synthesis of functionalized benzotriazoles 11 and 12.

Conclusion

We have compared three commonly used models for rationalizing regioselectivity in reactions of 3-haloarynes. Our experimental and computational study shows that regioselectivity in these systems is explained by the *Aryne Distortion Model*. Moreover, by virtue of the tandem aryne trapping / cross-coupling sequence developed, we have demonstrated the synthetic utility of 3-haloarynes for the assembly of functionalized heterocyclic compounds. We expect that these

studies of reactivity, regioselectivity, and synthetic applications will help propel the use of unsymmetrical arynes in complexity-generating transformations.

Acknowledgements: The authors are grateful to the NIH-NIGMS (R01 GM090007 to N. K. G.), the National Science Foundation (CHE-1361104 to K.N.H.), Boehringer Ingelheim, Bristol–Myers Squibb, DuPont, Eli Lilly, Amgen, AstraZeneca, Roche, the A. P. Sloan Foundation, the S. T. Li Foundation, the Dreyfus Foundation, the University of California, Los Angeles, and the UCLA Cota Robles Fellowship Program (J. M. M.) for financial support. This work used the Extreme Science and Engineering Discovery Environment (XSEDE), which is supported by the National Science Foundation (OCI-1053575) along with the UCLA Institute of Digital Research and Education (IDRE). We thank the Garcia–Garibay laboratory (UCLA) for access to instrumentation. These studies were supported by shared instrumentation grants from the NSF (CHE-1048804) and the National Center for Research Resources (S10RR025631).

Supporting information available: Detailed experimental procedures, as well as characterization data for all new compounds is available. Computational data and Cartesian coordinates of all structures are also provided. This material is available free of charge via the Internet at <http://pubs.acs.org>.

Reference

(1) For the application of distortion energies to regioselectivity of cycloaddition reactions, see: (a) Ess, D. H.; Houk, K. N. *J. Am. Chem. Soc.* **2007**, *129*, 10646–10647. (b) Ess, D. H.; Houk, K. N. *J. Am. Chem. Soc.* **2008**, *130*, 10187–10198. (c) Lam, Y.-h.; Cheong, P. H.-Y.; Blasco Mata, J. M.; Stanway, S. J.; Gouverneur, V.; Houk, K. N. *J. Am. Chem. Soc.* **2009**, *131*, 1947–1957. (d) Hayden, A. E.; Houk, K. N. *J. Am. Chem. Soc.* **2009**, *131*, 4084–4089. (e) Schoenebeck, F.; Ess, D. H.; Jones, G. O.; Houk, K. N. *J. Am. Chem. Soc.* **2009**, *131*, 8121–8133. (f) Osuna, S.; Houk, K. N. *Chem. Eur. J.* **2009**, *15*, 13219–13231. (g) Paton, R. S.; Kim, S.; Ross, A. G.; Danishefsky, S. J.; Houk, K. N. *Angew. Chem. Int. Ed.* **2011**, *50*, 10366–10368. (h) Lan, Y.; Wheeler, S. E.; Houk, K. N. *J. Chem. Theory Comput.* **2011**, *7*, 2104–2111. (i) Liang, Y.; Mackey, J. L.; Lopez, S. A.; Liu, F.; Houk, K. N. *J. Am. Chem. Soc.* **2012**, *134*, 17904–17907. (j) Gordon, C. G.; Mackey, J. L.; Jewett, J. C.; Sletten, E. M.; Houk, K. N. *J. Org. Chem.* **2013**, *78*, 1576–1582. (l) Lopez, S. A.; Houk, K. N. *J. Org. Chem.* **2013**, *78*, 1778–1783. (m) Kamber, D. N.; Nazarova, L. A.; Liang,

Y.; Lopez, S. A.; Patterson, D. M.; Shih, H.-W.; Houk, K. N.; Prescher, J. A. *J. Am. Chem. Soc.* **2013**, *135*, 13680–13683. (n) Liu, F.; Paton, R. S.; Kim, S.; Liang, Y.; Houk, K. N. *J. Am. Chem. Soc.* **2013**, *135*, 15642–15649. (o) Yang, J.; Liang, Y.; Šečkutė, J.; Houk, K. N.; Devaraj, N. K. *Chem. Eur. J.* **2014**, *20*, 3365–3375. (p) Hong, X.; Liang, Y.; Griffith, A. K.; Lambert, T. H.; Houk, K. N. *Chem. Sci.* **2014**, *5*, 471–475. (q) Liu, F.; Liang, Y.; Houk, K. N. *J. Am. Chem. Soc.* **2014**, *136*, 11483–11493. (r) Cao, Y.; Liang, Y.; Zhang, L.; Osuna, S.; Hoyt, A.-L. M.; Briseno, A. L.; Houk, K. N. *J. Am. Chem. Soc.* **2014**, *136*, 10743–10751. (s) Hong, X.; Liang, Y.; Brewer, M.; Houk, K. N. *Org. Lett.* **2014**, *16*, 4260–4263.

(2) For the application of distortion energies to regioselectivity of palladium-catalyzed cross coupling reactions, see: (a) Legault, C. Y.; Garcia, Y.; Merlic, C. A.; Houk, K. N. *J. Am. Chem. Soc.* **2007**, *129*, 12664–12665. (b) Garcia, Y.; Schoenebeck, F.; Legault, C. Y.; Merlic, C. A.; Houk, K. N. *J. Am. Chem. Soc.* **2009**, *131*, 6632–6639.

(3) For the application of distortion energies to understanding selectivities in C–H functionalization reactions, see: (a) Zou, L.; Paton, R. S.; Eschenmoser, A.; Newhouse, T. R.; Baran, P. S.; Houk, K. N. *J. Org. Chem.* **2013**, *78*, 4037–4048. (b) Green, A. G.; Liu, P.; Merlic, C. A.; Houk, K. N. *J. Am. Chem. Soc.* **2014**, *136*, 4575–4583.

(4) For the application of the distortion / interaction model to explain stereoselectivity in epoxidation reactions, see: Kolakowski, R. V.; Williams, L. J. *Nat. Chem.* **2010**, *2*, 303–307.

(5) For early studies and reviews regarding the aryne distortion model, see: (a) Cheong, P. H.-Y.; Paton, R. S.; Bronner, S. M.; Im, G.-Y. J.; Garg, N. K.; Houk, K. N. *J. Am. Chem. Soc.* **2010**, *132*, 1267–1269. (b) Im, G.-Y. J.; Bronner, S. M.; Goetz, A. E.; Paton, R. S.; Cheong, P. H.-Y.; Houk, K. N.; Garg, N. K. *J. Am. Chem. Soc.* **2010**, *132*, 17933–17944. (c) Bronner, S. M.; Goetz, A. E.; Garg, N. K. *Synlett* **2011**, *18*, 2599–2604. (d) Goetz, A. E.; Garg, N. K. *J. Org. Chem.* **2014**, *79*, 846–851.

(6) For the application of the aryne distortion model to 3-silylbenzynes, see: Bronner, S. M.; Mackey, J. L.; Houk, K. N.; Garg, N. K. *J. Am. Chem. Soc.* **2012**, *134*, 13966–13969.

(7) (a) van Zeist, W.-J.; Bickelhaupt, F. M. *Org. Biomol. Chem.* **2010**, *8*, 3118–3127. (b) Fernández, I.; Cossío, F. P.; Bickelhaupt, F. M. *J. Org. Chem.* **2011**, *76*, 2310–2314. (c) Fernández, I.; Bickelhaupt, F. M. *J. Comput. Chem.* **2012**, *33*, 509–516. (d) Fernández, I.; Sola, M.; Bickelhaupt, F. M. *Chem. Eur. J.* **2013**, *19*, 7416–7422. (e) Fernández, I.; Bickelhaupt, F. M. *Chem. Soc. Rev.* **2014**, *43*, 4953–4967.

(8) For pertinent reviews, see references 5c, 5d, and the following: (a) Pellissier, H.; Santelli, M. *Tetrahedron* **2003**, *59*, 701–730. (b) Wenk, H. H.; Winkler, M.; Sander, W. *Angew. Chem. Int. Ed.* **2003**, *42*, 502–528. (c) Sanz, R. *Org. Prep. Proced. Int.* **2008**, *40*, 215–291. (d) Chen, Y.; Larock, R. C. In *Modern Arylation Methods*; L. Ackermann, Wiley-VCH: Weinheim, 2009; pp 401–473. (e) Tadross, P. M.; Stoltz, B. M. *Chem. Rev.* **2012**, *112*, 3550–3577. (f) Gampe, C. M.; Carreira, E. M. *Angew. Chem. Int. Ed.* **2012**, *51*, 3766–3778. (g) Yoshida, H.; Takaki, K. *Synlett* **2012**, *23*, 1725–1732. (h) Dubrovskiy, A. V.; Markina, N. A.; Larock, R. C. *Org. Biomol. Chem.* **2013**, *11*, 191–218. (i) Wu, C.; Shi, F. *Asian J. Org. Chem.* **2013**, *2*, 116–125. (j) Hoffmann, R. W.; Suzuki, K. *Angew. Chem. Int. Ed.* **2013**, *52*, 2655–2656. (k) Bhunia, A.; Biji, A. T. *Synlett* **2014**, *25*, 608–614.

(9) For studies of 3-silylarynes or 3-borylbenzynes, which are not the major focus of the current study, see reference 6 and the following: (a) Ikawa, T.; Nishiyama, T.; Shigeta, T.; Mohri, S.; Morita, S.; Takayanagi, S.-i.; Terauchi, Y.; Morikawa, Y.; Takagi, A.; Ishikawa, Y.; Fujii, S.; Kita, Y.; Akai, S. *Angew. Chem. Int. Ed.* **2011**, *50*, 5674–5677. (b) Ikawa, T.; Takagi, A.; Goto, M.; Aoyama, Y.; Ishikawa, Y.; Itoh, Y.; Fujii, S.; Tokiwa, H.; Akai, S. *J. Org. Chem.* **2013**, *78*, 2965–2983. (c) Takagi, A.; Ikawa, T.; Kurita, Y.; Saito, K.; Azechi, K.; Egi, M.; Itoh, Y.; Tokiwa, H.; Kita, Y.; Akai, S. *Tetrahedron* **2013**, *69*, 4338–4352. (d) Takagi, A.; Ikawa, T.; Saito, K.; Masuda, S.; Ito, T.; Akai, S. *Org. Biomol. Chem.* **2013**, *11*, 8145–8150.

(10) For a recent study of a 3-alkoxycyclohexyne, see: Medina, J. M.; McMahon, T. C.; Jiménez-Osés, G.; Houk, K. N.; Garg, N. K. *J. Am. Chem. Soc.* **2014**, *136*, *Just Accepted Manuscript*, DOI: 10.1021/ja508635v.

(11) For examples involving the *Charge Distribution* and *Steric Models* to rationalize regioselectivities in trapping experiments of 3-substituted arynes, see: (a) Kessar, S. V. In *Comprehensive Organic Synthesis*; Trost, B. M.; Fleming, I. Eds.; Pergamon Press: Oxford, England, 1991; Vol. 4, pp 483–515. (b) Liu, Z.; Larock, R. C. *J. Org. Chem.* **2006**, *71*, 3198–3209. (c) Liu, Z.; Larock, R. C. *Org. Lett.* **2003**, *5*, 4673–4675. (d) Tadross, P. M.; Gilmore, C. D.; Bugga, P.; Virgil, S. C.; Stoltz, B. M. *Org. Lett.* **2010**, *12*, 1224–1227. (e) Yoshida, H.; Sugiura, S.; Kunai, A. *Org. Lett.* **2002**, *4*, 2767–2769. (f) Hamura, T.; Ibusuki, Y.; Sato, K.; Matsumoto, T.; Osamura, Y.; Suzuki, K. *Org. Lett.* **2003**, *5*, 3551–3554.

(12) In a somewhat related sense, it has also been argued that the presence of an adjacent inductively withdrawing group causes regioselectivity in aryne reactions due to stabilization of the developing carbanion, which we would be formed upon nucleophilic addition to the substituted benzyne. However, arynes undoubtedly react through very early transition states with low enthalpic barriers, so this explanation is inadequate.

(13) Calculations shown are at the B3LYP/6-311+G(d,p) level of theory and LANL2DZ for the Br and I atoms with tight convergence criteria and an ultrafine integration grid. Angles were also calculated at this level of theory. See the SI for calculations of angles of reactants and TSs with M06-2X and MP2. Because the potential energy surface of the reaction of **1b** has no maximum, a variational transition state search was performed to locate a saddle point. Although B3LYP overestimates the regioselectivities, it predicts the correct trend in reactivity.

(14) (a) Becke, A. D. *J. Chem. Phys.* **1993**, *98*, 5648–5652. (b) Lee, C.; Yang, W.; Parr, R. G. *Phys. Rev. B* **1988**, *37*, 785–789. (c) Vosko, S. H.; Wilk, L.; Nusair, M. *Can. J. Phys.* **1980**, *58*, 1200–1211. (d) Stephens, P. J.; Devlin, F. J.; Chabalowski, C. F.; Frisch, M. J. *J. Phys. Chem.* **1994**, *98*, 11623–11627.

(15) (a) Hay, P. J.; Wadt, W. R. J. *J. Chem. Phys.* **1985**, *82*, 270–283. (b) Wadt, W. R. J.; Hay, P. J. *J. Chem. Phys.* **1985**, *82*, 284–298. (c) Hay, P. J.; Wadt, W. R. J. *J. Chem. Phys.* **1985**, *82*, 299–310.

(16) Gaussian 09, Revision D.01, Frisch, M. J.; Trucks, G. W.; Schlegel, H. B.; Scuseria, G. E.; Robb, M. A.; Cheeseman, J. R.; Scalmani, G.; Barone, V.; Mennucci, B.; Petersson, G. A.; Nakatsuji, H.; Caricato, M.; Li, X.; Hratchian, H. P.; Izmaylov, A. F.; Bloino, J.; Zheng, G.; Sonnenberg, J. L.; Hada, M.; Ehara, M.; Toyota, K.; Fukuda, R.; Hasegawa, J.; Ishida, M.; Nakajima, T.; Honda, Y.; Kitao, O.; Nakai, H.; Vreven, T.; Montgomery, J. A., Jr.; Peralta, J. E.; Ogliaro, F.; Bearpark, M.; Heyd, J. J.; Brothers, E.; Kudin, K. N.; Staroverov, V. N.; Kobayashi, R.; Normand, J.; Raghavachari, K.; Rendell, A.; Burant, J. C.; Iyengar, S. S.; Tomasi, J.; Cossi, M.; Rega, N.; Millam, M. J.; Klene, M.; Knox, J. E.; Cross, J. B.; Bakken, V.; Adamo, C.; Jaramillo, J.; Gomperts, R.; Stratmann, R. E.; Yazyev, O.; Austin, A. J.; Cammi, R.; Pomelli, C.; Ochterski, J. W.; Martin, R. L.; Morokuma, K.; Zakrzewski, V. G.; Voth, G. A.; Salvador, P.; Dannenberg, J. J.; Dapprich, S.; Daniels, A. D.; Farkas, Ö.; Foresman, J. B.; Ortiz, J. V.; Cioslowski, J.; Fox, D. J. Gaussian, Inc., Wallingford CT, 2009.

(17) (a) Bronner, S. M.; Goetz, A. E.; Garg, N. K. *J. Am. Chem. Soc.* **2011**, *133*, 3832–3835. (b) Goetz, A. E.; Bronner, S. M.; Cisneros, J. D.; Melamed, J. M.; Paton, R. S.; Houk, K. N.; Garg, N. K. *Angew. Chem. Int. Ed.* **2012**, *51*, 2758–2762.

(18) For select examples of studies pertaining to 3-haloarynes, see ref 17a and the following: (a) Biehl, E. R.; Nieh, E.; Hsu, K. C. *J. Org. Chem.* **1969**, *34*, 3595–3599. (b) Moreau-Hochu, M. F.; Caubere, P. *Tetrahedron* **1977**, *33*, 955–959. (c) Ghosh, T.; Hart, H. *J. Org. Chem.* **1988**, *53*, 3555–3558. (d) Hart, H.; Ghosh, T. *Tetrahedron Lett.* **1988**, *29*, 881–884. (e) Wickham, P. P.; Reuter, K. H.; Senanayake, D.; Guo, H.; Zalesky, M.; Scott, W. J. *Tetrahedron Lett.* **1993**, *34*, 7521–7524. (f) Gokhale, A.; Scheiss, P. *Helv. Chem. Acta* **1998**, *81*, 251–267. (g) Goetz, A. E.; Garg, N. K. *Nat. Chem.* **2013**, *5*, 54–60. (h) Hendrick, C. E.; McDonald, S. L.; Wang, Q. *Org. Lett.* **2013**, *15*, 3444–3447. (i) Kirkham, J. D.; Delaney, P. M.; Ellames, G. J.; Row, E. C.; Harrity, J. P. A. *Chem. Commun.* **2010**, *46*, 5154–5156.

(19) Using Kobayashi's strategy, silyltriflates readily undergo conversion to the corresponding aryne upon treatment with fluoride sources; see: Himeshima, Y.; Sonoda, T.; Kobayashi, H. *Chem. Lett.* **1983**, *12*, 1211–1214.

(20) Silyltriflate **4a** was obtained from commercial sources. The syntheses of silyltriflates **4b–4e** are described in the SI. For an alternative synthesis of **4c**, see: (a) Hall, C.; Henderson, J. L.; Ernouf, G.; Greaney, M. F. *Chem. Commun.* **2013**, *49*, 7602–7604. For the prior synthesis of **4d**, see: (b) Dai, M.; Wang, Z.; Danishefsky, S. J. *Tetrahedron Lett.* **2008**, *49*, 6613–6616.

(21) For the addition of heteroatom nucleophiles to benzyne generated from silyltriflate precursors, see reference 11d.

(22) Although the atomic radii increase steadily from F to I, the corresponding A-values only increase from F to Cl, and then remain nearly constant for Cl, Br, and I. This is due to the increased C–X bond length as atom size increases.

(23) (a) Shi, F.; Waldo, J. P.; Chen, Y.; Larock, R. C. *Org. Lett.* **2008**, *10*, 2409–2412. (b) Campbell-Verduyn, L.; Elsinga, P. H.; Mirfeizi, L.; Dierckx, R. A.; Feringa, B. L. *Org. Biomol. Chem.* **2008**, *6*, 3461–3463.

(24) Given that reaction yields are not quantitative, and that computational free energies have some standard error, the predicted and experimental ratios should be taken with a grain of salt. Nonetheless, the general trends seen in the experimental and computation data of Tables 5 and 6 entirely correlate to predictions made by the aryne distortion model (i.e., highest selectivity is observed and calculated for the most distorted 3-haloaryne, **1b**, whereas the lowest selectivity is observed and calculated with the least distorted 3-haloaryne, **1e**).

(25) Weinhold, F.; Landis, C. R. *Discovering Chemistry with Natural Bond Orbitals*; John Wiley & Sons, Inc: Hoboken, New Jersey, 2012.

(26) The net attractive energy was calculated by separately determining the Coulombic interactions between the point charge and C1 and C2, using the aforementioned calculated NBO charges for **1b**, and then adding these values.

(27) Houk, K. N. *Acc. Chem. Res.* **1975**, *8*, 361–369.

(28) Bent, H. *Chem. Rev.* **1961**, *61*, 275–311.

(29) Although not the main focus of this study, it should be noted that steric effects are important in reactions of other unsymmetrical arynes, such as 3-silylbenzynes; for further discussion, see references 6 and 9.

(30) An array of aryne cycloaddition reactions are available in the literature using silyltriflate precursors; see reference 8.

(31) (a) Hassan, J.; Sevignon, M.; Gozzi, C.; Schulz, E.; Lemaire, M. *Chem. Rev.* **2002**, *102*, 1359–1469. (b) *Topics in Current Chemistry*, Vol. 219; Miyaura, N., Ed.; Springer Verlag: New York, 2002. (c) *Metal-Catalyzed Cross-Coupling Reactions*; Diederich, F., Meijere, A., Eds.; Wiley-VCH: Weinheim, 2004. (d) Corbet, J.; Mignani, G. *Chem. Rev.* **2006**, *106*, 2651–2710. (e) Negishi, E. *Bull. Chem. Soc. Jpn.* **2007**, *80*, 233–257. (f) *Application of Transition Metal Catalysis in Drug Discovery and Development: An Industrial Perspective*; Shen, H. C., Crawley, M. L., Trost, B. M., Eds.; John Wiley & Sons, Inc.: Hoboken, NJ, 2012

(32) Gong, L.; Jahangir, A.; Reuter, D. C. US Patent US2010160360A1, 2010.

(33) For recent reviews regarding Ni-catalyzed cross-couplings, see: (a) Rosen, B. M.; Quasdorf, K. W.; Wilson, D. A.; Zhang, N.; Resmerita, A.-M.; Garg, N. K.; Percec, V. *Chem. Rev.* **2011**, *111*, 1346–1416. (b) Li, B.-J.; Yu, D.-G.; Sun, C.-L.; Shi, Z.-J. *Chem. Eur. J.* **2011**, *17*, 1728–1759. (c) Mesganaw, T.; Garg, N. K. *Org. Process Res. Dev.* **2013**, *17*, 29–39. (d) Tasker, S. Z.; Standley, E. A.; Jamison, T. F. *Nature* **2014**, *509*, 299–309.

(34) For our previous studies of Ni-catalyzed Suzuki–Miyaura couplings, see: (a) Quasdorf, K. W.; Tian, X.; Garg, N. K. *J. Am. Chem. Soc.* **2008**, *130*, 14422–14423. (b) Quasdorf, K. W.; Riener, M.; Petrova, K. V.; Garg, N. K. *J. Am. Chem. Soc.* **2009**, *131*, 17748–17749. (c) Quasdorf, K. W.; Antoft-Finch, A.; Liu, P.; Silberstein, A. L.; Komaromi, A.; Blackburn, T.; Ramgren, S. D.; Houk, K. N.; Snieckus, V.; Garg, N. K. *J. Am. Chem. Soc.* **2011**, *133*, 6352–6363. (d) Ramgren, S. D.; Hie, L.; Ye, Y.; Garg, N. K. *Org. Lett.* **2013**, *15*, 3950–3953.

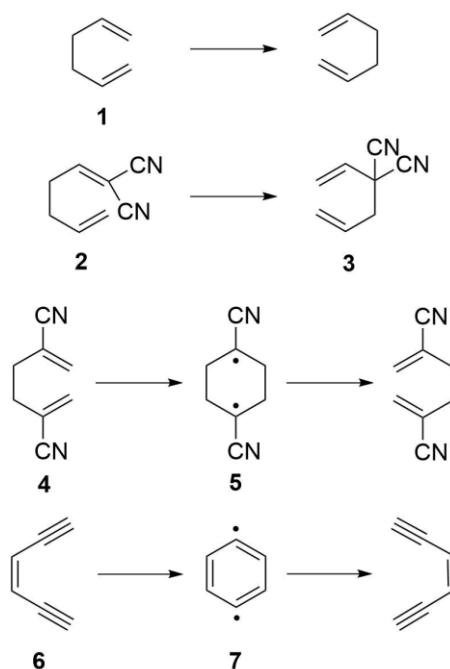
(35) For our previous studies of Ni-catalyzed amination reactions, see: (a) Mesganaw, T.; Silberstein, A. L.; Ramgren, S. D.; Fine Nathel, N. F.; Hong, X.; Liu, P.; Garg, N. K. *Chem. Sci.* **2011**, *2*, 1766–1771. (b) Ramgren, S. D.; Silberstein, A. L.; Yang, Y.; Garg, N. K. *Angew. Chem. Int. Ed.* **2011**, *50*, 2171–2173. (c) Hie, L.; Ramgren, S. D.; Mesganaw, T.; Garg, N. K. *Org. Lett.* **2012**, *14*, 4182–4185.

5. Molecular Dynamic Investigations of Cope Rearrangements and a Bergman Rearrangement: Probing the Nature of a Chameleonic Transition State

Introduction

Pericyclic reactions comprise a wide range of reactions that are extremely important in organic chemistry. While the synthetic utility of pericyclic reactions is incredibly important, they are also the subject of mechanistic interest, focused on the timing of bond formation and breaking. One such reaction is the Cope rearrangement. First discovered in 1940 by Arthur Cope and Elizabeth Hardy,¹ this prototypical 3,3-sigmatropic rearrangement now bears Cope's name.

Scheme 6. Reactions which illustrate the unique nature of the Cope and Bergman rearrangements.



Although the Cope rearrangement can be a pericyclic reaction in which the bonds are formed and broken in a concerted fashion around a circle, the nature of its mechanism depends heavily on its substitution (Scheme 6). While the parent Cope has been shown through Gajewski's measured secondary deuterium isotope effects to be nearly synchronous and

aromatic, the substituted 1,5-hexadiene systems in Scheme 6 give very asynchronous transition states.² Figure 29 illustrates the nature of the transition state due to substitution. Dicyano groups in the 3,3 position have a lot of bond breaking before much bond forming while 2,5-diphenyl give a large amount of bond forming but little bond breaking in the transition state.

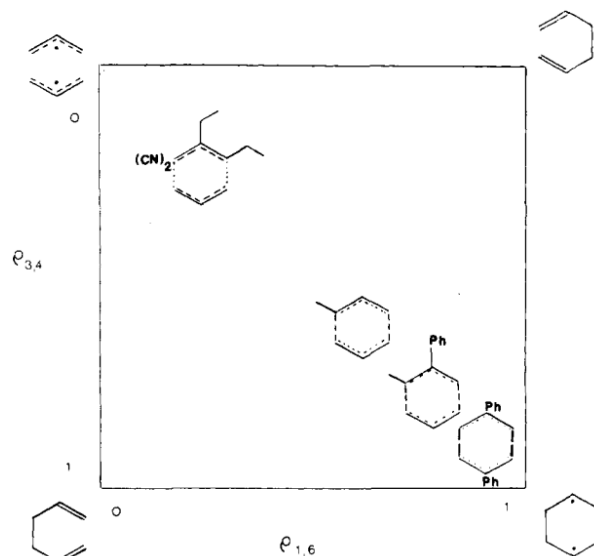


Figure 29. A More O'Ferrall-Jencks plot showing the effects of substitution on the timing of bond formations during a Cope rearrangement.

Depending on the substituent position, 3 possible mechanisms have been suggested for the Cope rearrangement by Doering and Roth.³ These include two allyl radicals, an “aromatic” concerted transition state and cyclohexane-1,4-diyl as shown in Figure 30. Much computational study has been done on both the parent systems and various substituted systems including the dicyanohexadienes.⁴ The results show a chameleonic nature of the transition state that depends on the substitution pattern of the 1,5-hexadiene. Similar to the results from secondary deuterium isotope effects, when substituents that stabilize the 1,4-diyl are present, the transition state is much more associative with the bond forming process much further along than the bond breaking process. When substituted by groups that stabilize the allyl radicals, the transition state becomes dissociative and the bond breaking process is much advanced in the transition state with little bond forming. In the 2,5-dicyano-1,5-hexadiene system, an intermediate is located on

the PES and a stepwise intermediate is found to be very similar in energy to the concerted transition state. This suggests that there might be some 1,4-diyli intermediate formed during the reaction; however, it may also simply be skipped, since the intermediate is only 4 kcal/mol lower in energy than the transition state that leads back to reactants or products.

This work uses molecular dynamics to probe the time spent as an intermediate for the 2,5-dicyano-1,5-hexadiene system and the number of trajectories that simply bypass the intermediate completely. We also look at the time spent in the transition zone and how synchronous or asynchronous the bond forming and breaking processes are in a time resolved mechanism for all systems studied. We performed molecular dynamics on the Bergman cyclization due to its highly associative nature and stabilized intermediate. It was of interest to investigate if it also had trajectories that could bypass the intermediate and continue on to products in a very short amount of time.

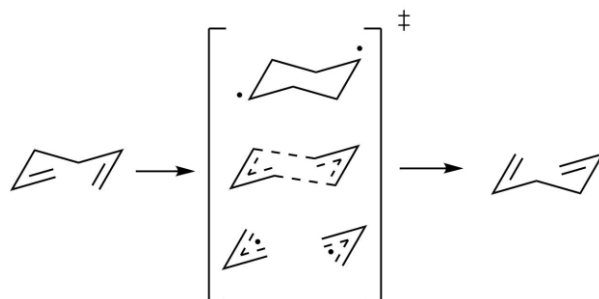


Figure 30: Three possible mechanisms for the Cope rearrangement.

Computational Methods

Quantum mechanical calculations were performed using Gaussian09 software.⁵ Optimized structures were obtained using the B3LYP⁶ and M06-2X density functionals.⁷ Frequency calculations were performed to verify all stationary points and intrinsic reaction coordinate calculations were performed when appropriate to verify the validity of the intermediate. All contour surfaces are generated by a 2d scan of the forming and breaking bonds near the

transition state. The grid starts at 1.5Å (1.3Å for the Bergman rearrangement) for each bond involved in the rearrangement and stops at 3.5Å. The step taken is 0.04Å. The energy used for the contour surfaces is electronic energy. All surfaces are created using an unrestricted wavefunction to make sure the structures that are diradical are correctly located.

Quasiclassical trajectories were initialized at the stepwise saddle points for each system in Scheme 6 (unless there is only a concerted TS) by transition state normal mode sampling.⁸ The software package used to initialize the TS structures is Daniel Singleton's PROGDYN.⁹ The sampling procedure in this work uses the harmonic frequencies and normal modes at the transition state to generate a set of coordinates and momenta that approximate a quantum mechanical Boltzmann distribution of vibrational levels on the transition state dividing surface.

All normal modes are given a Boltzmann sampling of energy for the 298.15 K along with its zero point energy. The initial velocities are given a random phase and sign and for the imaginary frequency. Trajectories are run in the forward and reverse direction to generate a full reactant to product trajectory. The time step used is 1 fs, and the propagation of the trajectories are done using the Verlet algorithm. The Hessian is updated every step. The trajectories are stopped once either reactants, products, or 500 fs is reached. Forming bonds are "formed" when they reach 1.6Å (1.5Å for the Bergman rearrangement) and breaking bonds are "broken" once they reach 3.5Å.

Results

Quantum mechanical investigations. Before running dynamic simulations, energy profiles and geometries were calculated for all systems studied. Comparison to experiments allows for validation of the chosen QM method. While we have studied simple substituted systems, experiments have been performed on similar systems with only slight differences.

Experimental studies to probe the mechanisms via secondary kinetic isotope effects, energies of activation, and entropies have been performed in systems similar to those in this

work.¹⁰ Activation barriers of the substituted hexadiene systems are presented alongside the computation results used for MD simulations in Table 7. For the substituted hexadiene systems, the experimental results show a lowering of 9-10 kcal/mol for the activation energy and ΔG^\ddagger for both the dissociative and associative substitution patterns. This is in good agreement with the B3LYP computational results that are used for molecular dynamics. For the 2,5-dicyano-1,5-hexadiene system, the transition state energy for both the concerted and stepwise mechanisms are nearly identical for electronic and enthalpic barriers, with only 0.4 kcal/mol difference in free energy. The intermediate that forms through the stepwise mechanism is only 4.4 kcal/mol lower than the electronic activation barrier. B3LYP slightly underestimates the enthalpic barriers but slightly overestimates the free energy barriers. The differences are around 2 kcal/mol in either direction.

Experimental work on the Bergman^{10f,g} cyclization suggest barrier heights in-between the parent Cope rearrangement and the substituted systems. Our computational results overestimate the barriers by 2-2.5 kcal/mol, similar to the Cope results, but our calculations predict a more stabilized intermediate by 3.8 kcal/mol.

Table 7: QM and electronic energetics for the Cope and Bergman reactions. The computed energies are in kcal/mol and the method and basis set are given.

		Computational Results										Experimental Results						
		B3LYP/6-31g(d)					M06-2X/6-31g(d)					E _a (kcal/mol)	ΔS‡ (J/Mol*K)	ΔG‡ (kcal/mol)	ΔH _{int} (kcal/mol)			
		TS		Intermediate			TS		Intermediate									
		ΔE	ΔH	ΔG	ΔE	ΔH	ΔG	ΔE	ΔH	ΔG	ΔE	ΔH	ΔG					
		34.4	33.2	36.2	N/A	N/A	N/A	N/A	N/A	N/A	N/A	N/A	N/A	239-299C 34.2±0.4	-13.4	35.8-36.0	N/A	
		24.6	23.3	25.1	N/A	N/A	N/A	N/A	N/A	N/A	N/A	N/A	N/A	130C 25.8	-11.7	26.9	N/A	
		Concerted 25.4	24.7	27.8	21.0	20.8	23.2	Concerted 27.5	26.5	29.5	25.2	24.9	27.0	70-90C 23.8±0.7	-14.2	25.0	N/A	
		Stepwise 25.4	24.7	27.4				Stepwise 28.4	26.8	29.1								
		31.8	30.6	32.5	3.6	4.7	7.7	35.7	34.3	36.1	5.0	6.1	8.9	197C 28.2±0.5	-10.2	29.2	8.5	

The computed structures are presented in Figure 30. The parent 1,5-hexadiene (**1**) has a symmetric transition state with distances of 1.97Å between the carbons of the forming and breaking bonds. The reactant and product are identical. The 1,1-dicyano-1,5-hexadiene reactant (**2**) has a more dissociative transition state with the breaking bond process far along at 2.32Å and the bond forming process in early stages at 2.21Å. This reaction is not degenerate and results in 3,3-dicyano-1,5-hexadiene. The 2,5-dicyano-1,5-hexadiene reaction proceeds through an associative mechanism with the newly forming bond almost complete at 1.83Å and the breaking bond slightly elongated at 1.67Å. This reaction has an intermediate that is symmetric. This reactant and product are also identical. The Bergman cyclization of (*Z*)-hexa-3-ene-1,5-diyne proceeds through an associative mechanism with a stabilized intermediate. The bond length of the forming bond in the TS is 1.98, and the reactant and product of this reaction are also degenerate.

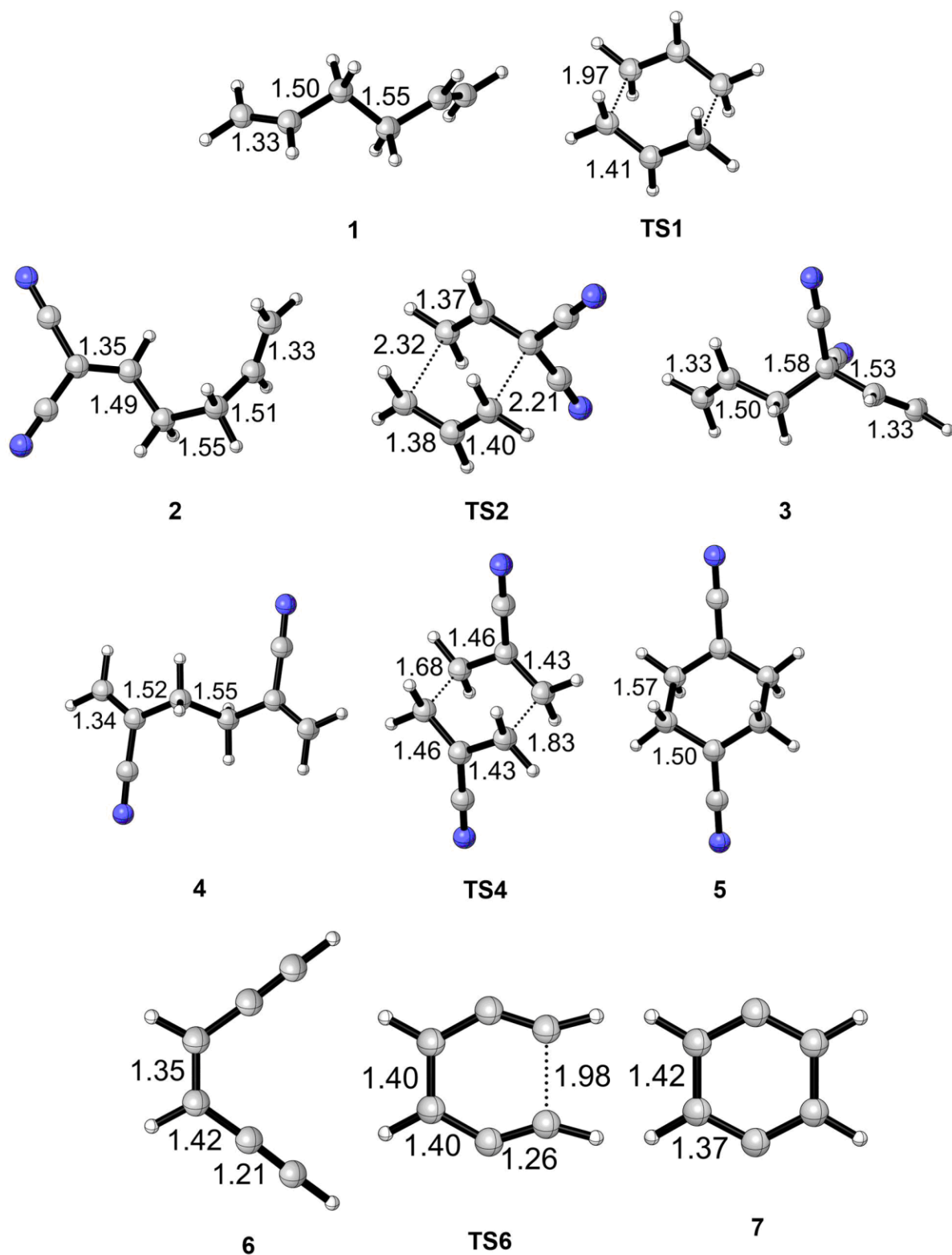


Figure 31. Computed reactants, transition states, intermediates and products. These structures list important bond lengths in the transition states and intermediates of the reactions studied.

Contour map of the potential energy surfaces studied. A 2D bond scan was performed for each system studied near the transition state. The scanned bonds are the forming and breaking bonds required to convert reactants to products or intermediates. These scans were used to generate contour maps of the potential energy surface near the transition state for the reaction of **1**, **2**, **4**, and **6**. The contour maps are orientated to mimic the More O'Ferrall-Jencks plot used by Gajewski in his secondary kinetic isotope experiments (Figure 29).² The reactants in Figure 31 are located in the bottom left while the products are in the upper right corner. The bottom right corner represents when both bonds are formed and is a 1,4-diyli intermediate for the Cope systems and *m*-benzyne for the Bergmann cyclization. Transition states in this region indicate an associative mechanism is at play during the reaction. The upper left region of the contour maps is the region where both bonds are nearly broken. Transition states in this region are indicative of a dissociative mechanism. Transition states near the middle are more symmetric and suggests an "aromatic" mechanism typically expected for pericyclic reactions. This detailed analysis of the PES gives another look at the differences between the dissociative, aromatic, and associative mechanisms. The x-axis of each contour map in Figure 31 is the bond that is formed during the reaction process, while the y-axis is the breaking bond. Each contour map also has the position of the transition structure marked.

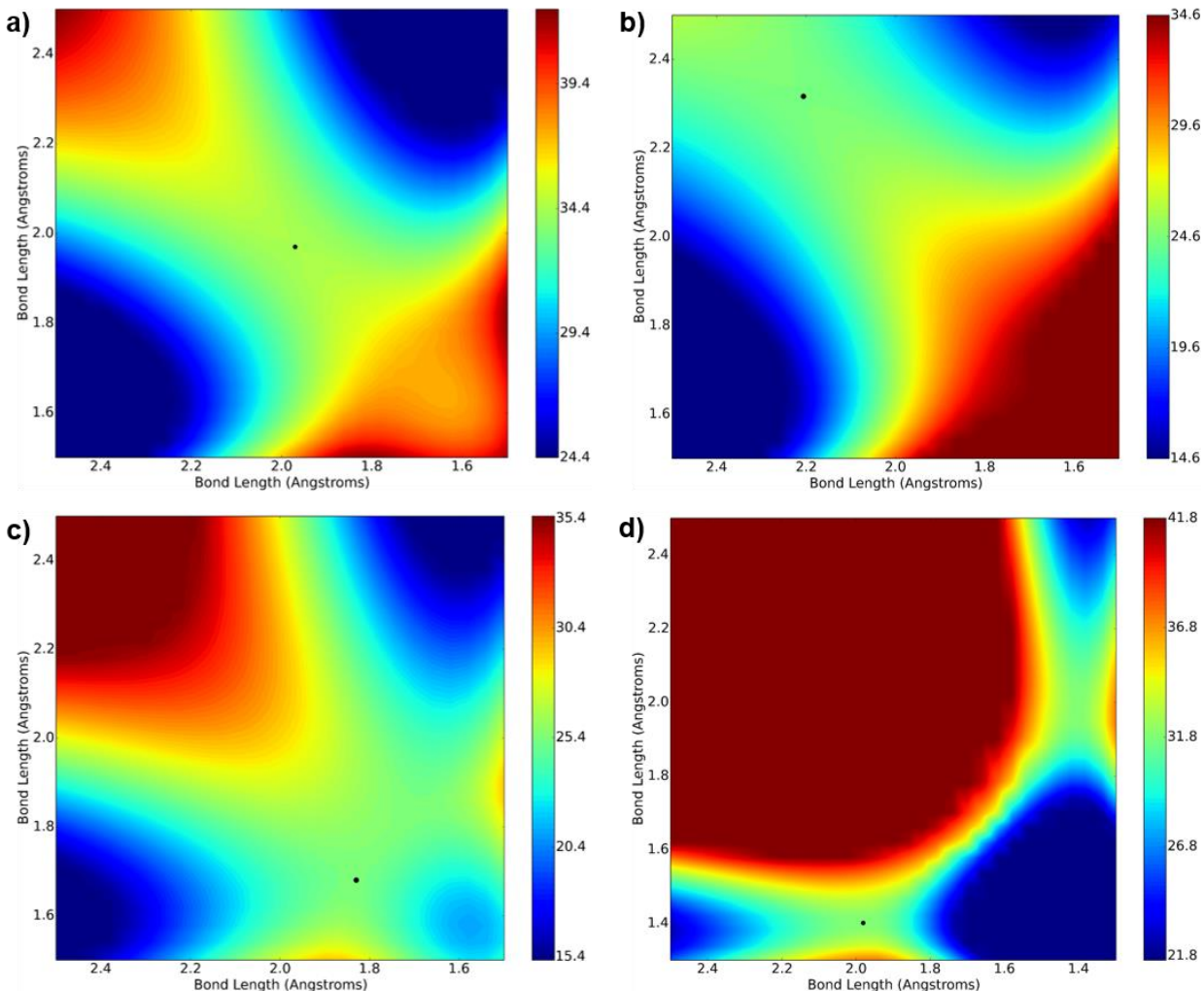


Figure 32. Contour maps of reactions 1, 2, 4, and 6. a) is the contour map of reaction of **1**. b) is the contour map of reaction **2**. c) is the contour map of reaction **4**. d) is the Bergman cyclization of **6**.

Examination of all the contour maps shows a clear relationship between substitution and the nature of the transition state. Contour map a) in Figure 31 is the reaction of the parent Cope system, **1**, and is symmetric with respect to the forming and breaking bonds. The energy rises near the associative, dissociative regions of the contour map. The Cope rearrangement of 1,1-dicyano-1,5-hexadiene shows that the transition state has an advanced broken bond with little forming bond character. The energy rises as the surface becomes more symmetrical and becomes very high in energy near the associative region of the contour map. The Cope

rearrangement of 2,5-dicyano-1,5-hexadiene shown in c) shows a stepwise transition state that leads to a very shallow intermediate well. This associative region of the contour map is low energy compared to the symmetric and dissociative regions for this substitution pattern. Finally, the parent Bergman cyclization is shown. When compared to the associative Cope rearrangement, there are strong similarities in the shape of the transition region. The major difference is due to the large stability of the *p*-benzyne (benzene-1,4-diyl). Trajectories that try to cross over and skip the *p*-benzyne have only a very narrow path to follow before falling into the intermediate well. Due to the triple bonds of the Bergman cyclization, the path from reactants to transition state are also very tight compared the Cope rearrangements double bonds.

Molecular dynamic results. Although these PES's give insight to the nature of the transition state, the molecular dynamic simulations provide a time-resolved mechanism of the reactions. The time spent traversing the transition zone can be used to determine if the reactions are dynamically concerted even though they may be dissociative. Finally, the ability for trajectories to skip intermediates is well known,¹¹ and these simulations reveal if the shallow intermediate of the associative Cope rearrangement can be bypassed.

Molecular dynamic simulations were performed and are summarized in Table 8. The number of trajectories for the parent and dissociative reactions are a little lower as all the trajectories behaved statistically and no anomalies were found. All trajectories passed through the transition zone and formed products. There were no recrossing events. The number of trajectories for the associative Cope reaction, **4**, was 304 while the Bergman rearrangement, **6**, was 343. For the trajectories simulated for the Cope rearrangement of **4**, 84 link from reactant to product within 500 fs (27.6%), 140 start from reactants but remained 1,4-diyl intermediates after 500 fs (46.1%), 67 trajectories formed the intermediate and then exited the intermediate well and returned to reactants (22.0%), finally, 13 trajectories headed to intermediates when pushed forward and reverse along the PES (4.2%). Finally, The Bergmann cyclization only had 3

trajectories in which the reactants escaped the intermediate well and formed product within 500 fs. (0.9%), 297 trajectories ended in the intermediate well after 500 fs (86.6%), 25 trajectories started from reactants and after entering the intermediate, came back out to form reactants again (7.3%), lastly, 18 trajectories headed to intermediates when pushed forward and reverse along the PES (5.2%).

Table 8: Summation of trajectories performed on reactants. Included is the results of these trajectory runs.

	Number of trajectories	R → P	R → Int	R → R	Int → Int
1	233	233	0	0	0
2	266	266	0	0	0
4	304	84	140	67	13
6	343	3	297	25	18

For the parent Cope rearrangement, **1**, the trajectories behaved as expected. All trajectories pass through the transition state and form product. Reactions passing through the transition zone in less than 60 fs are defined as being dynamically concerted. To determine this time, a transition zone is defined by taking 0.25Å on either side of the breaking or forming bond and calculating how long the trajectory spends crossing that region. Note that the following contour maps extend out to 3.5Å to better showcase the reactant and product pieces of each trajectory. The first contour map in Figure 32 shows all the starting points after normal-mode sampling overlaid on the PES contour map. These points are the dividing line between reactants and products and represent the transition state of this reaction. The second contour map is all the trajectories overlaid on the PES and show nicely that the trajectories do not wander far from the dividing surface. They sample some of the low energy areas around the transition point, but there are no recrossing events, and none that travel to the dissociative or associative areas of the PES. Finally, an overlay of all the structures generated through normal-mode sampling are given. The overlay of structures gives a more correct sense of the transition state of the reaction which is an average of all transition states on the dividing surface. All 233 trajectories behave normally and

there are no unusual trajectories. The transition zone for this reaction is 1.77Å to 2.22Å and take 47.0 fs \pm 17 fs.

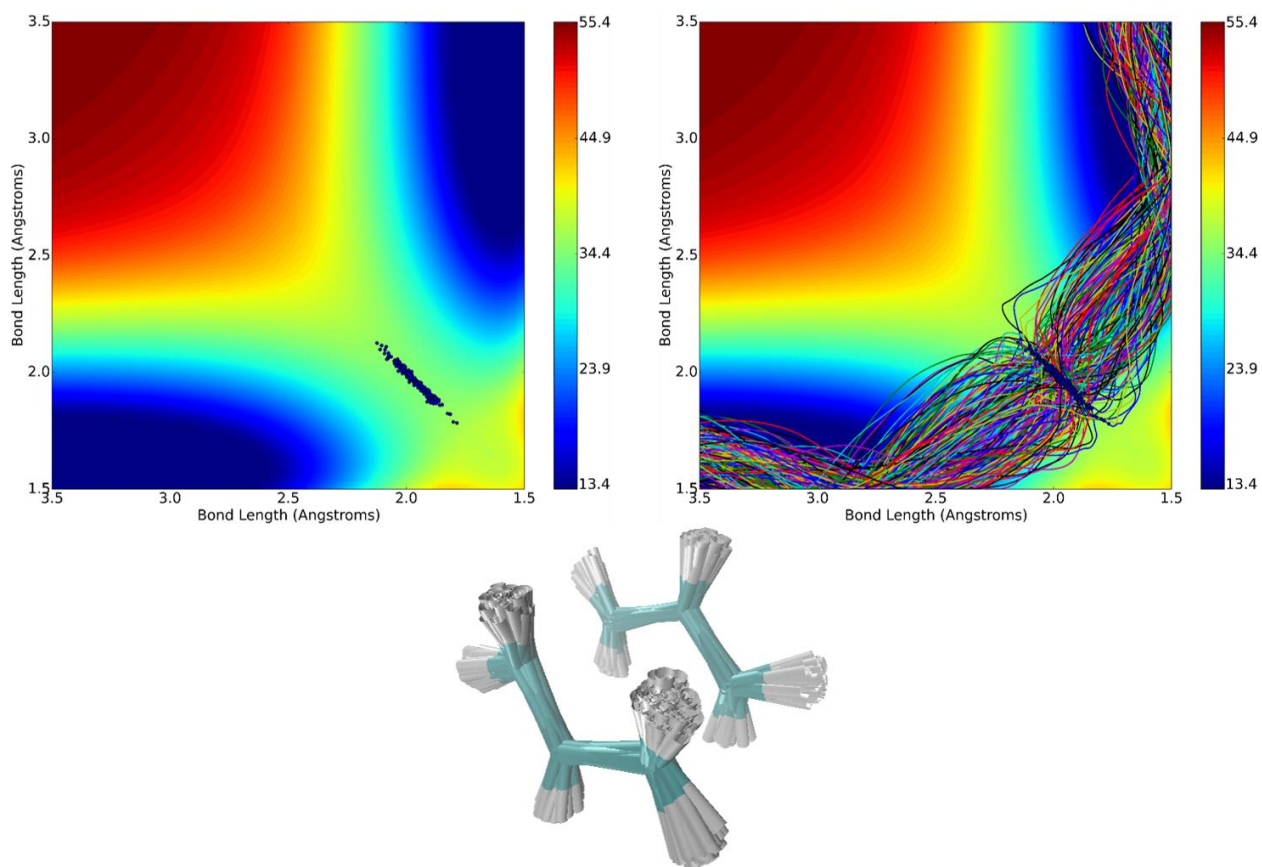


Figure 33. Overlay of starting points and trajectory paths on the PES contour map of reaction 1.

The reaction of **2**, while a more dissociative mechanism and transition state, also behaves normally during molecular dynamic simulations. The first contour map in Figure 33 is the starting points after normal-mode sampling of the transition structure. These structures are in the dissociative region of the contour map. The second contour map in Figure 33 overlays all 266 trajectories. There are no abnormal trajectories as all of them passed through the dividing surface onto products. Also shown is the overlay of all transition structures to get a better picture of the real transition state. Although this reaction is more dissociative, there is no evidence to suggest that the reaction forms 2 allyl radicals that then reform to make the product (or return to starting materials). The transition zone for this reaction is a bit more complex due to the asynchronicity of

the transition state. The transition zone timing for reactions of this nature will start when either the bond forming or breaking first crosses its threshold ($\pm .25\text{\AA}$ in either direction from the computed transition state distances) into the transition zone and stop when both have passed out of their respective zones. For the breaking bond, the transition zone ranges from 2.07-2.57 \AA . The forming bond ranges from 1.96-2.46 \AA . The time it takes to cross the transition zone for this reaction is 65.0 fs \pm 20.0 fs, on the borderline between dynamically concerted and stepwise, and approximately 15 fs longer than the parent system passing through the symmetric transition state.

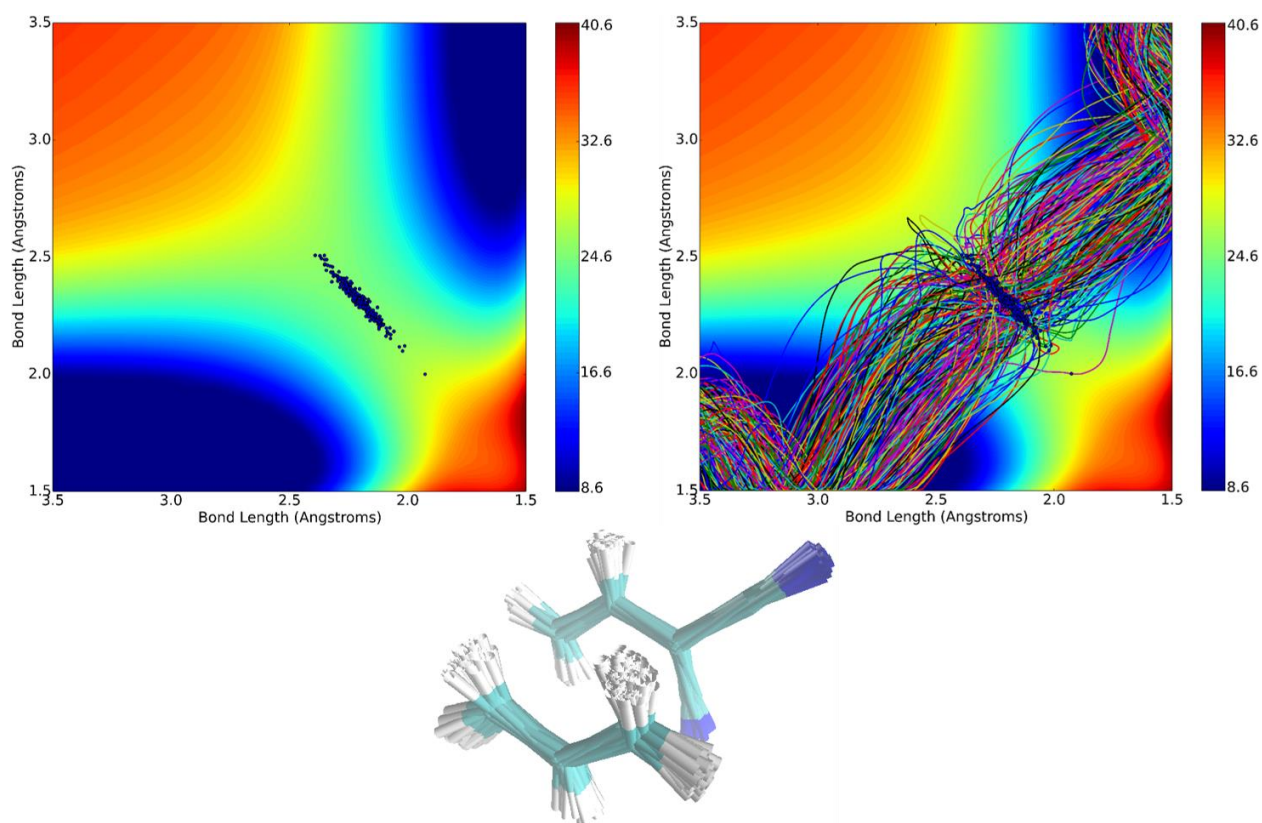


Figure 34. Overlay of starting points and trajectory paths on the PES contour map of reaction 2.

While the previous systems have all had trajectories that behaved normally, the associative Cope reaction, **4**, has some trajectories that do show non-statistical behavior. The first contour map in Figure 34 gives an overlay of transition structures from normal-mode sampling. They are in the region in which there is significant bond-forming progress, but virtually

no bond breaking. Due to an intermediate linking the reactants and products, this stepwise process in a bond forming and then a bond breaking reaction. It follows that there is another transition state for the reaction to overcome once it forms the intermediate. This transition state is the same as the first, except that the process is a bond breaking one.

The second contour shows the overlay of all the trajectories on the PES. All trajectories do sample the intermediate region of the PES but are not thermally equilibrated, but rather continue directly to product. The final image is the overlay of transition structures that better represents the actual transition state. Because the first transition state is especially the bond forming process, the transition zone will be defined using only that bond. The transition zone is still $\pm 0.25\text{\AA}$ from the distance in the transition zone (1.83\AA). For this reaction, the transition zone is 1.58\AA to 2.08\AA and the time to cross it is $39.5\text{ fs} \pm 14.5\text{ fs}$.

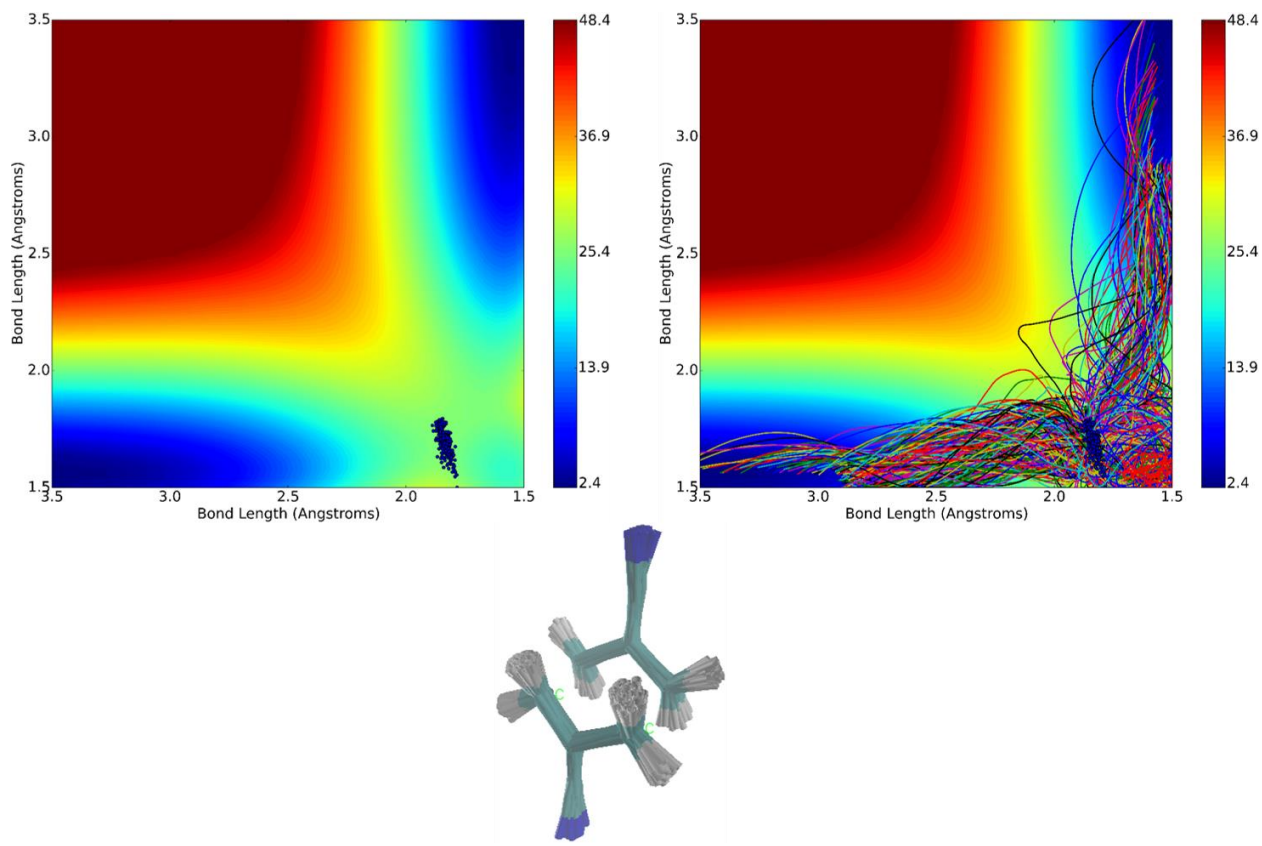


Figure 35. Overlay of starting points and trajectory paths on the PES contour map of reaction 4.

Of the 84 trajectories that formed product within 500 fs, 44 do so within 100 fs. An example trajectory is shown in the first contour map in Figure 35. These trajectories completely skip the intermediate well altogether or send less than one C-C bond vibration as a diradical. Interestingly, as the forming bond nears the transition state in most of these trajectories, the breaking bond is just finishing a bond compression and is ready to start stretching. This primes it for skirting the intermediate well and as the forming bond finishes, the breaking bond starts breaking and continues through its transition state and forms the product. The second contour map in Figure 35 shows what the other 40 trajectories look like. They behave as expected but they finish within 500 fs. They enter the intermediate region by forming a diradical 1,4-diyli intermediate and leave once the C-C bond that needs to break gets the energy to pull apart and form the 2 π bonds of the product.

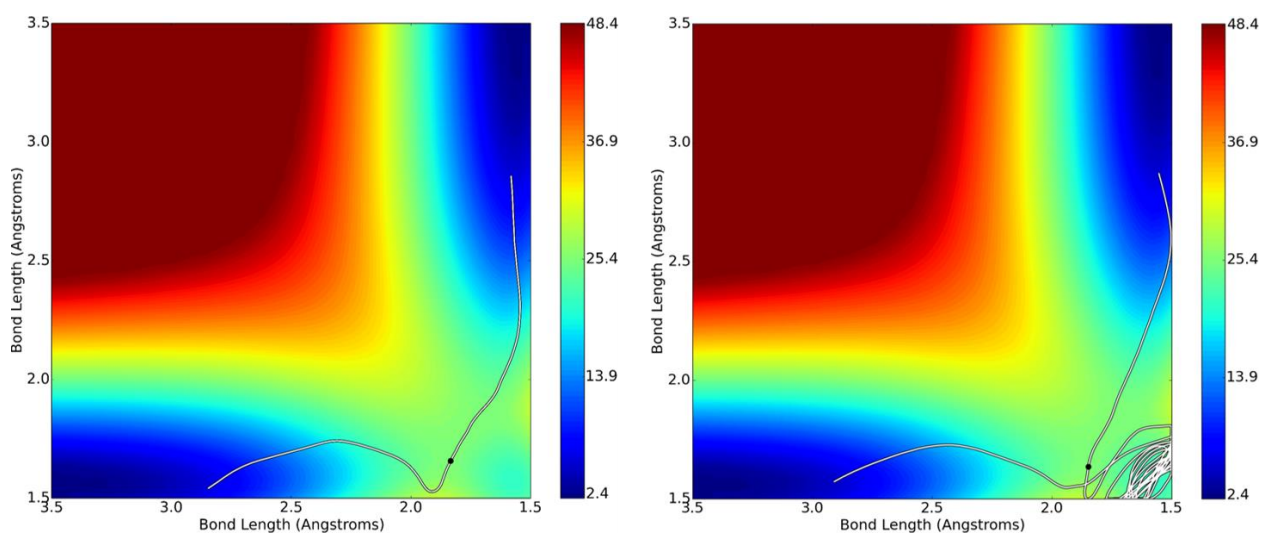


Figure 36. Representative samples of a trajectory that bypasses the intermediate and a normal short trajectory.

The associative Bergman reaction has very different results from that of the Cope rearrangement. The Bergman reaction of **6** is a two-step process in which only one bond is broken or formed at a time. The first contour map in Figure 36 shows the PES with the transition states generated through normal-mode sampling. This grouping of transition states is not nearly as

broad as the previous reactions due to narrow nature of the PES from reactants to products. The second contour map is the overlaid trajectories that pass through the transition points. Of note, only 3 trajectories formed product and are seen here exiting the intermediate well and proceeding to product.

This reaction deals with carbons that have much stiffer force constants for bond stretching due to the increased number of π systems involved in the breaking and forming bonds from reactant to product. This results in a much steeper energy cost to stretch these bonds as opposed to the previous studied Cope relations. This manifests as a very narrow path from reactant to intermediate to product on the PES. Finally, there is also an overlay of all the transition structures that gives a real sense of what the actual transition state is. The time spent crossing the transition zone is nearly identical to that of the associative Cope rearrangement time gap. Again, the transition zone for this process is based on the forming bond as the breaking bond does not start to break until it reached the intermediate. The transition zone is 1.73-2.23 with a time gap of $40 \text{ fs} \pm 13 \text{ fs}$.

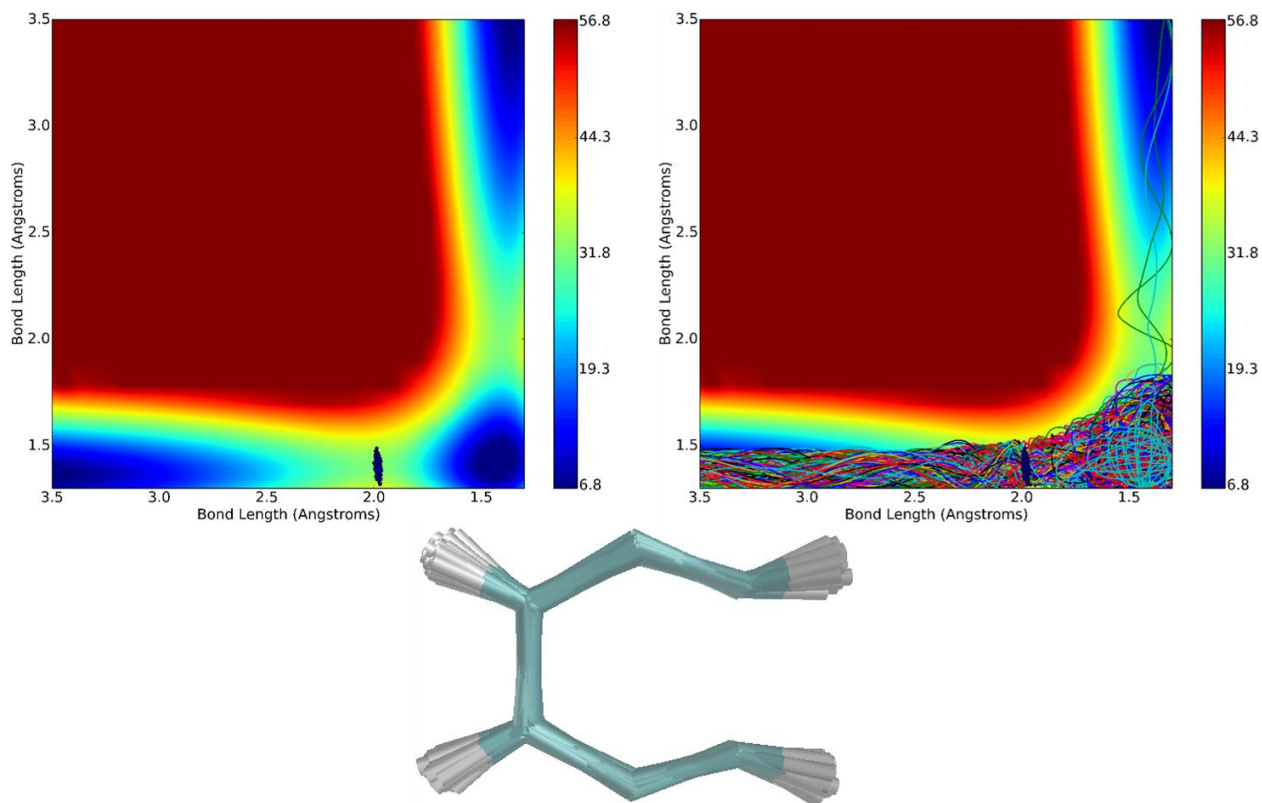


Figure 37. Overlay of starting points and trajectory paths on the PES contour map of reaction 6.

Dynamic calculations have shown that only 3 trajectories out of 343, about 1%, formed product before the 500 fs cut off criteria was reached. The first contour map in Figure 37 shows the 3 trajectories overlayed on the PES. They spend between 400 and 440 fs sampling the intermediate well before coming over the barrier to products. No trajectories went straight from reactants to products directly. Some of the trajectories rebounded back to starting material after entering the intermediate well and only sampling it for less than 20 fs. The number of trajectories that rebounded were 25, about 7.3%. The second contour map in Figure 37 shows the typical trajectory that had this behavior. While the forming bond compresses and then springs open, the bond that would normally break to form product has very little oscillation. This is observed in a majority of the rebound trajectories.

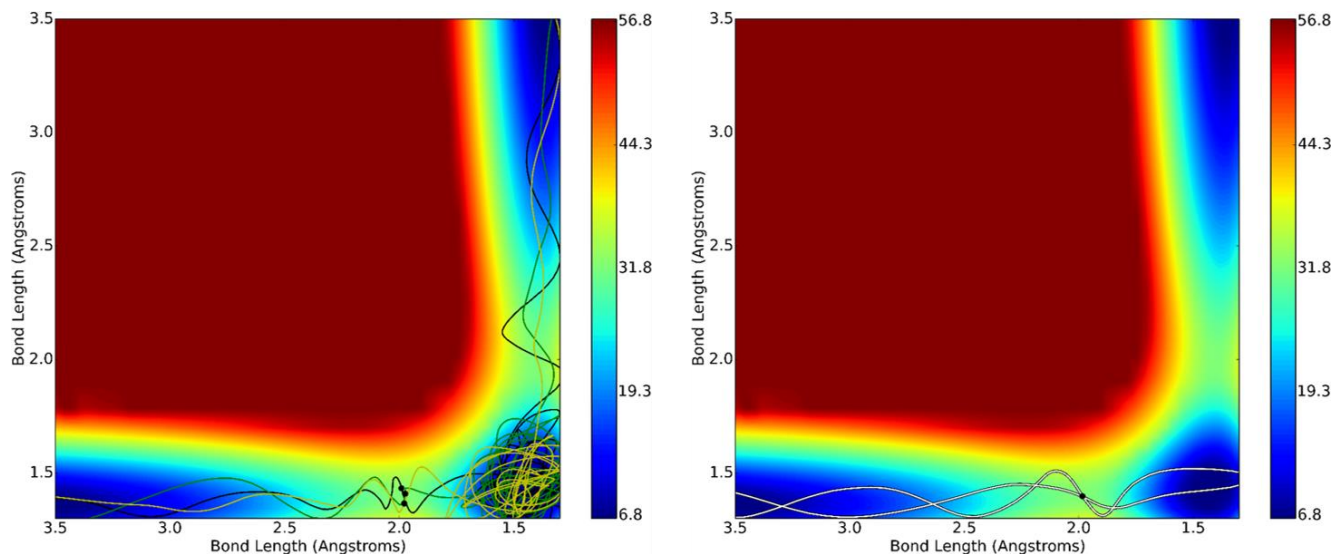


Figure 38. Trajectories that lead to product and a trajectory that rebounds.

Finally, there are about 18 trajectories, about 5%, that recrossed. Recrossing is normally defined as a trajectory going to reactants in both trajectory directions. This happens when the true transition state is a little earlier or later than the electronic transition state that is used to generate initial starting points for trajectories. With this Bergman reaction, the recrossing happens when the starting transition state moves in reverse direction back to reactants but ends up reversing direction and falling into the intermediate well. The last contour map in Figure 38 showcases a trajectory with this behavior. The forward reaction behaves normally and becomes the intermediate and remains until the 500 fs cutoff criteria is met for the trajectory. This suggests that the true transition state is in fact a bit earlier than the electronic transition state.

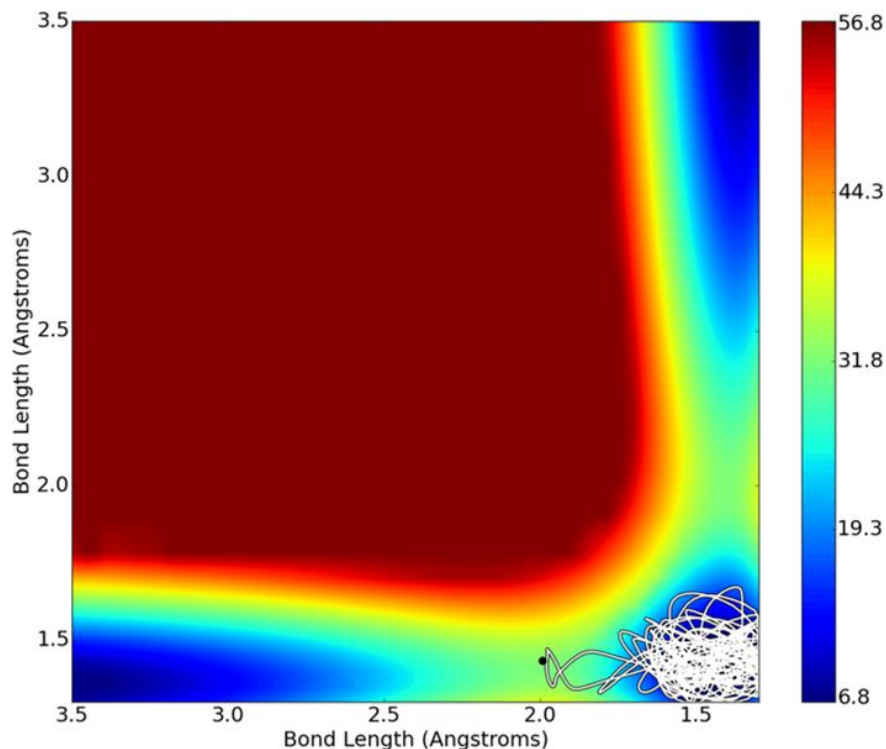


Figure 39. Trajectory that recross in the Bergman reaction.

Conclusion

Molecular dynamics allows for exploration of the timing of the bond making and breaking process. The study of these Cope rearrangements is of interest due to the shifting nature of the transition state. Aromatic and dissociative reactions give the expected statistical outcomes. The more interesting cases are the associative mechanisms in which an intermediate is accessible. For the case of a shallow intermediate, non-statistical trajectories showcased the ability of some of the trajectories to skip over completely or spend a very small amount of time as an intermediate. The related Bergman rearrangement is also associative but has a much deeper intermediate well and trajectories suggest that only a small fraction, less than 1%, will exit the intermediate to become product in under 500 fs and none ever skip the intermediate all together.

References

-
- 1) Cope, A. C.; Hardy, E. M. *J. Am. Chem. Soc.*, **1940**, 62, 441.

-
- 2) Gajewski, J. J.; Conrad, N. D. *J. Am. Chem. Soc.* **1979**, *101*, 6693.
- 3) Doering, W. v. E.; Roth, W. R. *Tetrahedron*, **1962**, *18*, 67.
- 4) a) Hrovat, D. A.; Borden, W. T.; Vance, R. L.; Rondan, N. G.; Houk, K. N.; Morokuma, K. *J. Am. Chem. Soc.*, **1990**, *112*, 2018-2019. b) Hrovat, D. A.; Morokuma, K.; Borden, W. T. *J. Am. Chem. Soc.*, **1994**, *116*, 1072. c) Wiest, O.; Black, K. A.; Houk, K. N. *J. Am. Chem. Soc.*, **1994**, *116*, 10336. d) Houk, K. N.; Gonzalez, J.; Li, Y. *Acc. Chem. Res.*, **1995**, *28*, 81-90. e) Hrovat, D. A.; Beno, B. R.; Lange, H.; Yoo, H.-T.; Houk, K. N.; Borden, W. T. *J. Am. Chem. Soc.*, **1999**, *121*, 10529-10537. f) Hrovat, D. A.; Chen, J.; Houk, K. N.; Borden, W. T. *J. Am. Chem. Soc.*, **2000**, *122*, 7456-7460. g) Staroverov, V.; Davidson, E. R. *J. Am. Chem. Soc.*, **2000**, *122*, 7377-7385. h) Balavins, J. J.; Cooper, D. L.; Karadakov, P. B. *J. Phys. Chem. A*, **2004**, *108*, 194-202.
- 5) Frisch, M. J.; et al. Gaussian 09, revision D.01; Gaussian, Inc.: Wallingford, CT, **2013**.
- 6) a) Becke, A. D. *J. Chem. Phys.*, **1993**, *98*, 5648-5652. b) Lee, C.; Yang, W.; Parr, R. G. *Phys. Rev. B*, **1988**, *37*, 785-789. c) Vosko, S. H.; Wilk, L.; Nusair, M. *Can. J. Phys.*, **1980**, *58*, 1200-1211. d) Stephens, P. J.; Devlin, F. J.; Chabalowski, C. F.; Frisch, M. J. *J. Phys. Chem.*, **1994**, *98*, 11623-11627.
- 7) Zhao, Y.; Truhlar, D. G. *Theor. Chem. Acc.*, **2008**, *120*, 215-241.
- 8) a) Chapman, S.; Bunker, D. L. *J. Chem. Phys.*, **1975**, *62*, 2890-2899. b) Doubleday, C. E.; Bolton, K.; Hase, W. L. *J. Phys. Chem. A*, **1998**, *102*, 3648-3658. c) Peslherbe, G. H.; Wang, H. B.; Hase, W. L. "Monty Carlo Methods in Chemical Physics" **1998**, Wiley, New York, 171-201.
- 9) Ussing, B. R.; Hang, C.; Singleton, D. A. *J. Am. Chem. Soc.*, **2006**, *128*, 7594-7607.
- 10) a) Bellus, D.; Hansen, H.-J. *Helv. Chim. Acta*. **1977**, *60*, 1325-1356. b) Humski, K.; Malojcic, R.; Borcic, S.; Sunko, D. E. *J. Am. Chem. Soc.* **1970**, *92*, 6534-6538. c) Bellus, D.; Hansen, H.-J. *Helv. Chim. Acta*. **1977**, *60*, 1325-1356. d) Humski, K.; Malojcic, R.; Borcic, S.; Sunko, D. E. *J. Am. Chem. Soc.* **1970**, *92*, 6534-6538. e) Foster, F. G.; Cope, A. C.; Daniels, F. *J. Am. Chem. Soc.*, **1947**, *69*, 1893-1896. f) Roth, W. R.; Hopf, H.; Horn, C. *Chem. Ber.*, **1994**, *127*, 1765-1779. g) Roth, W. R.; Hopf, H.; Wasser, T.; Zimmermann, H.; Werner, C. *Liebigs Ann.*, **1996**, *10*, 1691-1695.
- 11) a) Berson, J. A.; Nelson, G. L. *J. Am. Chem. Soc.* **1967**, *89*, 5503-5504. b) Baldwin, J. E.; Belfield, K. D. *J. Am. Chem. Soc.* **1988**, *110*, 296-297. c) Klaerner, F. G.; Drewes, R.; Hasselmann, D. *J. Am. Chem. Soc.* **1988**, *110*, 297-298. d) Carpenter, B. K. *J. Am. Chem. Soc.* **1995**, *117*, 6336-6344. e) Carpenter, B. K. *J. Am. Chem. Soc.* **1996**, *118*, 10329-10330. f) Roth, W. R.; Wollweber, D.; Offerhaus, R.; Rekowski, V.; Lennartz, H. W.; Sustmann, R.; Müller, W. *Chem. Ber.* **1993**, *126*, 2701-2715. g) Debbert, S. L.; Carpenter, B. K.; Hrovat, D. A.; Borden, W. T. *J. Am. Chem. Soc.* **2002**, *124*, 7896-7897.